Investigation of Stall Inception in Centrifugal Compressors Using Isolated Diffuser Simulations

by

Jonathan Everitt

M.Eng., M.A. (Cantab), University of Cambridge (2005)

Submitted to the Department of Aeronautics and Astronautics
in partial fulfillment of the requirements for the degree of

Master of Science in Aeronautics and Astronautics

at the

MASSACHUSETTS INSTITUTE OF TECHNOLOGY

September 2010

Author .....
Department of Aeronautics and Astronautics
August 20, 2010

Certified by .....
Zoltán S. Spakovszky
H. N. Slater Associate Professor
Thesis Supervisor

Accepted by .....
Eytan H. Modiano
Associate Professor of Aeronautics and Astronautics
Chair, Graduate Program Committee

Investigation of Stall Inception in Centrifugal Compressors Using Isolated Diffuser Simulations

by

Jonathan Everitt

Submitted to the Department of Aeronautics and Astronautics
on August 20, 2010, in partial fulfillment of the
requirements for the degree of
Master of Science in Aeronautics and Astronautics

Abstract

In compression systems the range of stable operating is limited by rotating stall and/or surge. Two distinct types of stall precursors can be observed prior to these phenomena: the development of long-wavelength modal waves or a short-wavelength, three-dimensional flow breakdown which is typically known as a "spike". The cause of the latter is not well understood; in axial machines it has been suggested that over-tip spillage flow has a significant role, but spikes can also occur in shrouded vaned diffusers of centrifugal compressors, where these flows are not present, suggesting an alternative mechanism may be at play.

Unsteady Reynold's Averaged Navier-Stokes simulations are performed for an isolated vaned radial diffuser from a highly loaded centrifugal compressor. Key to their success is the definition of pitchwise "mixed out" averaged inlet conditions derived from the impeller exit flow field from separate single passage stage calculations. This guarantees the relevant flow features are carried into the diffuser model, particularly the spanwise profile of flow angle and total pressure. It is shown that the isolated diffuser model compares well with experimental data and time-averaged, unsteady, full wheel simulations.

The stability of the flow is tested via numerical forced response experiments whereby the inlet conditions are perturbed by a total pressure forcing small in temporal and spatial extent. An unstable rotating stall precursor is observed at low diffuser inlet corrected flow, due to the spanwise non-uniform flow angle and total pressure at the diffuser inlet. The radial pressure gradient imposed by the highly swirling bulk flow leads to flow angles in excess of 90° in the shroud endwall flow. This results in shroud-side separation at the diffuser vane leading edge and a region of recirculating flow in the vaneless space. Vorticity shed from the diffuser vane leading edge convects back to the vaneless space and joins the vortical structures within the recirculating flow. This is suggested to lead to spike stall inception.

Thesis Supervisor: Zoltán S. Spakovszky
Title: H. N. Slater Associate Professor

Acknowledgments

Firstly I would like to thank Prof. Zoltán Spakovszky, who as my advisor eased me back into academia and provided support, helpful suggestions and much patience. Prof. Nick Cumpsty provided a fresh pair of eyes at regular intervals, for which I am very grateful, and Prof. Edward Greitzer and Dr. Choon Tan were always on hand to help with questions or lend a reference text. Holly Anderson is also gratefully acknowledged for her role in keeping the lab and all the projects running smoothly.

The research described here builds upon the work of past members of the "ABB Team" here at the GTL, and I would like to thank Björn Benneke and Andy Hill (who took time out of flying helicopters to visit me) for their guidance at the beginning of this project.

All of the graduate students at the GTL have assisted me at some stage by answering questions, providing a sounding board for ideas, or listening to my problems. There are some in particular I'd like to thank - firstly, Jeff Defoe, who has taken on responsibility for maintaining and expanding the GTL cluster, on which my project and many others depend. My current and past office mates, Andreas, Francois, Jeff, Sho and Alex, began as people with whom I shared office space but are now (very international!) good friends.

I would like to thank my parents and the rest of my family for their support and encouragement throughout my education. Most importantly, I extend my thanks and love to my fiancèe Liz, who is always there for me but who has been particularly encouraging and patient during the writing of this thesis.

This project was enabled and supported by ABB Turbo Systems Ltd., under the supervision of Dr. Daniel Rusch. I would like to thank Dr. Rusch, Dr. Jan-peter Kühnel and Dr. Hans-Peter Dickmann for their input in regular telephone and video conferences, Dr. Niklas Sievers for kindly providing the volute mesh, and Dr. Matthias Schleer for his support during visits to Baden. I much look forward to working with ABB further as I continue my graduate studies here at the MIT GTL.

Contents

List of Figures

List of Tables

Nomenclature

Abbreviations

CFD	Computational Fluid Dynamics
CO_2	Carbon Dioxide
EGR	Exhaust Gas Recirculation
FINE/Turbo	Flow INtegrated Environment for Turbomachinery Flows
GTL	The MIT Gas Turbine Laboratory
NASA	National Aeronautics and Space Administration
NO_X	Oxides of Nitrogen
O4H	Grid structure description: O-ring with four hexahedral blocks
PDPR	Peak Diffuser Pressure Rise
RANS	Reynolds Average Navier-Stokes
SDCF	Standard Day Corrected Flow
VLS	Vaneless Space

Roman Symbols

A	area (m^2)
B	blockage (-)
c	speed of sound (m/s)
c_p	specific heat at constant pressure (kJ/kgK)
C_p	Pressure coefficient, $(p - p_{upstream})/(p_t - p)_{upstream}$
c_v	specific heat at constant volume (kJ/kgK)

$d()$	differential quantity
h	enthalpy (kJ/kg)
m	number of multigrid levels (-)
$\dot{m}$	mass flow (kg/s)
M	Mach number (-)
n	number of impeller main blades (-)
p	static pressure (Pa)
p_{ref}	100 kPa
p_t	stagnation pressure (Pa)
r	radius (m)
R	gas constant (kJ/kgK)
t	time (s)
T	static temperature (K)
T_{ref}	298 K
T_t	stagnation temperature (K)
$\dot{V}$	volume flow (m^2/s)
V	velocity (m/s)
w	axial depth of diffuser (m)
U	rotor speed (m/s)
X_i	Number of mesh nodes in a given dimension, i (-)
z	axial dimension (m)

Greek Symbols

α	flow angle from radial, positive in direction of rotor rotation (°)
β	compound compressible flow indicator (-)
γ	ratio of specific heats, $(\frac{c_p}{c_v})$ (-)
δ	ratio of total pressure to reference value (-)
δz	small element in z direction, defined by mesh spacing

η_p	polytropic efficiency (-)
θ	angular position (°)
θ	ratio of total temperature to reference value (-)
π	pressure ratio (-)
ρ	density (kg/m^3)
σ	slip (-)
χ	metal angle, defining blade geometry (°)
ω	vorticity, $\nabla \times V$ (1/s)
Ω	angular velocity (rad/s)

Subscripts

TS	total-to-static
0	stagnation conditions upstream of impeller
1	impeller leading edge location
2	impeller trailing edge location
3	diffuser leading edge position
4	diffuser trailing edge position
m	average (mean)
r	radial (e.g. velocity)
ref	reference value
tip	impeller tip
θ	tangential (e.g. velocity)
vls	vaneless space

Conventions

Unless otherwise noted, spanwise position is taken as the proportion of the span from the hub e.g. "10% span" is 10% of the span from the hub surface. See also Figure 1-1.

Chapter 1

Introduction

1.1 Background and Motivation

Turbochargers use centrifugal compressors to increase the density of the air into an internal combustion engine. By increasing the density of the air, it is possible to burn more fuel per stroke while maintaining the desired fuel/air ratio, thus increasing the engine's specific power (power output per unit weight). In addition, using a turbine driven by exhaust gases to power the compressor offers the opportunity to increase the efficiency of the internal combustion engine through the extraction of work from the exhaust gases.

A further advantage of turbocharging is the opportunity to lower emissions. While high pressure ratio turbochargers can improve efficiency and hence help to reduce carbon dioxide emissions, typically increasing boost pressure results in an increase in emissions of nitrogen oxides (NO_X), due to increased temperatures. However, the combination of high boost pressures and other technologies, such as exhaust gas recirculation (EGR) or advanced Millar timing, offer the opportunity to reduce NO_X emissions while simultaneously improving efficiency [9, 10]. With environmental and cost pressures on fuel burn and CO_2 emissions, and environmental and legislative pressures on NO_X emissions, the development of high pressure ratio turbochargers is important for engine and turbocharger manufacturers.

Turbochargers utilize centrifugal compressors (Figure 1-1) which are able to achieve

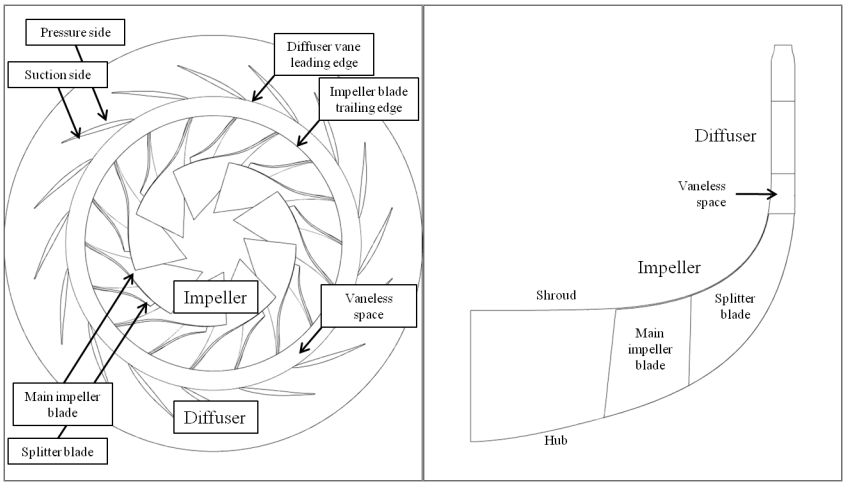

Figure 1-1: Basic geometry of a centrifugal compressor: axial view (left) and meridional passage (right).

a high pressure ratio from a single stage while simultaneously achieving a broad operating range. These qualities stem from the fact that the centrifugal compressor is able to achieve much of its compression from centrifugal effects rather than deceleration of the flow (as encountered in an axial machine), such that it is less limited by boundary layer growth and separation due to adverse pressure gradients [11]. However, as the pressure ratio is increased, the range of stable operation tends to decrease due to compressibility effects and the challenge of diffusing the high Mach number flow at the outlet of the impeller.

The design of a centrifugal compressor is therefore tailored to application. For the turbocharger application, a broad operating map is desirable with a good margin between the operating line and the surge line (shown in Figure 1-2 on the left), and the pressure ratio achieved from a single stage is typically a maximum of 5 or 6. For a different application, for example an helicopter engine, the characteristic is narrow but the pressure ratio may exceed 10 (Figure 1-2 on the right).

One way to improve the range of stable behavior is to employ increased backsweep in the impeller design [12]. The problem is that this introduces a bending stress in the impeller blade due to centrifugal accelerations while simultaneously requiring increased rotor speed to achieve the same pressure ratio. Enhanced materials (e.g. titanium alloys) which can support these stresses are commercially undesirable due to

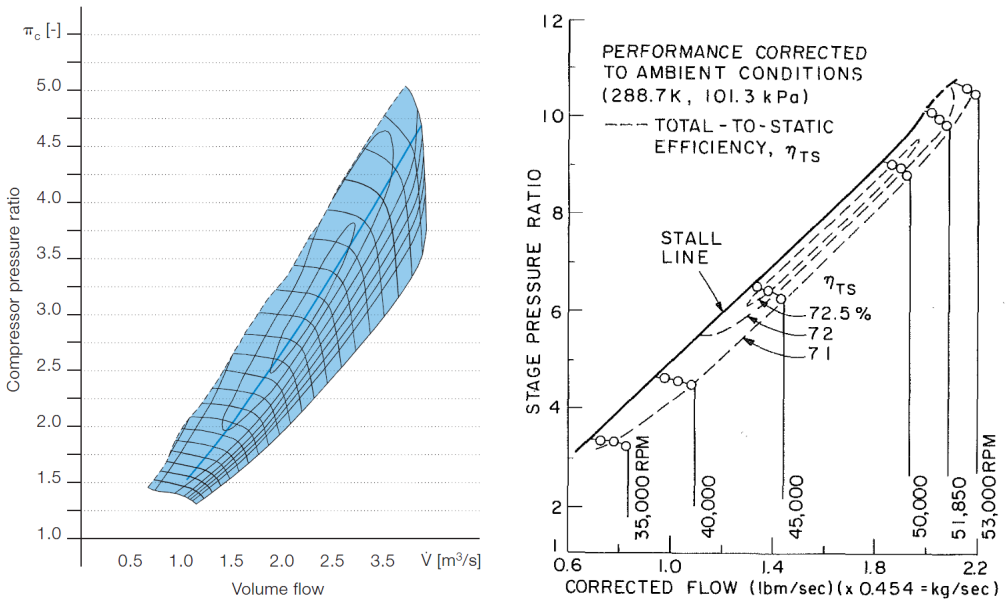

Figure 1-2: Typical centrifugal compressor maps. Left shows a compressor for turbocharging application [1]. Right shows a compressor designed for high pressure ratio [2].

high material and machining costs; as such, large turbocharger impellers are typically manufactured from aluminum alloys.

The motivation for this research is thus to improve understanding of the fluid mechanics which govern the onset of instability, to enable design of compressors which are better able to meet the simultaneous requirements for high pressure ratios, a wide range of stable operation and manufacture from aluminum alloys.

1.1.1 Compressor Instability

For a given rotational speed, the stable operation of compressors (either axial or centrifugal) is limited by choking at high flows and rotating stall or surge at low flows. Choking is a compressible flow effect that limits the maximum mass flow through a certain geometry, such that the corrected flow becomes independent of the back pressure (as seen in Figure 1-2). Rotating stall and surge are instabilities which occur at low flows, and are marked on the compressor map by a "stall line" or a "surge line". Compressors must be controlled to prevent operation near this line, and a surge margin is provided to allow some factor of safety. The phenomena of rotating stall

and surge are well documented (a comprehensive review is provided in [3]), but a brief overview is provided here for completeness.

Rotating stall comprises one or more stall cells, in which some blades experience stalled operation similar to an airfoil at high angles of attack. The stalled region may include one or more blades, and extend across all or part of the span. The mass flow in this region is typically small in comparison to the flow past unstalled blades. The stall cells propagate around the circumference at a fraction of the rotor speed typically between 20-70%. The presence of rotating stall is undesirable as it causes vibrational stresses on the blading and often leads to severely degraded performance (for example much lower efficiencies).

Surge is a system wide instability which causes flow reversal through the entire system. Surge can occur following rotating stall or directly, but requires a volume of fluid downstream of the compressor which, when at high pressure, provides stored energy (analogous to a gas spring). In the simplest sense, if a breakdown of flow occurs in the compressor and the pressure ratio is momentarily compromised, the high pressure fluid in the downstream volume can cause flow reversal. Once this potential energy is released, the compressor can recover and a period of forward flow occurs. The compressor enters a limit cycle with low frequency oscillations between forward and reversed flow which is typical of surge.

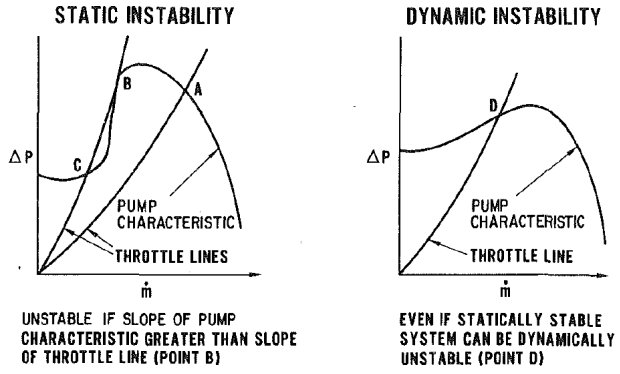

Figure 1-3: Static and dynamic instability in a compression system, from Greitzer [3].

As mentioned above, it is important to identify the conditions under which the compression system can become unstable. The onset of instability can be related to the slope of the curve of pressure rise coefficient against corrected flow, and again the reader is referred to Greitzer [3] for further detail. The compressor is statically unstable if the slope of the compressor characteristic

is greater than the slope of the downstream throttle characteristic (Figure 1-3, point B). When a small reduction in mass flow occurs, the compressor is unable to achieve the pressure rise required by the throttle line, and there is pure exponential divergence until a new equilibrium position is found, typically with significantly reduced pressure rise. Dynamic instability has a more complex criterion for its occurrence, as it is related to oscillatory fluid motion within the compression system, and this links to the dynamic behavior of the system as described above.

The different parts of the compression system can be broken down into:

- The compressor or pump, which acts as an active damper (the compressor can add or remove energy from a oscillatory disturbance)
- Ducts, the fluid in which has inertia, analogous to mass in a mechanical oscillating system;
- Fluid volumes, which can act as gas springs, storing and releasing potential energy (if large enough[1], ducts also act as gas springs); and
- The throttle, which always removes energy from the oscillatory motion.

An analysis can then be performed on the energy within the oscillatory motion. On the positive slope of the compressor characteristic curve (Figure 1-3, point D), a small increase in mass flow causes a small increase in the pressure rise, and the product, which relates to the energy change to an oscillatory motion, is positive. A small reduction in mass flow (such that $d\dot{m} < 0$) results in a small reduction in pressure rise ($d(\Delta p) < 0$) such that the product is again positive. In this case, any infinitesimal disturbance to the flow will increase in magnitude and lead to instability.

The analysis of dynamic stability can be performed one-dimensionally, but can also be extended to two dimensions, with variation in the pitchwise direction, such that it can be used to describe either the onset of surge or rotating stall. It is noted that the two phenomenon are not isolated; while rotating stall is localized in terms of

[1] "large enough" has to be quantified in a non-dimensional sense; a "small" or "compact" duct has $\omega L/c \ll 1$, where ω is the frequency of the oscillatory disturbance, L is the length of the duct and c is the local speed of sound. Further detail can be found in Greitzer et al. [13].

the overall compression system, it impacts the slope of the compressor characteristic curve and therefore can lead directly to surge.

Particularly in centrifugal compressors, it is common practice to break down the compressor further into subcomponents and determine their pressure rise characteristic separately to identify the stabilizing or destabilizing elements. Published literature on centrifugal compressors (e.g. Dean [14], Hunziker and Gyarmathy [15] and, more recently, Spakovszky and Roduner [7]) appear to agree that the the change in gradient of the pressure rise characteristic of the diffuser inlet region plays an important role in the onset of instability.

1.1.2 Stall Inception

Prior to the fully developed instability described in the previous section, certain behaviors are evident in the compressor which can be described as stall precursors. Detection and understanding of these behaviors is important to allow sufficient margin over unstable behavior in the operation of the compressor and to enable the design of compressors with an improved range of stable operation.

Camp and Day [4] described the phenomena of stall inception in a low speed axial compressor, identifying two distinct routes to instability: modal oscillations and a short length-scale "spike" phenomena. These are illustrated in Figure 1-4 below, which shows the unsteady traces from hot-wire anemometers distributed around the circumference of an axial machine. Modal oscillations can be seen as long wavelength (of the order of the circumference) pressure fluctuations, which rotate and grow over time before eventually triggering full-scale instability. These stall precursors are theoretically predicted by the system model of Moore and Greitzer [16], discussed in more detail in Chapter 3, and are a consequence of oscillations within the flow field.

In contrast, spike stall inception can be distinguished by their short wavelength and a different rotation speed. The spike is caused by a local, three-dimensional flow breakdown (described by Camp and Day as an "embryonic stall cell") and is not captured by the Moore and Greitzer model.

Camp and Day hypothesized that stall is initiated when the incidence on a blade

exceeds a critical value. This can occur due to circumferential variations introduced via modal waves at or near the peak of the total-to-static pressure rise characteristic. Alternatively, it can occur before the peak of the pressure rise characteristic is reached; in this case, it is suggested that stall inception will be via the "spike" phenomenon. However, the mechanism which initiates the spike is not clearly understood. A comprehensive review of spike stall inception is provided by Tan et al.[17], and further discussion is presented in the next Chapter. Briefly, however, Camp and Day have suggested tip-leakage effects play a role, and extensive research has been performed examining the tip region in axial compressors. However, Spakovszky and Roduner [7] showed spike stall inception can also occur in the shrouded diffuser of a centrifugal compressor. Given tip leakage effects cannot play a role in the stall inception in the shrouded diffuser, it is suggested that tip leakage flow may not be a necessary condition. This is a particular focus of this research.

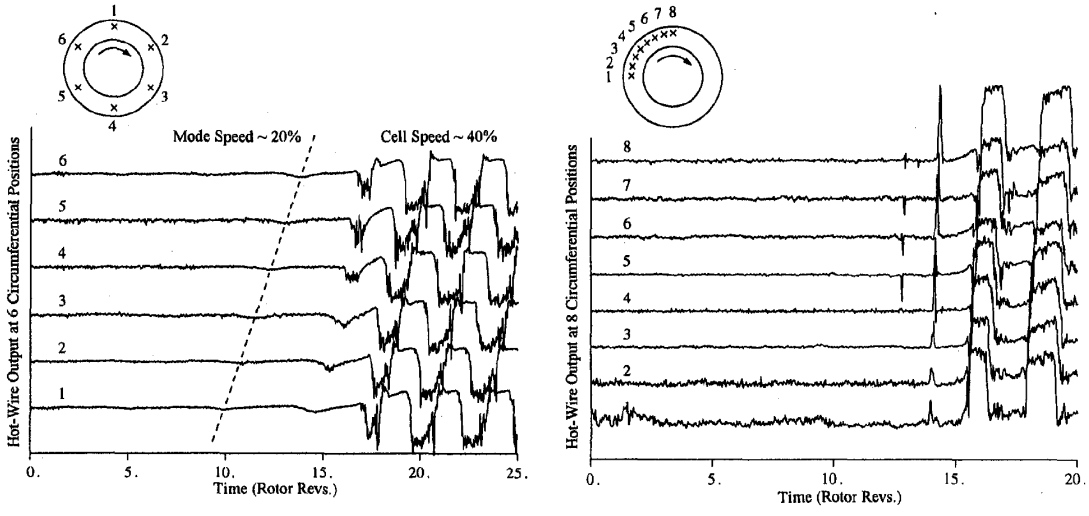

Figure 1-4: Pre-stall behavior: modal stall precursors (left) and spike stall precursors (right), from [4].

1.2 Research Objectives

The objectives of this research project are as follows:

- Develop a model using 3D RANS CFD software that allows capture of stall inception in vaned diffusers. It is suggested that an isolated diffuser model is sufficient for this purpose.
- Utilize the model developed to analyze the flow field to determine the mechanism for spike stall inception.
- Develop a criterion for spike stall inception.
- Parametrically change variables which are thought to affect stall inception to assist in the development of a criterion or to test its adequacy.

With these objectives in mind, Chapter 2 sets out the technical approach for the project, including a justification of the choice of an isolated diffuser model. Chapter 3 provides an overview of the current state-of-the-art in terms of stall inception in the vaned diffusers of centrifugal compressors, as well as a discussion of the efforts in numerical modeling of stall inception. Chapter 4 describes the numerical scheme and computational setup used in this project. Chapter 5 discusses the critical topic of diffuser matching as it relates to this project, and Chapter 6 discusses the results of the stability analysis performed using the model developed.

1.3 Thesis Contributions

The contributions of this research effort can be summarized as follows:

- The challenges of transonic flow, combined with strong pitchwise non-uniformities caused by the impeller jet-wake structure and the upstream influence of the diffuser, is shown to prevent the convergence of generic mixing planes used for the steady simulations of a highly loaded centrifugal compressor near to the surge line. Pitchwise non-uniformities on the diffuser side of the mixing plane result in inaccurate representation of the diffuser flow field.

- A methodology is developed for consistent pitchwise averaging of the impeller exit flow field and matching of an isolated diffuser simulation with an separate simulation of the impeller flow, enabling isolated diffuser simulations which agree well with experimental data and full wheel unsteady simulations.

- It is shown that the volute has a significant impact on the blade-to-blade flow non-uniformity in the diffuser. In addition, the effect of the volute on stability is discussed; although this discussion is introductory in nature, there is little such discussion elsewhere in published literature. It is suggested that the once-per-revolution non-uniformity caused by the upstream influence of the volute tongue may have a role in disrupting the development of stall precursors, particularly when the non-uniformity causes the development of a supersonic diffuser passage, as this prevents the upstream propagation of rotating pressure waves. Guidelines and recommendations for future research on the volute can be drawn from the simulations performed here; it seems likely that full compressor (impeller, diffuser and volute) simulations are necessary to fully capture the effects of the volute.

- An unstable stall precursor has been modeled in an unsteady simulation of the isolated diffuser, triggered by a forcing in total pressure small in temporal and spatial extent. The precursor has the form of a convecting perturbation in axial vorticity near to the shroud, which grows due to the shedding of vorticity from the separated flow near the shroud at the leading edge of the diffuser leading edge. The precursor rotates around the diffuser in the same direction as the rotor at a rate of 33% in the simulations, correlating well with experiments which indicated rotational rates of approximately 20%.

- Criteria for the development of a spike stall precursor in a centrifugal compressor with a shrouded vaned diffuser are developed for the first time. It is proposed that the spanwise flow non-uniformity at the diffuser inlet is responsible for high flow angles (in excess of 90° from radially outwards) at the shroud side at the diffuser vane leading edge, leading to (a) separation at the diffuser

vane leading edge, causing vorticity to be shed here as the disturbance passes which convects into the vaneless space between impeller and diffuser; and (b) recirculating flow which allows for vorticity perturbations to travel around the entire circumference and build over time. A link can be made with the criteria put forth for spike stall inception by Vo et al. [18], who determined that the tip clearance spillage flow convected parallel to the leading edge of the blade row in an axial compressor. In this case, the blade-to-blade convection is allowed via the spanwise non-uniformity and the highly swirling flow at diffuser inlet, as opposed to tip spillage in axial machines.

Chapter 2

Technical Approach

2.1 Project Hypotheses

Given the objectives of the research enumerated in the previous chapter, the research described in this thesis aims to test a number of hypotheses.

Hypothesis I: The first hypothesis is implicit in the approach: that an isolated diffuser model is capable of simulating stall inception. This requires that the flow features relevant to stall inception are carried into the model through the inlet boundary conditions, defined by the impeller exit flow profile, and that the model itself is capable of capturing the relevant mechanisms which govern the onset of instability.

Hypothesis II: Related to Hypothesis I, it is suggested that the unsteady blade-to-blade non-uniformities (the viscous blade wakes and the jet-wake structure caused by the Coriolis accelerations within the impeller passages) do not play a significant role in the stall inception process with spike stall precursors.

Hypothesis III: Spanwise flow non-uniformity at diffuser inlet plays an important role in the stall inception process.

Hypothesis IV: Lastly, it is hypothesized that the volute is not a necessary component within the simulation in order to capture the stall inception mechanism. The volute has the potential to effect the instability in many ways, for example determining whether the compressor surges or enters rotating stall, and introducing blade-to-blade variations in flow angle and mass flux within the diffuser due to its upstream influ-

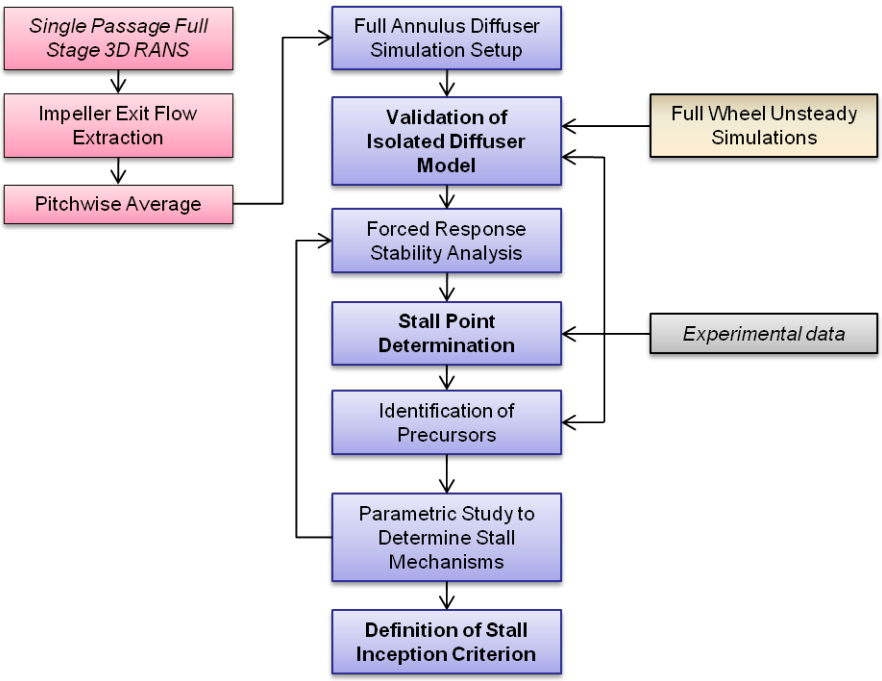

Figure 2-1: Project roadmap. Critical junctures are in highlighted in bold, and the results of previous research efforts are italicized. Compressor models are color coded, with the isolated diffuser shown in blue.

ence. It is recognized that these effects may alter the fully developed stall behavior and the corrected flow rate at which the diffuser flow enters an unstable regime, but it is hypothesized that the stall mechanism itself can be captured without the additional complexity introduced by the volute.

The technical approach used to test these hypotheses is set out in the next section. The hypotheses are based on previous research, which is described in more detail below and in Chapter 3.

2.2 Project Roadmap

The project roadmap is illustrated in the flow chart in Figure 2-1. Key to the successful implementation of the isolated diffuser model is the definition of the inlet conditions from the impeller. The project leverages off single passage, steady, mixing plane simulations previously run in the GTL (and described by Hill [5] and Benneke [19]) to define the conditions at impeller exit. The flow field at this location

is appropriately averaged to define a pitchwise uniform flow field which retains the hub-to-shroud non-uniformity.

Once the inlet conditions to the isolated diffuser model are defined, steady simulations are performed to test whether the isolated diffuser adequately captures the diffuser flow field. To determine the adequacy, the simulations are compared with experimental data from the experiments of Spakovszky and Roduner [7]. Additionally, unsteady simulations are performed with the full wheel (impeller and diffuser) for the purposes of validating the isolated diffuser model.

To investigate stability, a numerical "forced response" experiment is performed on the isolated diffuser model. The flow field is perturbed with a total pressure forcing and the resulting response is analyzed. Should the perturbation grow over time, the operating point is deemed unstable. Through testing a number of different operating points, the limit of stable operation is established. The unstable operating points allow analysis of stall precursors.

In addition to the simulations of the isolated diffuser, both steady and "forced response" simulations are also performed with the diffuser and the downstream volute. These are compared with the isolated diffuser simulations to determine the effect of the volute on the stability.

To elucidate the criteria for spike stall inception, the final step of the approach is a parametric study to vary the diffuser inlet flow. For example, simulation of an equivalent diffuser flow but with spanwise uniform flow at inlet allows one to test the hypothesis that spanwise flow non-uniformity plays an important role in stall inception. In addition, the sensitivity of the model can be tested - for example the form of perturbation used in the forced response analysis.

Apart from preliminary work performed by Hill [5], the approach for testing stability through the use of numerical forced response experiments on isolated diffusers is unique. The work here expands significantly on Hill's research, resolving implementation issues as well as considerably improving the fidelity of the modeling. The inclusion of the volute in modeling the onset of instability in centrifugal compressors is also unique. The challenges of this approach are discussed following a review of the

published literature.

2.3 Justification for an Isolated Diffuser Model

An isolated diffuser model, using a pitchwise averaged but spanwise non-uniform inlet flow, is desirable not least because it simplifies the problem of modeling and identifying stall inception in vaned diffusers. The flow is physically isolated from the impeller flow, such that the complex and unsteady impeller-diffuser interaction is removed. Whether this is sufficient to capture stall inception is topic of much of the discussion below. However, before addressing this issue, there are two other advantages in using an isolated diffuser model: it reduces the computational complexity through reduction of the computational domain, and it allows careful control of the diffuser inlet flow. With reference to the project roadmap, it would not be straightforward to perturb the diffuser inlet flow in a stage simulation (without altering the CFD code and possibly deliberately contravening the conservation of mass, momentum and energy), nor would it be possible to perform a parametric study varying diffuser inlet conditions. As this is a principal objective of this research, an isolated diffuser model is necessary.

Much discussion exists on whether the unsteady blade-to-blade non-uniformities have a significant effect on the diffuser performance, and there exists conflicting data within the literature. The flow at the impeller exit has a distinctive jet-wake structure, caused by a combination of inviscid effects due to the Coriolis accelerations in the impeller (described for example by Greitzer et al. [13]) and viscous boundary layer effects. Dawes [20] performed an isolated diffuser simulation using pitchwise averaged but spanwise non-uniform inlet conditions and compared it to the unsteady simulation run with impeller and diffuser (from which he had derived the inlet conditions). He determined that the performance of the diffuser was similar - notably the mass flow was the same as in the unsteady simulation for the same diffuser pressure ratio - although the unsteady flow from the impeller tended to increase blockage. Peeters and Sleiman [21] performed a comparison of steady, mixing plane, single pas-

sage simulations and unsteady, full wheel simulations. In the latter, after time and pitchwise averaging, they observed a uniform impeller exit pressure. This lead them to conjecture that there was no good reason for a coupled calculation (i.e. the mixing plane was redundant), since an isolated impeller simulation could be run which could then be used to provide inlet conditions for an isolated diffuser simulation. However, these simulations were not performed or compared with the unsteady case.

Shum et al. [22] performed a series of 3D RANS CFD simulations of the full wheel, isolated diffuser and isolated impeller, with the objective of determining the effect of unsteadiness on both the diffuser and impeller flows (the impeller encountering unsteadiness from the time-varying pressure field from the downstream diffuser). They concluded that the unsteadiness had more effect on the impeller flow, where it caused losses due to increased impeller tip leakage flows, than it did on the diffuser, by a factor of seven.

There has been equal discussion on experimental observations, with emphasis on whether wakes mix out quickly. Cumpsty [23] reviews the work of several authors and concludes that wakes mix out "quite rapidly" but that there is likely to be strong unsteadiness at inlet to the diffuser when the vane leading edge occurs at a radius ratios less than 1.2. The conclusion that the jet-wake structure is present at the diffuser leading edge is borne out by many later studies of impeller-diffuser interaction (e.g. Roduner et al. [24], Ziegler et al. [25], Cukurel et al. [26]), which also note that unsteadiness persists through the diffuser.

However, an analysis of experiments using a stationary swirl-generating rig with no vanes (Baghdadi [27]) indicates that the unsteadiness of the diffuser inlet flow does not have a significant effect on the diffuser aerodynamics, which Baghdadi suggested was due to the combination of rapid mixing and the high frequency of the unsteadiness. Cumpsty's suggestion was that "the unsteadiness of the flow seen by the diffuser as a result of the circumferential non-uniform flow out of the impeller is of secondary importance" and "the diffuser can be studied (and probably modeled) whilst ignoring the blade-to-blade variations of the impeller." Taken with the work of Shum et al., this supports the isolated diffuser approach.

One precautionary note on this conclusion is that stability was not considered in much of the above cited work, with the focus being on the pressure rise achieved or on loss (or equivalently, efficiency). Shum et al. comment that the effect of unsteadiness on the diffuser near stall may be larger than at the design point, which was where their simulations were performed. Also, Spakovszky [28] showed that vorticity waves shed from the impeller play an important role in modal stall inception. As a criterion for spike stall inception does not exist, it remains only a hypothesis that an isolated diffuser simulation can capture this phenomenon without the unsteady effects of impeller blade passing.

Chapter 3

Stall Inception in Vaned Diffusers

3.1 Modal Stall Pre-Cursors

The theoretical model of Moore and Greitzer [16] predicts the occurrence of modal stall precursors in a compression system. The time-evolution of modal oscillations is linked to the time-mean background flow field, which governs the damping of the oscillations. Under certain conditions, the damping can become negative such that energy input into the oscillations from the rotor exceeds the energy dissipated. This will lead to the growth of modal oscillations and the instability of the compression system. Longley discussed the Moore and Greitzer model and further developments in a review paper [29].

Spakovszky [28, 30] removed some of the shortcomings of the Moore and Greitzer model highlighted by Longley by further breaking down the compression system to resolve the dynamics of the individual blade rows, interblade gaps and intermediate ducts. The Spakovszky model predicted the occurrence of backward traveling modal waves in a centrifugal compressor (i.e. waves which traveled in the opposite direction to that of the impeller rotation), which were then observed for the first time experimentally in experiments on a NASA high speed centrifugal compressor. Spakovszky showed these are caused by interaction of pressure waves and the unsteady vortex shedding of the impeller; the radial spacing between impeller and diffuser vanes was critical and defined whether the modal wave traveled forward or backward. An energy

analysis revealed the strongest activity was in the vaneless space.

Modal waves can occur across a range of frequencies, but are characterized by a wavelength which spans a number of blades. The growth of modal waves, governed by the damping of the compression system, can lead directly to the onset of instability through triggering rotating stall when the critical incidence of the downstream blade row is exceeded.

3.2 Spike Stall Inception

During spike stall inception a characteristic "spike" is seen in traces of static pressure or velocity (either an increase in pressure or a reduction in velocity) due to local stagnation of the flow. In axial compressors, which have seen the most attention on the subject of spike stall inception (see Tan et al. [17] for a review of current understanding), the wavelength is very short, typically affecting only one or two blades.

Camp and Day [4] observed the spike occurs at the tip of the axial compressor blade, and it has been hypothesized that the spike occurs due to the instability of the overtip leakage flows. Vo et al. [18] performed RANS CFD simulations using both single- and multiple-passage models, and determined two criteria for spike stall inception relating to the tip leakage flows:

1. The interface between tip clearance spillage flow and the oncoming flow becomes parallel to the blade leading edge plane; and

2. Backflow occurs within the tip leakage flows at the trailing edge plane, stemming from fluid in an adjacent passage.

Tan et al. reference a number of different simulations, including a body-force approach [31], which have served to show these features are common near stall in axial compressors exhibiting spike-type stall inception[1]. In response to the findings of Vo et al., Deppe et al. [32] have reported the same features present in experiments.

[1]Semi-actuator disk models used to capture modal pre-stall behavior, such at the Moore and Greitzer model, are not appropriate for the short wavelength and fully three-dimensional spikes.

However, very little is known regarding spike stall inception in centrifugal compressors with vaned diffusers. Spakovszky and Roduner [7] reported spike-type stall inception in centrifugal compressors for the first time, when performing experiments with an advanced, high speed centrifugal compressor (their experiments are further discussed in Section 3.3). They showed that the spike originated in the vaned diffuser, which was shrouded and thus has no tip leakage flows. This suggests either that a different mechanism is present in centrifugal compressors with vaned diffusers, or that the underlying physics may be more complex than that put forth by Vo et al.

Benneke [19] used a body-force approach to model the same compressor, and found that both modal and spike-type stall could be modeled; however, spike was only shown to occur with a mismatched impeller and diffuser. To the author's knowledge, there exists no other published references on spike stall inception in centrifugal compressors with vaned diffusers.

3.3 Spanwise Flow Non-Uniformity at Diffuser Inlet

In the experimental work by Spakovszky and Roduner [7], both modal and spike pre-stall behaviors were detected in a highly loaded centrifugal compressor with a vaned diffuser. Different behavior was detected depending on whether leakage flows were present between the impeller and diffuser. As discussed in their paper, leakage flows are present in turbochargers for secondary air systems, for example to provide sealing air for the bearing compartments. The mass flow rate of the leakage flow can be very small - in their experiments it was 0.5% of the throughflow - and yet it had a significant effect on the pre-stall behavior and compressor operating range, with 50% reduction in stable operating range when leakage flow is present.

It was conjectured that the extraction of fluid from the hub boundary layer alters the spanwise flow profile at impeller exit and destabilizes the highly loaded diffuser. With bleed flow, blockage is removed at the diffuser throat, increasing the loading in the vaneless space and reducing the loading in the semi-vaneless space. The gradient of the pressure rise characteristic in the semi-vaneless space is reduced, such that

the slope flattens out at higher flows. In turn, this reduces the compression system damping and leads to the onset of modal waves, which grow in amplitude as the flow rate is further reduced before triggering stall.

Without bleed flow the additional blockage serves to increase the loading on the semi-vaneless space which increases the compression system damping. This increases the stable operating range by approximately 50%, and changes the pre-stall behavior such that, instead of modal waves, stall is initiated by a spike in the vaneless space.

This observation led Spakovszky and Roduner to put forth an alternative criterion for spike stall inception: that spikes would occur in centrifugal compressors with vaned diffusers when the gradient of the static pressure rise coefficient characteristic for the semi-vaneless space becomes zero before that of the overall diffuser. It also leads to the third hypothesis tested in this project: that spanwise flow non-uniformity at diffuser inlet plays an important role in the stall inception process.

That spanwise flow non-uniformity is important to the performance on the diffuser is another subject which has received considerable attention within the literature. Several authors (e.g. Cumpsty [23] and Dawes [20]) suggested spanwise flow non-uniformity influences the performance of the diffuser, while Dawes and Peeters and Sleimen [21] note this non-uniformity should be retained in performing isolated diffuser simulations (also see Section 3.5 below). However, Filipenco et al. [6] and Deniz et al. [33] performed experiments with a swirl generator which was capable of producing a variety of spanwise profiles, and determined that it had little effect on the stall point of the vaned diffuser (the same conclusion was reached regarding diffuser inlet Mach number). They identified that the momentum averaged flow angle was the critical parameter in determining the performance and stall point. Phillips [34] performed isolated diffuser simulations to verify these results. However, at the point when this research was being performed, spike stall inception had not been identified in centrifugal compressors and no unsteady data was recorded. It is possible that that the compressor tested underwent modal stall inception, in which case the spanwise flow non-uniformity would have less importance. The evidence of Spakovszky and Roduner [7] is compelling in the suggestion that spanwise flow non-uniformity has

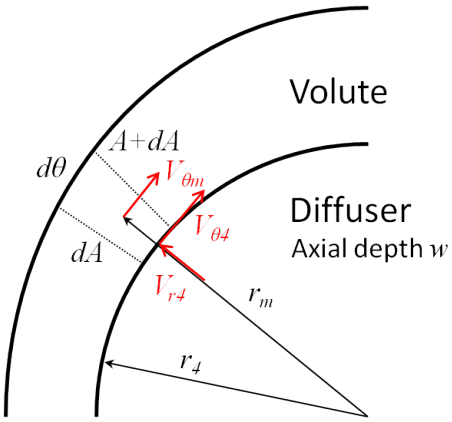

Figure 3-1: Sketch indicating important parameters for the flow from diffuser to volute.

some role in the distinction between spike and modal stall inception.

3.4 Effect of the Volute

The volute, an integral part of the centrifugal compressor, is often not included in modeling of centrifugal compressors. More generally, the volute receives significantly less attention in published literature than impeller and diffuser flows, and there remains further understanding to be gained about how it influences the centrifugal compressor system, particularly in terms of stability.

A simplified analysis is presented here to provide insight into the volute flow. Firstly, it is assumed the flow in the volute is incompressible such that density is constant. This is justified because the Mach number in the volute is low ($M^2 \ll 1$). The following analysis follows the notation in Figure 3-1.

Angular momentum for the flow from the diffuser into the volute, assuming a frictionless volute, requires the product rV_θ to be constant:

$$r_4 V_{\theta 4} = r_m V_{\theta m} \tag{3.1}$$

The one-dimensional momentum equation can be written in its general form as:

$$dp/\rho V^2 = dV/V \tag{3.2}$$

If we consider the volute simply as an unwrapped, quasi-1D duct[2], and further require the pressure to be circumferentially uniform, Equation 3.2 can be used to show:

$$V_{\theta m} = constant \tag{3.3}$$

Now, considering conservation of mass in the volute, it is possible to write:

$$\rho V_{\theta m} A + d\dot{m} = \rho(V_{\theta m} + dV_{\theta m})(A + dA) \tag{3.4}$$

$d\dot{m}$ is the incremental additional mass flow from the diffuser; this is defined by $d\dot{m} = \rho V_{r4} w\, r_4 d\theta$. It has already been shown that, for uniform pressure, $dV_{\theta m} = 0$.

Combining Equations 3.4 and 3.1 and rearranging, it is possible to relate the volute cross sectional area distribution directly to the diffuser exit flow angle:

$$\frac{1}{w r_4}\frac{dA}{d\theta} = \frac{r_m}{r_4}\cot\alpha_4 \tag{3.5}$$

In a vaned diffuser, where the flow angle is defined by the diffuser vane trailing edge metal angle via the Kutta condition, this equation sets the area distribution around the circumference. This is determined only for a singular value of compressor mass flow, and illustrates the important matching criteria which relates the diffuser exit flow angle to the volute geometry. Off design, the static pressure at inlet to the volute will no longer be uniform, and Equation 3.4 shows that this requires a circumferential variation in mass flow through the diffuser. This couples the flow through the impeller to the volute geometry.

Another cause of pressure non-uniformity is the tongue. At the design point, the local pressure rise at the tongue region, where there must exist a stagnation point, is small since the flow path is designed to be smooth into the volute pipe. However, off design, the flow past the tongue can involve significant streamline curvature and the development of a high and/or low pressure area, as flow is diverted into the exit

[2]This assumption is strictly only valid if the radial dimension of the volute cross-sectional area is small compared to the mean radius, or $\frac{(r_m - r_4)}{r_m} \ll 1$

diffuser.

An alternative way of viewing the volute is as an additional blade row comprising a single vane, wrapped around the circumference. Viewed in this manner, it is clear that the upstream influence on pressure will be of the length scale of the circumference. In fact, the upstream influence of the volute extends through the entire machine - the presence of the volute can be detected even upstream of the impeller [23]. An important consequence is that the flow angles at the diffuser leading edge can be affected by the upstream influence of the volute; this potentially affects the stability of the compressor, given Camp and Day's criteria for stall inception (exceeding a critical leading edge incidence).

Recently, it has been suggested that the volute has a further role in the onset of instability. Guo et al. [35] perform a system analysis using 3D RANS software with centrifugal compressor with a vaneless diffuser, volute and plenum, and suggested standing waves are set up in the volute which eventually trigger instability. The standing waves were suggested to be triggered by periodic instabilities within the vaneless diffuser, so whether this has an effect in a compressor with vaned diffusers is questionable.

Another impact of the volute concerns wave reflections. The impeller sheds vorticity and entropy waves as an effect of the blade boundary layers, which convect with the flow through the diffuser. The impeller also causes periodic pressure waves at impeller blade passing frequency. The reflection of pressure waves from the downstream blade row interacting with the convecting vorticity waves is the mechanism suggested by Spakovszky [30] to create backward traveling modal stall precursors in centrifugal compressors with vaned diffusers. Pressure waves can also be reflected from the change in impedance encountered as the flow enters the volute. This also has the potential to affect stability but does not appear to have been investigated in the literature to date.

The numerical aspects of wave reflections are discussed in Chapter 4. It was found reflections from the diffuser exit strongly affected the stability predicted by the simulations, and this is further discussed in Chapter 6.

3.5 Computational Fluid Dynamics Modeling

The computational study of compressors can be broadly separated into two different types: reduced order, system modeling (e.g. the semi-actuator disk models of Moore and Greitzer or Spakovszky discussed above), and higher fidelity, discretized flow field simulations (such as Reynolds-averaged Navier Stokes computational fluid dynamics (RANS CFD)). Here we consider the development of models for centrifugal compressors in the latter field, which will from hereon be simply referred to as "CFD".

Modeling centrifugal compressors using CFD is challenging due to the complex nature of the flow. A high pressure ratio, single stage centrifugal compressor has a fully three-dimensional, unsteady, highly swirling flow with supersonic flow likely either in the inducer (relative to the blades) or the diffuser inlet or both, as well as significant changes in density. This has meant centrifugal compressors have not seen the same attention as axial machines. However, as CFD capability and computing power has improved and with demand for higher performance centrifugal compressors, more work is being directed to this area. The validation work performed by the authors below indicate that CFD is reaching the capability where it is able to provide useful insights in the field of centrifugal compressors.

Published research on the use of CFD to analyze the stability of centrifugal compressors is limited. One potential reason for this is that off-design behavior is particularly challenging to model given the inherent limitations of CFD. Denton [36] observes that accurately capturing the point of stall is almost invariably beyond that capacity of CFD, partly due to modeling limitations (for example, being unable to model blade untwist and erosion or upstream and downstream components) but also because the occurrence of stall relates to the onset of large scale separation and therefore is limited by turbulence modeling. Dickmann et al. [37] also observe that solutions often cannot be obtained near stall when using a simplified compressor model (e.g. single passage steady simulations with a mixing plane or a frozen rotor), whereas experimental results or full annulus, unsteady CFD simulations reveal operation is possible at significantly lower mass flows.

The discussion below summarizes potential models for the centrifugal compressor, their advantages and limitations, as well as briefly exploring published literature using these models.

3.5.1 Single Passage Models with Mixing Planes

Single passage models with mixing planes are a popular method for analyzing centrifugal compressors due to the ability to capture the flow at a reasonable level of accuracy for a reasonable computational cost. The simulations can be performed in a steady framework, with flow in the impeller and diffuser being solved in the relative and absolute frame respectively. The two components exchange boundary conditions across the mixing plane interface. The downstream side is treated as an inlet face with the boundary conditions defined by averaged flow properties at the impeller exit. The upstream impeller side can be seen as an outlet face with the exit flow condition being provided by the diffuser inlet flow.

The mixing plane interface implemented in the commercial RANS CFD code Numeca FINE/Turbo is typical and is described in detail in the user manual [38]. The objective is to ensure mass, momentum (in axial, tangential and radial directions) and energy fluxes are conserved across the interface, at each spanwise location. For each flux and at each spanwise location, the time-marching method aims to match the flux on the downstream surface of the interface with the pitchwise averaged flux on the upstream surface. The exception to this rule is the meridional momentum flux which has to take into consideration the upstream influence of the downstream blade row. Thus the upstream surface applies the pitchwise averaged pressure field from the downstream surface. For situations with flow reversal at some spanwise location, the solver determines the sense of flow direction from the mass flux.

This methodology ensures flux conservation, which is especially important in multistage simulations. However, unsteady effects are obviously not captured, and interpolation errors are introduced in calculating the base variables from the transferred fluxes.

Steady, single passage simulations with a mixing plane suffer two particular limi-

tations: by definition they cannot capture the unsteady flow encountered in stall and surge; and it is impossible to capture the circumferentially non-uniform exit pressure imposed by the volute. In addition, work carried out here has highlighted limitations associated with the mixing plane which shall be discussed in depth in Section 5.3. These relate specifically to challenges which exist uniquely in centrifugal compressors, namely the strong circumferential non-uniformities associated with the jet-wake structure from the impeller blades and the strong upstream influence from the diffuser vanes.

The mixing plane (albeit implemented in a different code) was also suggested to be an unreliable tool in work by Peeters and Sleiman [21], who compared experimental data to both full wheel unsteady simulations and single passage mixing plane simulations. Peeters and Sleiman analyzed the steady state performance of the compressor and noted the pressure rise through the diffuser was as much as 20% lower in the steady mixing plane solution than in the experimental results and unsteady simulation, due to increased blockage. They did not explicitly consider the stability of the compressor.

3.5.2 Full Annulus Unsteady Models

An alternative to performing single passage, mixing plane models is to use a sliding mesh, full wheel unsteady simulation. This removes many of the shortcomings of the mixing plane model: the impeller-diffuser interface is treated as a continuous flow path (although depending on the type and quality of the mesh, small numerical errors can be introduced in the interpolation of data across the two grids) and modeling the full wheel allows circumferentially non-uniform effects such at the volute to be included. However, the main problem is the computational requirements for these types of simulations, and for this reason it is only recently that such models have become feasible. Each timestep must be solved through iteration, with the additional unsteady terms of the equations of motions, and it may take many timesteps before a steady state solution is reached. If the full wheel is modeled the mesh size and hence the computational load can increase by an order of magnitude or more. Some authors

have used reduced blade count when the number of diffuser blades is equal to, or an integer multiple of, the number of impeller blades, or have even approximated the number of blades if they are close to a common multiple (e.g. Dawes [20]).

Varying levels of fidelity are available: these range from simulations extending from the upstream pipe and inlet bend to the volute (Dickmann et al. [37]) to simplified models of just impeller and diffuser, where the blade count is reduced as described above. An interesting alternative is the body force approach, as described by Gong [31] and Benneke [19], whereby the physical blades are replaced by a description of the pressure and viscous forces which would produce the equivalent accelerations. In this manner, it is possible to utilize an Euler model and to reduce mesh sizes through not requiring resolution of blade boundary layers.

One of the first published studies of an unsteady model was that of Dawes [20], who showed the method was capable of providing insight to the impeller-diffuser interaction. Peeters and Sleiman [21] determined that the steady simulation of impeller and diffuser was inadequate. Dickmann et al. modeled operating points close to stall and close to choke, coupling the CFD with finite element codes to analyze the unsteady stresses on the impeller blade. Cui [39] compared vaneless and vaned diffusers in unsteady simulations which included the volute geometry. None of these authors considered stall, although Dickmann et al. determined that steady simulations could not be obtained near stall whereas unsteady solutions could. Guo et al. [35] modeled stall, but considered a vaneless diffuser. Their work is discussed in Section 3.4.

The work of Benneke [19] expressly considered the onset of instability. Benneke showed that both modal and spike-type stall precursors in a centrifugal compressor could be captured in a body force model (the capability of a body force model for capturing stall inception in axial machines having previously been established by Gong [31]). However, the work was limited to low speed cases, and spike-type stall inception was only demonstrated with a mismatched impeller and diffuser which was not representative of a real compressor. The work described in this thesis complements Benneke's work by allowing a detailed examination of the diffuser flow to define the mechanisms which cause stall inception.

3.5.3 Isolated Diffuser Models

Isolated diffuser simulations have been attempted by a number of researchers. The work of Dawes [20], Phillips [34] and Shum [22] has already been discussed. In addition, Casartelli et al. [40] perform isolated diffuser simulations with the aim of improving the diffuser vane leading edge design. None of these authors expressly consider stability.

Hill [5] performed isolated diffuser simulations addressing the stability of the diffuser flow, and this project is a development of his work. Hill's work was limited in terms of grid resolution, size of domain (four passages only were modeled) and the definition of the boundary conditions but, importantly, he suggested that isolated diffuser models have the potential to model stall precursors.

3.6 Specific Challenges to Simulation of Stall Inception in an Isolated Diffuser Model

The analysis of previous work on stall inception in vaned diffusers raises a number of challenges for the modeling of stall inception using an isolated diffuser model:

1. Matching the diffuser inlet flow to the impeller exit flow is of critical importance and this is addressed in Chapter 5.

2. To model modal stall precursors, past research indicates the necessity of modeling the unsteady effects of the upstream impeller passing the diffuser vanes; by excluding these it is unlikely to capture modal stall precursors.

3. The cause of spike stall precursors within centrifugal compressors is not known, therefore the precise modeling requirements cannot be known a-prioiri. It is known that the spike originates within the vaneless space between impeller and diffuser so the full extent of this should be included within the model. This however requires the mixing that occurs downstream of the impeller to be modeled in an artificial manner to derive steady inlet conditions.

4. The effect of the downstream volute may impact stability and this is addressed in Chapter 5. The inclusion of the volute within the model necessitates a full annulus simulation, with the associated increase in computational demand that this entails. Regardless of this, a full annulus simulation is desirable to properly capture the number and rotation rate of the stall precursors.

5. It is often not possible to model centrifugal compressors near to the stall point in steady simulations, so it is challenging to use simple steady simulations as a starting point for the analysis.

6. Reflections, both physical and numeric in origin, must be dealt with appropriately. This is addressed in Chapter 6.

Chapter 4

Computational Setup

The research performed for this thesis uses a numerical tool to gain physical insight into the diffuser flow, and this chapter briefly describes that tool. The chapter is organized in the following manner: first, the test compressor and the CFD software are introduced. Although the focus is on isolated diffuser models, several other models were used in the course of the research and are discussed in this thesis: single passage, full stage steady simulations with a mixing plane; full stage, full annulus, unsteady simulations; and diffuser and volute simulations. Information common to all the simulations is described first, including an overview of the subject of boundary conditions. Finally, elements unique to each simulation are set out. Further information on the compressor modeled and the CFD software can be found in references [7] and [38, 41] respectively.

4.1 Test Compressor

The compressor geometry chosen for this project is the same as that used in the experiments of Spakovszky and Roduner [7] and in the modeling of Hill [5] and Benneke [19]. The compressor is an advanced design, pre-production turbocharger compressor with a design pressure ratio of 5. The compressor comprises an impeller with 9 main vanes and 9 splitter vanes, and has tip Mach number, $U_{tip}/\sqrt{\gamma RT_{t0}}$, greater than unity at design speed. The vaned diffuser has 16 airfoil vanes, with the leading edge

at 111.5% of the impeller tip diameter. The application for the turbocharger is large diesel engines used in heavy industrial equipment.

4.2 CFD Tool Description

The commercial Reynold's Averaged Navier-Stokes (RANS) CFD code Numeca FINE/Turbo was used for all the simulations described in this thesis. FINE/Turbo is an integrated CFD package tailored for turbomachinery applications. The package includes tools for grid generation, flow solving and post-processing.

FINE/Turbo utilizes a structured hexahedra grid for speed and accuracy. Multi-block grids for turbomachinery can be generated efficiently using the built-in meshing software "Autogrid," which incorporates both a wizard for fully automatic mesh generation of common turbomachinery geometries (e.g. axial compressor stage, centrifugal impeller, radial diffuser) as well as functionality to create meshes in a semi-automated fashion. The wizard is used in the project to create an optimized diffuser mesh for the diffuser and volute simulations, but the majority of simulations used the latter method.

All diffuser grids share same basic topology, utilizing the common O4H structure. The impeller is modeled in a similar manner, although presence of splitter vanes and the impeller tip gap requires more careful definition of the blocks. The volute grid structure is discussed in Section 4.4.3.

FINE (Flow INtegrated Environment) is the graphical user interface used to input parameters for the model, which is solved using the flow solver EURANUS. The solver is capable of using a "multigrid" technique. Starting with a coarse grid, an approximate solution is found before increasing the grid resolution by doubling the number of nodes in each dimension. Evidently, this must be preceded by creating a grid in Autogrid with the number of nodes in each dimension defined by:

$$X_i = a(2^{m-1}) + 1 \tag{4.1}$$

where X_i is the number of nodes in a given dimension i, and a can be freely chosen

to provide the grid density required and m is the number of multigrid levels desired.

4.3 Common Input Parameters

Despite the different models used in the project for describing the compressor, many of the parameters used in the computational setup were kept constant. Apart from ensuring the same operating point is modeled, this allows consistent comparison between the models. The following parameters, controlled in FINE, are maintained throughout all the different models:

Rotational speed. Only the 100% corrected speedline was considered for this work. Different operating points were defined by varying the back pressure or mass flow.

Spatial resolution. The size of the numerical meshes used for this project ranged from 1.2 million mesh nodes in the single passage full stage simulations, to 13 million mesh nodes used in the full stage unsteady simulations. Table 4.1 provides an overview of the number of grid nodes used in the individual meshes.

Mesh	Nodes
Single Passage, Impeller and Diffuser (Stage)	1,250,000
Full Wheel, Impeller and Diffuser (Stage)	13,000,000
Isolated Diffuser (without buffer zone)	3,520,000
Isolated Diffuser (with buffer zone)	3,850,000
Diffuser and Volute	3,620,000

Table 4.1: Mesh nodes for compressor models

The diffuser mesh generated for this project was a development of that used by Hill [5], which was created following industry guidelines. The developments comprised work to reduce cell skew and improve resolution of the diffuser vane boundary layer, and resulted in a small increase in the number of grid nodes. In his work, Hill noted no appreciable difference in stage performance through increasing or decreasing the multigrid level by one (i.e. increasing or decreasing the number of grid points by a factor of eight), and the mesh improvements made for this project also made no appreciable difference in the solution. It is concluded that the grid resolution is sufficient. Hill reduced the resolution when using an isolated diffuser model for stability

assessment by decreasing the multigrid level. This work removes that limitation.

Temporal resolution. For unsteady simulations, the timestep was defined as 1/144th of a rotor revolution - i.e. 16 timesteps per main rotor blade passing. To determine whether this was sufficient, and no clocking effects were present given the even factor between timesteps and blade count, a simulation run for stability assessment (Chapter 6) was rerun with 211 timesteps per revolution - i.e an increase of approximately 50%. The results obtained with the smaller timestep were found to be identical, indicating the timestep was sufficiently fine to capture the relevant features. It could be possible to further optimize the timestep to minimize computational demand but due to time constraints this was not performed as part of the project. In the future, a study to determine the minimum requirement for temporal resolution would be beneficial.

Turbulence modeling. The Spalert-Allmaras turbulence model was used for each simulation, following industry practice. The Spalart-Allmaras model is described as a "single-equation" turbulence model, using an eddy-viscosity transport equation to determine the Reynolds stresses. These are lumped with the fluid viscosity to form the "turbulence viscosity". Further details can be found in references [41] and [42]. Significant effort was devoted to the validation of the diffuser model (as discussed in Section 5.2) which indicates the performance trends of the diffuser were well captured, but a study to determine the effect of the turbulence model chosen is suggested as future work. It was noted by Denton [36] that the onset of stall is often associated with separation, which is an effect often not well captured by turbulence modeling.

Solution initialization. The first simulation was initialized using constant velocities and pressures throughout the domain. Following this, it was possible to initialize each successive simulation from the results of the previous one.

4.3.1 Inlet Boundary Conditions

The inlet conditions were defined in all cases by total pressure, total temperature and normalized velocity vectors. For full stage simulations, a singular value for each parameter was adequate to set the inlet conditions. However for simulations where the inlet was defined at the impeller exit, a spanwise profile was defined while the pitchwise

direction was uniform. The derivation of these inlet conditions is of critical importance as careful matching is required with the impeller exit flow. The methodology and results are discussed in detail in Chapter 5.

4.3.2 Outlet Boundary Conditions

In experiments the flow through is controlled by a throttle valve at the exit of the compressor as illustrated in the sketch in Figure 4-1. The intersection of the throttle characteristic line and the compressor operating line marks the operating point of the compressor. In the numerical simulations, the user must make a choice whether to set the operating point via a pressure or mass flow boundary condition. The choice of which to use is dependent on the operating point. Close to surge, a small change in pressure ratio (defined here by the back pressure, as inlet conditions are constrained) can result in a large variation of mass flow. In fact, where the pressure rise characteristic has zero slope or reverses from a negative to a positive slope, multiple solutions exist for a single pressure ratio, and the numerical scheme is either unstable or tends towards one possible solution with no control from the user. Whereas the throttle characteristic allows testing across the entire range, the implementation within the numerical simulations require a change between the pressure exit boundary condition (near choke) to a mass flow boundary condition (near surge). Benneke [19] showed the two options yielded very similar results at the "elbow" of the operating line (i.e. midway between choke and the surge line, where the gradient of the characteristic curve changes rapidly), as implemented in FINE/Turbo. At 125% and 135% impeller tip radius, the maximum difference in radial Mach number and total pressure between the two options was less than 1% of their respective mean vaneless space value.

There are further sub-options within each main type of boundary condition, relating to the implementation within the numerical scheme. First considering the pressure boundary condition, the user can select to apply either a uniform pressure, an averaged pressure, or a user-defined pressure distribution, and each is appropriate in different cases. Where a flow exits subsonically into a large body of fluid (or to atmosphere), the exit pressure is defined by the pressure in the body. In this case, uni-

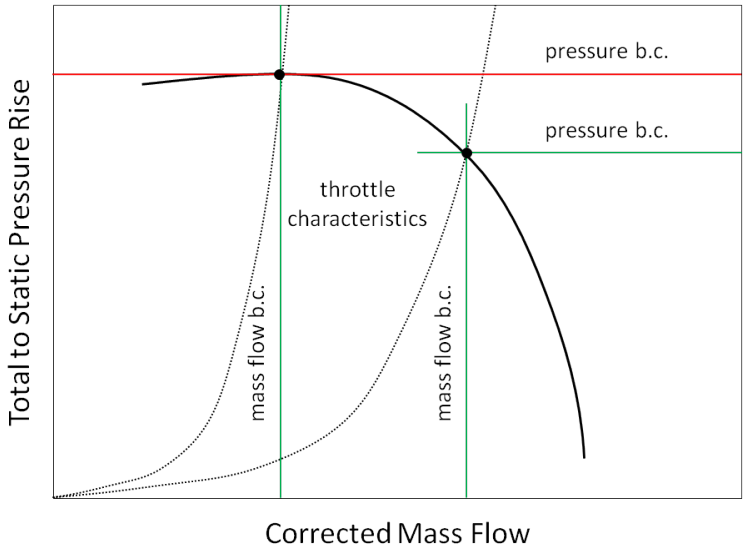

Figure 4-1: Sketch of compressor and throttle characteristics, illustrating pressure and mass flow exit boundary conditions, adapted from [5]. The throttle allows testing across the entire operating range, whereas using a pressure boundary condition can lead to numerical divergence near to stall (red), c.f. static instability.

form exit pressure is justified. For a boundary in the center of a device (e.g. between stages in a multi-stage axial turbomachine), the average pressure may be the most appropriate. When the exit pressure distribution can be defined (e.g. the pressure distribution around the volute inlet, when known from previous research), evidently it would be prudent to apply that boundary condition. However, for simulations with an exit boundary at diffuser exit where the volute pressure distribution is not known a-priori, it is not obvious which boundary condition should be used.

Simulations with diffuser and volute were used to elucidate the problem. The pressure distribution at diffuser exit shows a distinct variation around the circumference due to the upstream influence of the volute, as shown in Figure 5-16 and discussed in Chapter 3. The pressure variation is dependent on the operating point, but there is a clear pattern: there exists a region of influence near the volute tongue and a distribution of pressure around the circumference (as described in Section 3.4). From this we take the following: pressure variations that occur on the lengthscale of the volute (i.e. once-per-revolution) are much more significant than pressure variations on the length scale of the diffuser vane pitch, which are relatively small. For this

reason, a uniform exit pressure condition is chosen to be more representative of the fluid flow in the real device than the average pressure condition, where the effect of the volute is to be neglected.

FINE/Turbo provides two options for implementing a mass flow boundary condition. The first is through adaption of the pressure on the exit surface ("pressure adaptation"). At each iteration, the algorithm calculates the error between the specified mass flow and the actual mass flow. For the next iteration, the backpressure is adjusted by a factor of this error, thus theoretically driving the error to zero. The static pressure is uniform on the exit surface, and the user provides the initial estimate. The second option directly scales the velocity vectors on the exit boundary surface, again based on a factor of the mass flow error. There is no stipulation regarding uniformity at the exit, therefore the exit static pressure is non-uniform using this condition; this is the main difference between the two mass flow options when performing steady simulations.

The different options available have an impact upstream of the diffuser exit, as illustrated by Figure 4-2. It is for this reason it is especially important to select an option that is physically representative. The choice of a constant pressure exit condition is considered most representative of centrifugal compressor diffuser exit flow where there exists a downstream volute.

A further difference between the different exit boundary condition options is the treatment of oncoming pressure and vorticity waves. This was important for the stability assessment and is fully addressed in Section 4.5.

4.4 Numerical Models for the Vaned Diffuser

4.4.1 Single Passage Full Stage with a Mixing Plane

The single passage computational domain comprises one main impeller blade, one splitter blade, and one diffuser vane, with periodic boundaries where the grid face aligns with an adjacent passage, as shown in Figure 4-3. A mixing plane is used

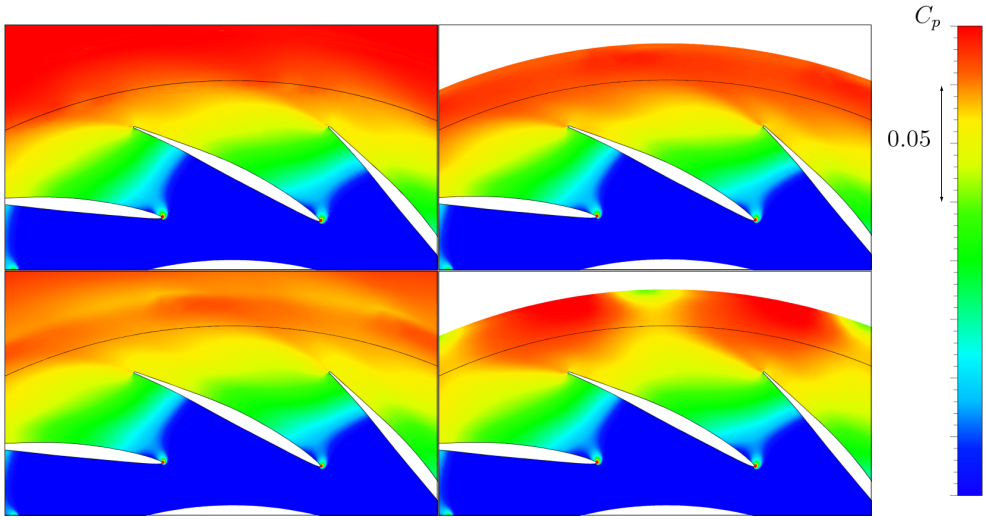

Figure 4-2: Static pressure contours at mid-span for four different diffuser exit boundary conditions: modeling the volute (top left, showing passage opposite to tongue); constant pressure (top right); buffer zone with constant pressure (bottom left); and mass flow with velocity scaling (bottom right). Specifying an average pressure yields similar result to velocity scaling. Volute inlet diameter indicated by solid black line.

(described in the previous chapter), located between impeller and diffuser at 106.7% impeller tip radius. Further information can be found in Hill [5] and [38, 41].

4.4.2 Isolated Diffuser

The isolated diffuser is meshed from immediately downstream of impeller (101.1% impeller tip radius) in order to capture the majority of the vaneless space. The mesh extended well beyond the diffuser exit, such that a buffer zone could be utilized to help prevent reflecting waves affecting the stability prediction simulations (as discussed in Section 4.5). The buffer zone had no significant impact on the diffuser performance with the steady-state pressure rise through the diffuser subcomponents being equal with or without the buffer zone. The full annulus of the diffuser was modeled to allow any stall precursors to develop in a natural manner i.e. without the use of periodic boundary conditions. This allows the number of stall precursors and their rotation and growth rate to be accurately determined.

The mesh is illustrated in Figure 4-4.

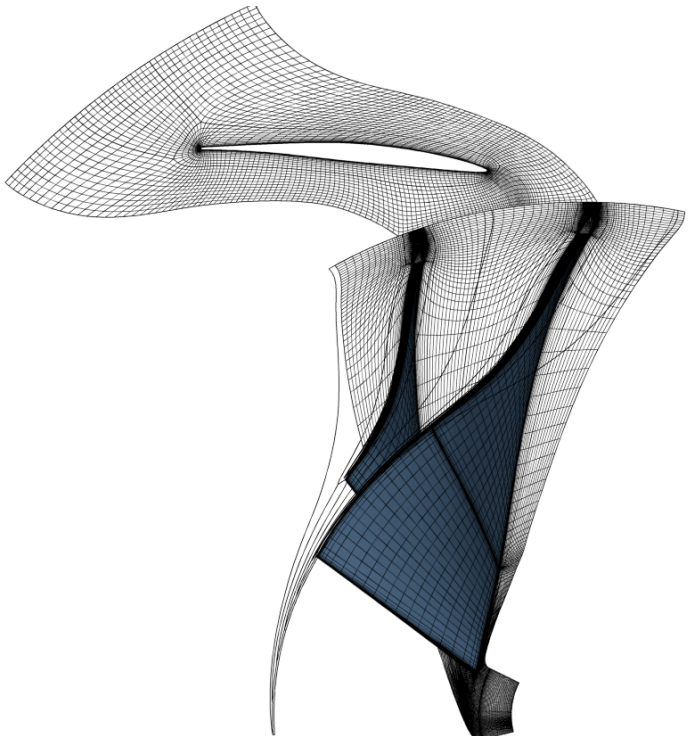

Figure 4-3: Single passage stage mesh.

4.4.3 Diffuser and Volute

The addition of the volute required modification of the diffuser mesh. The computational domain still begins at 101.1% of the impeller tip diameter, but the diffuser exit definition was changed in order to match with the volute mesh; the diffuser mesh now ends in the same location as the physical diffuser. An optimized mesh was created using the "wizard" feature of Autogrid, which comprised 2.6 million mesh nodes, with an additional block both upstream and downstream of the diffuser vanes compared to the original isolated diffuser mesh. The new mesh was checked for consistency with the original diffuser mesh, and little difference in subcomponent pressure rise were detected: less than 1% in the channel, less than 5% in the semi-vaneless space and less than 10% in the vaneless space, where the pressure rise is low. The difference in the vaneless space suggests that the reduction in grid density in this region may have a small effect on the solution.

Challenges exist in modeling the non-symmetric volute, in particular the tongue region, to ensure adequate grid density and consistency with the diffuser mesh. A

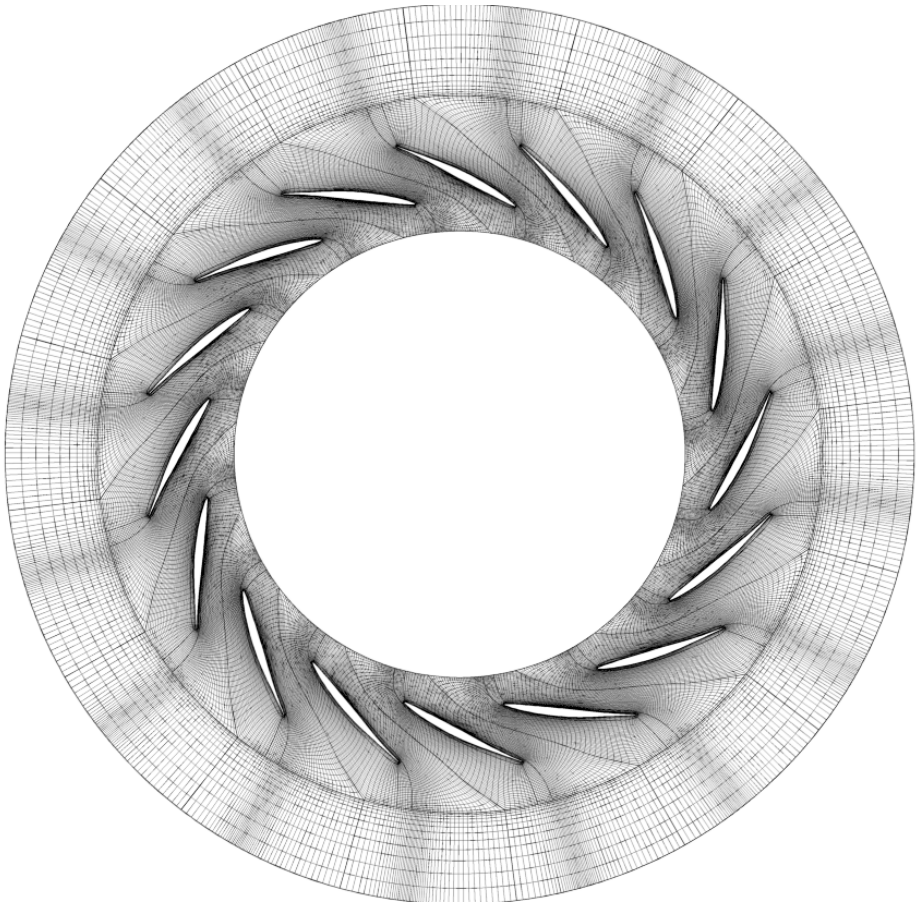

Figure 4-4: Isolated diffuser mesh with buffer zone.

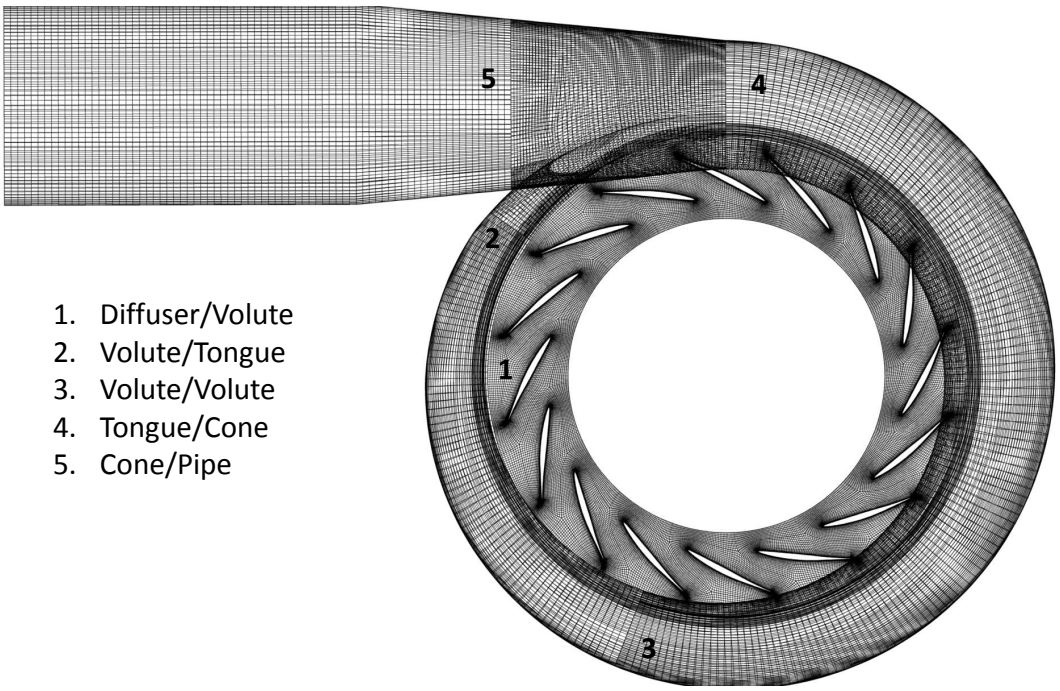

Figure 4-5: Diffuser and volute mesh showing non-matching grid interfaces.

high level of detail was not required for the volute flow; the main purpose of including the volute was to set the boundary condition for the diffuser, to allow the upstream influence to be captured. Some compromises were therefore accepted - a lower grid density, with fewer cells in the boundary layer, and five non-matching grid interfaces (between diffuser and volute and in various circumferential locations around volute, as illustrated in Figure 4-5). The blocks were set out to allow the increasing area of the volute to be meshed with reasonably uniform grid density, and the volute comprised approximately 1 million mesh nodes.

The flow in the volute and downstream pipe has much lower velocity than that in the diffuser, and the flow path is considerably increased in comparison to the isolated diffuser. The physical time required for a fluid particle to pass through flow domain (or unsteadiness to pass through flow domain) is thus significantly increased. In addition, steady simulations of the diffuser and volute showed numerical divergence, and only transient simulations could be used to reach a steady state. The unsteady simulations

thus required significant physical time to be modeled in order to reach a steady state solution. One strategy successfully implemented to reduce computational time was to increase the time step used for initialization calculations. Even so, simulations were computationally involved.

The diffuser was aligned within the volute consistently with the experiments ran by Spakovszky and Roduner [7], i.e. the angular position of the tongue relative to a diffuser vane leading edge was ensured consistent. It is noted that the effect of different alignment is not well known.

4.4.4 Full Wheel, Full Stage with Sliding Mesh

The full wheel unsteady simulations included the full annulus for the impeller wheel and the diffuser, but did not include the volute. The mesh was generated by repeating the single passage mesh for each blade passage, resulting in approximately 13 million mesh nodes.

The impeller mesh is rotated at the correct angular velocity, and the impeller mesh and the diffuser mesh slide at the interface location. Interpolation is used to pass information between the non-matching meshes at each timestep.

4.5 Numerical Strategy for Stability Assessment

The stability of the diffuser flow is tested through applying a perturbation to the diffuser flow and determining the response, in a "forced response" experiment. Should the disturbance die out and the flow return to the same steady-state condition as prior to the perturbation, the flow is deemed to be stable. The forcing is chosen to be in total pressure, as described in Chapter 6, and is applied through a temporary change to the inlet boundary conditions used for the isolated diffuser simulations. This is representative of a disturbance entering the diffuser from the impeller.

The application of the perturbation requires three different unsteady calculations to be run: firstly, an initialization calculation for the flow to reach steady state; secondly, a calculation with the definition of the boundary condition in total pressure

adjusted to include a perturbation; and finally, a calculation with the perturbation removed to see how the flow develops[1].

The perturbation occurs over a small pitchwise and spanwise extent, and thus changes the boundary condition from one which is pitchwise uniform (classified here as "one dimensional") to one which varies both in the pitchwise and spanwise directions ("two dimensional"). The parameters for the perturbation are described in Chapter 6.

One challenge to this approach is the ability of the CFD to obtain a steady state solution at operating points very close to stall. A converged, time invariant solution is required (using the unsteady solver) which can be perturbed a small amount to prompt unstable behavior. The difficulty is that, for operating points on the edge of stability, a time-marching method starting with an inexact initial solution could simply just become unstable; in other words, a "perturbation" already exists in the form of the initial solution, which is sufficient to trigger instability. It is observed that, by moving toward the stall line using small steps in corrected flow, it is possible to obtain a steady state solution close enough to the surge line that an additional perturbation (if located in the correct location and of sufficient magnitude) generates a flow instability within the time-accurate simulation.

4.5.1 Transition Between Simulations

For the stability assessment, each simulation is initialized from the last two timesteps of the previous simulation in order to provide a continuous transition. Two timesteps are required because EURANUS is second-order accurate in time.

As the simulations involve changing between a one-dimensional definition of the inlet boundary condition (only spanwise variation) to a two-dimensional definition (spanwise and pitchwise variation), it is necessary to define both in a common format to allow smooth transition. The 1D boundary condition is therefore applied repeat-

[1]Applying time-dependent boundary conditions is feasible in FINE/Turbo, but is limited to applying a time-varying (but spatially constant) factor to a defined spatial distribution. For example, the spanwise variation in total pressure can be defined and scaled uniformly by a time-varying factor, but a local adjustment for a small fraction of the span and pitch cannot currently be implemented.

edly at the same pitchwise locations that are used in defining of the 2D profile. If this is not performed, the small interpolation errors introduced with the application of the 2D profile creates a discontinuity between the simulations.

4.5.2 Exit Conditions in Unsteady Simulations

The different exit boundary condition options treat oncoming pressure and vorticity waves differently, which is important for stability assessment. When the perturbation in total pressure is applied at the inlet, the flow in the diffuser changes. The change is transmitted via a pressure wave which propagates through the domain, combined with entropy and vorticity waves which convect with the mean flow. It is known that a uniform pressure boundary condition (including the pressure adaptation mass flow method) has a tendency to reflect waves [43]. This is due to the exit boundary acting as a pressure node to traveling waves, causing artificial reflections. Physical reflections are possible within the compressor, due to the change in impedance resulting from the sudden change in area, as discussed in Chapter 3. However, analysis of cases run with the volute indicates that no reflections are detectable at the volute inlet location.

In simulations using a uniform pressure exit condition, numerical reflections could be detected as indicated in Figure 4-6. The figure shows a contour plot of the variation of pressure with time for a line of pressure taps at mid-passage, from diffuser inlet to diffuser exit. The pressure wave propagation speed was measured and was found to correctly match the local speed of sound, relative to the flow. This can be seen in Figure 4-6 by the fact the reflected wave travels back into the diffuser at a slower rate than it propagates outward.

Another effect observed on the exit boundary surface concerns the iterative boundary conditions which alter the exit pressure, including average pressure and both mass flow options. When unsteady simulations are restarted with the inclusion of the volute, the iterative processes attempt to maintain the same mass flow or average pressure. The change to the exit pressure that ensues propagates upstream in a wave which interferes with the development of stall precursors.

To perform the stability assessments, it was necessary to use a combination of

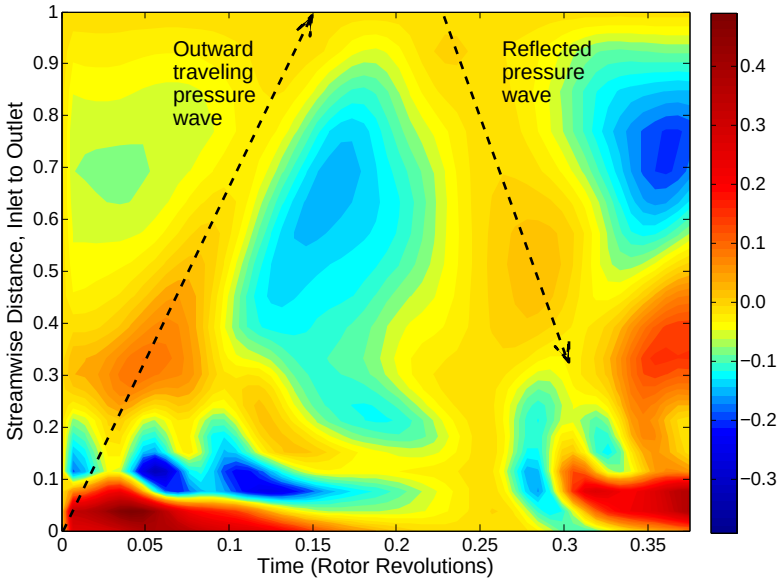

Figure 4-6: Reflection of pressure wave with constant pressure exit condition. Contours show static pressure variations as a percentage of diffuser inlet dynamic pressure. The ordinate is the streamwise distance along the diffuser mid-passage.

approaches. Firstly, a mesh is created with an extended region downstream of the diffuser (as illustrated in Figure 4-4). This "buffer zone" is used to damp out traveling waves through the use of cell stretching, a method presented by Efraimsson and Biela [44] for computational aeroacoustics. The stretched cells cause additional numerical damping which reduces the amplitude of outward traveling waves and any reflections from the boundary. Following the recommendations of Efraimsson and Biela, the cells are stretched by a factor of 1.2. Twelve cells are added in the radial direction; this is at the lower end of what is necessary to accomplish wave damping, but the radial geometry requires the cell size to increase also in the theta direction, reducing the effectiveness of the cell stretching.

The cell stretching was originally considered key in enabling a uniform exit pressure boundary condition to be used. However, as can be seen in Figure 4-7, while grid stretching appears to eliminate reflection at the exit boundary, some reflection is encountered as the wave enters the region with stretched cells. Efraimsson and Biela suggest grid stretching should be used in tandem with an increase in artificial viscosity, and identify the possibility of wave reflection from the stretched grid cells.

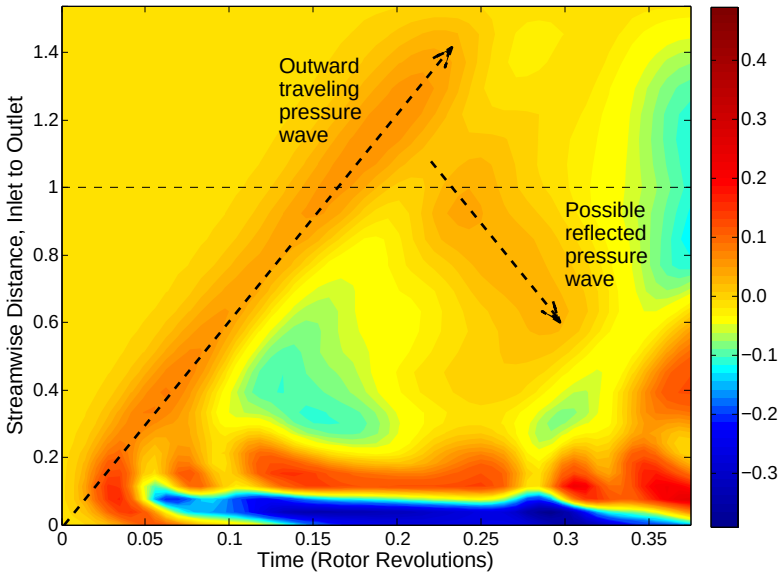

Figure 4-7: Treatment of pressure wave with the buffer zone, showing contours of static pressure change as percentage of diffuser inlet dynamic pressure. Ordinate defined consistent with Figure 4-6.

Additional artificial viscosity in the buffer zone requires local modification of fluid parameters and this was not feasible in the commercial code used. However, experiments with and without cell stretching appear to have a similar outcome, suggesting that the numerical pressure reflections do not have a significant impact on the development of instability. It is suggested that future work investigates whether the buffer zone could be improved (e.g. by changing the cell stretching factor), and, if successful, simulations should be run for comparison with those without the buffer zone. It would then be possible to definitively conclude whether the numerical pressure reflections effect the onset of instability. The similar results achieved here with and without the buffer zone, taken in tandem with the proposed mechanism for instability in Chapter 6, suggests that the buffer zone is not a necessary feature for the simulation of stall precursors.

To obtain the correct backpressure for a given operating point, a preliminary simulation is run with the exit mass flow defined. The pressure adaptation algorithm is used to adjust the backpressure to obtain a particular mass flow, and the exit pressure is then extracted for use in the three simulations outlined above (initialization,

perturbation, flow response). The use of the preliminary simulation with the pressure adaptation mass flow exit boundary condition allows the backpressure to be precisely defined even when the gradient of the pressure rise characteristic is near zero. The use of the buffer zone means a uniform pressure is no longer applied at the diffuser exit. However, the pitchwise pressure variations at diffuser exit are small (as shown in Figure 4-2) and it is considered that the diffuser remains well matched with the volute.

This approach ensures that (a) simulations near stall are feasible; (b) pressure reflections at the diffuser exit can be reduced or prevented; and (c) there are no changes in exit condition when changing over simulations.

4.6 Implementation Guidelines

There are a number of lessons learned in implementing the isolated diffuser model which can be summarized as a set of guidelines. These relate not only to isolated diffuser models for centrifugal compressors with vaned diffusers, and also to general compressor modeling.

- To model operating points near stall, it is necessary to use a mass flow exit boundary conditions as opposed to one which defines static pressure.

- In some cases, unsteady simulations will reach a steady state whereas steady simulations will not. This is the case for diffuser and volute simulations as well as single passage simulations with a mixing plane, compared with unsteady full wheel simulations. Assuming the compressor stability limit lies where the steady simulations no longer converge appears to provide only a very conservative estimate of the stable operating range.

- Steady state mixing plane simulations can provide misleading results, particularly for vaned diffusers operating near stall and with transonic conditions in the vaneless space between impeller and diffuser. This is the subject of Section 5.3. The results of such simulations should be treated with caution.

- The exit boundary condition chosen has an impact on the solution. Applying an average pressure or using the Numeca FINE/Turbo "velocity scaling" mass flow option provides a non-uniform pressure distribution on the exit surface, whereas a uniform pressure or the Numeca FINE/Turbo "pressure adaptation" mass flow option applies a uniform pressure on the exit surface. This impacts the upstream flow. For centrifugal compressors with vaned diffusers and volutes, applying a uniform pressure at exit suggests to be more representative of the actual device, although this neglects the once-per-revolution static pressure variation caused by the volute.

- Although not discussed above, it is found applying a mass flow exit boundary condition can allow two equally valid possible solutions, one subsonic and one supersonic. Within FINE/Turbo, it is possible to influence which solution is achieved through the initial estimate of the pressure on the exit surface, which is required in setting the initial condition for the time-marching scheme. A high exit pressure will cause the solver to tend towards a subsonic solution.

A number of guidelines apply only to the unsteady simulations:

- For simulations with large domains and low fluid velocities, a converged steady state solution can be reached in shorter time by initially using a larger timestep, before reducing it to achieve the desired temporal resolution.

- Methods for determining the exit condition using an iterative algorithm (e.g. velocity scaling or pressure adaptation mass flow options) cannot be used when inlet conditions are changing, as information is artificially inserted onto the exit surface. This can propagate into the flow domain in the form of a pressure wave and impact the solution.

- A uniform pressure boundary is typically reflective to oncoming waves, which can impact simulations with time-dependent inlet conditions and negatively affect simulations testing the onset of instability. This can be mitigated using a buffer zone and cell stretching.

- The pressure adaptation boundary condition can be used to accurately determine the back pressure for a particular operating point, even close to stall where the pressure rise characteristic has near zero gradient. The exit static pressure found in this manner can then be utilized for simulations at the same operating point using a constant pressure exit boundary condition. It is thus possible to resolve the conflict presented in the choice of exit boundary condition: that a mass flow boundary condition is necessary near to stall, but causes artificial pressure waves to propagate from the exit boundary when used with time-varying inlet conditions. This approach allows the numerical forced response experiments described in this thesis.

- When switching simulations, boundary conditions must be specified in the same format to prevent differences in interpolation e.g. should a boundary condition be defined via a matrix of pitchwise and spanwise points for one simulation (e.g. defining a perturbation in total pressure), it is necessary to define the inlet condition using the same format for prior and subsequent simulations, should a smooth transition be desired.

Chapter 5

Diffuser Matching

A particular challenge exists in the matching of the vaned diffuser flow with the upstream and downstream components. In matching with the impeller, the concept is to reduce complexity, taking the rotating (and hence time-varying) flow field coming from the impeller, and performing a pitchwise averaging procedure to create an equivalent steady flow as the inlet condition for the diffuser model. By pitchwise averaging, some information is lost from the original flow; to quote Pianko and Wazelt [45]: "no uniform flow exists which simultaneously matches all the significant stream fluxes, aerothermodynamic and geometric parameters of a non-uniform flow." The choice of how to perform the averaging is therefore critical.

Matching with the downstream volute reduces to the decision of how to apply the diffuser exit boundary condition such that the pressure distribution is representative. This was discussed in Chapter 4, but it is noted that, in accordance with Hypothesis IV, the circumferential non-uniformity caused by the upstream influence of the volute is not considered to be necessary to capture the stall inception mechanism. Thus the matching procedure simply sets the pressure at the diffuser exit boundary.

5.1 Approach

The single passage stage calculations, performed routinely as part of the design cycle, are utilized to provide data on the impeller exit flow. In fact, a similar pitchwise

averaging operation is performed in the stage calculations such that they can be solved within a steady framework; this is the purpose of the mixing plane, introduced in the previous chapter. However, the mixing plane is located approximately midway between impeller trailing edge and diffuser leading edge. This is further downstream than is desired for the inlet to the isolated diffuser simulations, given the goal of capturing the flow in the vaneless space. The mixing plane location is not moved upstream because it has been optimized to provide the best performance near design conditions. The second reason for not utilizing the standard mixing plane, which is more important and is discussed in Section 5.3, is that it can lead to an incorrect diffuser flow field, particularly near to stall.

A valid question is therefore whether the impeller flow is accurately captured, given the known discrepancies in the diffuser flow. It is assumed here that it is, and this assumption is tested through comparison with the unsteady full wheel stage simulations. The primary effect of the downstream diffuser is setting the pressure field at the impeller exit, and the mixing plane does appear to transfer this information in an adequate manner. This topic is returned to in Section 5.2.

The impeller exit flow is extracted from the stage calculations at each operating point with pitchwise and spanwise non-uniformities. It is desired to perform an averaging operation in the pitchwise direction to remove the unsteadiness of the impeller blade passing. The goal is to provide the parameters that define the time-mean inlet flow into the isolated diffuser simulation: a flow direction specified by normalized, absolute flow velocity vectors and the total conditions (pressure and temperature), each defined as a profile across the span. In particular, the definition of the spanwise flow angle distribution is deemed critical, consistent with Hypothesis III. It is also noted that the momentum-averaged flow angle at the diffuser inlet was found to determine the performance of the diffuser over and above any other parameter, according to the findings of Filipenco et al. [6], although their findings also indicated that spanwise flow non-uniformity had little role in the diffuser performance or stable operating range (see Chapter 3).

It is noted that defining total conditions and a flow direction at inlet to the

diffuser allows circumferential variation of static pressure and velocity magnitude; i.e. not all parameters are pitchwise uniform at diffuser inlet. In particular there exists a non-uniform static pressure field as stipulated by the upstream influence of the diffuser vanes and a non-uniform Mach number. Although the pressure field in non-uniform, one of the limitations of this approach is that the flow angle, which would also be expected to see circumferential non-uniformity due to the diffuser vane non-uniformity, is held constant. This does not appear to have a greatly adverse effect as discussed in section 5.2.

5.1.1 Inlet Conditions

Different methods of averaging a non-uniform flow are required for different purposes as discussed by Cumpsty and Horlock [46] and Greitzer et al. [13]. For example, to calculate the work output from a turbine, the non-uniform flow at inlet and outlet should be calculated via the work average, or for averaging a non-uniform flow into a nozzle, the thrust average should be computed. The purpose here is to provide a flow at the inlet of the isolated diffuser simulations which is equivalent to the flow output from the impeller but with pitchwise non-uniformities mixed out, consistent with the hypothesis that the unsteady blade-to-blade non-uniformities do not play a significant role in the stall inception process. It is now recognized that mixing does not, in fact, occur completely in the vaneless space, with pitchwise non-uniformities still present through the diffuser (see Chapter 2). However, if these non-uniformities do not significantly effect the aerodynamics of the diffuser, it can be assumed the mixing occurs instantaneously, at a plane near the impeller exit.

The approach is thus to compute the mixed out average for the conditions at the impeller outlet. The input is the pitchwise and spanwise non-uniform flow field at impeller exit taken from the single passage, stage calculation, and the output is a pitchwise uniform total pressure, total temperature and velocity direction to provide inlet conditions for the isolated diffuser simulation. A control volume is utilized with a constant area, defined by a small slice δz in the axial direction (the axial grid cell dimension provides the natural dimension, although an infinitesimal slice dz

could theoretically be used), and the main impeller blade pitch in the circumferential direction, $2\pi r_2/n$ (where there exists n main blades). The length of the control volume is theoretically zero - mixing is assumed to occur instantaneously.

The stagnation pressure is reduced by the mixing process and this has a consequence for the transonic diffuser inlet flow as it impacts the diffuser inlet corrected flow. An adjustment is therefore necessary as a later step in the matching process (discussed in Section 5.1.3). It is noted by Cumpsty and Horlock [46] that the mixed out average tends to provide a "pessimistic" averaged total pressure, as it assumes that the mixing processes are irreversible. However, Cumpsty notes in [23] that the contribution of reversible work transfer in mixing out the impeller non-uniformities are negligible, thus validating the approach.

The conservation equations used in the calculation of the averaged conditions are then as follows:

Conservation of mass:

$$\int_0^{\frac{2\pi}{n}} \rho V_r \, \delta z \, r_2 \, d\theta = \overline{\rho}\overline{V_r} \; (2\pi r_2/n) \; \delta z = \dot{m} \tag{5.1}$$

Conservation of radial momentum:

$$\int_0^{\frac{2\pi}{n}} \left(p + \rho V_r^2\right) \; \delta z \, r_2 \, d\theta = F_r = \left(\overline{p} + \overline{\rho}\overline{V_r}^2\right) \; (2\pi r_2/n) \; \delta z \tag{5.2}$$

The radial momentum equation is the only momentum equation involving a pressure term because the upstream and downstream surfaces of the control volume are perpendicular to the radial direction. The assumption here is that the downstream static pressure is uniform. In reality, the impeller rotates through the pressure field caused by the upstream influence of the diffuser. The pressure therefore fluctuates in time; this uniform pressure field is representative of the time-averaged pressure felt at the impeller exit.

Conservation of tangential and axial momentum:

$$\int_0^{\frac{2\pi}{n}} \rho V_r V_\theta \, \delta z \, r_2 \, d\theta = \overline{\rho}\overline{V_r V_\theta} \; (2\pi r_2/n) \; \delta z = \dot{m}\overline{V_\theta} \tag{5.3}$$

$$\int_0^{\frac{2\pi}{n}} \rho V_r V_z \, \delta z \, r_2 \, d\theta = \overline{\rho}\overline{V_r V_z} \; (2\pi r_2/n) \; \delta z = \dot{m}\overline{V_z} \tag{5.4}$$

Conservation of energy (assuming a perfect gas):

$$\int_0^{\frac{2\pi}{n}} \rho V_r c_p T_t \, \delta z \, r_2 \, d\theta = \overline{\rho}\overline{V_r} c_p \overline{T_t} \; (2\pi r_2/n) \; \delta z = \dot{m} c_p \overline{T_t} \tag{5.5}$$

From these equations it is evident that the mixed out average is equivalent to the "mass average" for the tangential and axial velocity and the total temperature. It therefore only remains to calculate the radial velocity (to allow the definition of the flow angle) and the total pressure.

The equation of state for a perfect gas and the definition of total temperature are required to provide a closed problem:

$$T_t = T + \frac{V^2}{2c_p} \tag{5.6}$$

$$p = \rho R T \tag{5.7}$$

Combining:

$$\bar{T_t} = \frac{\bar{p}}{\bar{\rho} R} + \frac{\bar{V_r^2} + \bar{V_\theta^2} + \bar{V_z^2}}{2c_p} \tag{5.8}$$

Equations 5.1, 5.2 and 5.8 form a set of three equations with three unknowns: $\bar{V_r}$, $\bar{\rho}$ and $\bar{p}$. These were solved for $\bar{V_r}$, providing a quadratic with sub- and supersonic solutions (the subsonic solution being taken):

$$\bar{V_r}^2 \left(\frac{\gamma + 1}{2\gamma} \right) - \bar{V_r} \, \frac{F_r}{\dot{m}} + \left(\bar{T_t} - \frac{\bar{V_\theta^2} + \bar{V_z^2}}{2c_p} \right) = 0 \tag{5.9}$$

The final step is to determine the mixed out total pressure. The mixed out average Mach number is computed, then the total pressure is determined from the calculated mixed out static pressure. This is a conventional calculation for compressible flows, thus the algebra is not presented here.

The above process is performed for each spanwise cell in the mesh, providing the desired spanwise distribution of total pressure, temperature and velocity direction.

The "momentum averaged" flow angle defined by Filipenco et al. [6] differs from this definition in that it uses a mass flow weighted average for both the radial velocity and the tangential velocity, rather than a control volume formulation. It is also noted that Filipenco et al. performed a complete pitchwise and spanwise average to define the diffuser inlet flow by a single value, rather than via a function of axial position.

The derivation of the inlet conditions also differs from that used by Hill [5]. Hill used an approximate mass-average when pitchwise averaging (approximate only because the meridional mass flux was chosen as the weighting factor, for a surface defined perpendicular to the radial direction - i.e. mass flux and area were not mutually perpendicular). The flow angle obtained as a result was similar to the momentum averaged angle as defined by Filipenco et al. [6].

The momentum averaged angle and Hill's inlet flow angle are both significantly lower than that found using the mixed out definition described above, as shown in Figure 5-1. The control volume formulation used to derive the mixed out average requires the modification of the radial velocity due to the pressure term in the radial momentum equation (Equation 5.2). Both the mixed out and mass flow weighted averages lead to the same algebraic expression for the average tangential velocity, but the mass flow weighted radial velocity would not conserve mass across a control volume. To satisfy mass continuity (dependent on V_r) and the radial momentum equation (dependent on V_r^2) simultaneously requires pressure changes between the non-uniform flow and the mixed out flow. This requirement leads to the difference in radial velocity, and thus flow angle, between the two approaches.

Figure 5-2 illustrates the main features of the spanwise profile in flow angle at impeller exit, with a comparison against the time-averaged unsteady full wheel simulation. The angle is measured from the radial direction, with the impeller rotation direction as positive, and both simulations are pitchwise averaged in the same manner. Further discussion of this validation is included in Section 5.2, but it is evident that the inlet conditions for the isolated diffuser simulations compare well to the im-

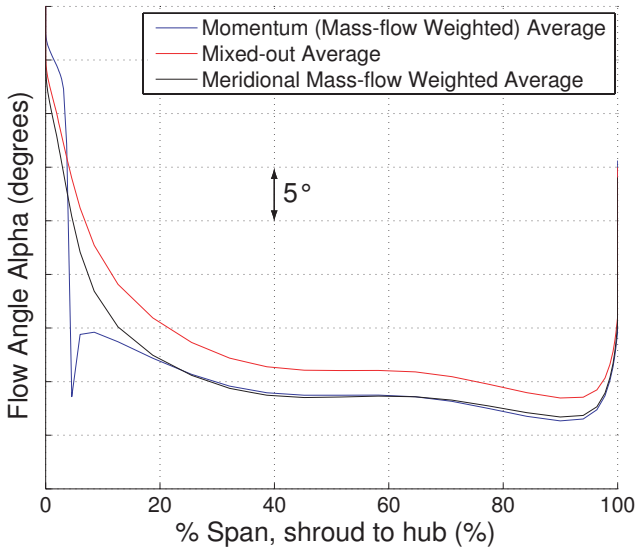

Figure 5-1: Comparison of different pitchwise averaging methods for the flow angle at impeller exit; the mixed out average flow angle is between 2-3° greater than the mass-flow weighted averages utilized by Filipenco et al. [6] and Hill [5].

peller exit flow from the time-averaged unsteady full wheel simulation. It is noted that this is effectively a comparison of unsteady full wheel and steady, single passage simulations, as it is this latter simulation on which the inlet conditions for the isolated diffuser are derived.

The flow at diffuser inlet is highly swirling - flow angles exceed 65 degrees across the span - and there exists significant spanwise variation. At the shroud, the radial velocity is negative in the time-averaged unsteady full wheel simulations, and the same is true in the isolated diffuser inlet conditions but for a limit applied during processing to aid convergence of the simulations (this will be discussed in the following section). The radial velocity remains low even as far as 30% of the span, illustrating that the shroud endwall flow cannot be described as a simple boundary layer, although this description holds more true for the hub endwall flow.

The jet part of the jet-wake structure is represented by the lower flow angle near the hub surface. Even following pitchwise averaging the flow near the hub has a high radial velocity and correspondingly low flow angle.

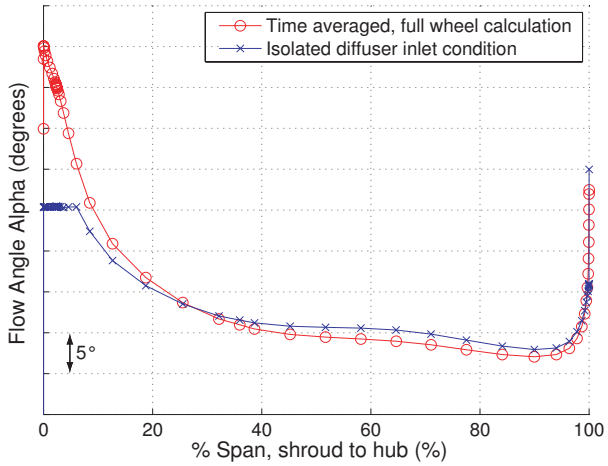

Figure 5-2: Spanwise profile for flow angle alpha, showing the typical features at impeller exit for an operating point near stall. The isolated diffuser inlet conditions are compared to the time-averaged, unsteady full wheel simulation as a preview to Section 5.2; good agreement is shown.

5.1.2 Flow Reversal on Shroud Side

The single passage full stage results indicated reversed flow at the the impeller exit for all of the operating points tested on the design speedline. Flow reversal occurs on the shroud side due to the tip clearance flows (which are modeled in the stage simulations) and the convex shroud surface, which tends to favor boundary layer detachment within the adverse pressure gradient. Including backflow within the inlet conditions for the isolated diffuser simulation results in an ill-posed numerical problem and provides challenges for the flow solver. Following the guidelines of Hill [5], the normalized radial velocity vector and the total pressure are limited to $V_r/|V| \geq 0.08$ and $P_{t2}/P_{t0} \geq 3.8$ on the shroud side.

The effect on blockage at the diffuser inlet, defined as:

$$B = 1 - \frac{\int \rho V_r \, dA}{\int (\rho V_r)_{max} \, dA} \tag{5.10}$$

is small but not negligible; the flow blockage is fairly constant between 21% and 22% across the operating range (with blockage calculated after pitchwise averaging), and the maximum change due to the limiter on radial velocity was 1.3 percentage

points. This maximum value occurred at the lowest flow operating point at which the steady, single passage simulations converged. The quantity of backflow monotonically increases as the compressor moves along the operating line towards stall.

The small increase in mass flow, caused by the limit on radial velocity, combined with the increase in the total pressure has the effect of canceling each other out in terms of corrected flow, defined by $\dot{m}\sqrt{c_p T_t}/A\,p_t$. However, the increase in physical mass flow outweighs the increase in total pressure such that the overall effect is an increase in the averaged corrected flow of 2.1% at the operating point with minimum flow. Through careful matching of mass flow at diffuser inlet, described in the following section, it is possible to take this into account.

For the purposes of this project the limits on total pressure and radial velocity were kept fixed. Some work was performed to determine whether it was possible to relax or remove them; trials suggested this was possible for some operating points but not others, and no consistent trend was identified. It is not known whether flow reversal at the inlet to the vaneless space has a significant impact on the stability of centrifugal compressors with vaned diffusers, although the presence of back flow forms part of the criteria of Vo et al. [18] (see Chapter 3) for spike stall inception in axial compressors. This presents an opportunity for future study.

A further effect of the flow reversal is a high sensitivity to numerical accuracy around the spanwise location of zero net forward flow. This can be seen as spiky profiles near the shroud in Figure 5-4.

5.1.3 Exit Conditions

Given the inlet conditions defined above, one further piece of information is required to constrain the problem; the total mass flux or the exit static pressure, both of which are defined via the exit boundary condition. The most straightforward approach would be to take the mass flow as defined in the stage calculations, guaranteeing conservation of mass, momentum and energy (excepting the modifications made to the radial velocity and total pressure profiles). However, given that the flow in the vaneless space is transonic for the speedline under consideration, the Mach number of

the flow is of considerable importance, defining the choking mass flow and the location and strength of any shocks. In addition, the adjustments on radial velocity and total pressure mean that the physical mass flow is not necessarily the most representative means of matching; what is required is a non-dimensional parameter that defines the flow at inlet to the diffuser.

The Mach number of the swirling flow at the impeller exit is a function of total temperature, total pressure, flow angle, and mass flow (assuming the compressor geometry and fluid properties are fixed):

$$M = f(T_t,\, p_t,\, \alpha,\, \dot{m})$$

This is more often expressed the opposite way around, in the non-dimensional relationship:

$$\frac{\dot{m}\sqrt{c_p T_t}}{A\, p_t} = f(M, \gamma) \tag{5.11}$$

where the area, A, must reflect the actual flow area, which is a function of both geometry and flow angle. The expression on the left hand side of Equation 5.11 is sometimes referred to as the "corrected flow per unit area" or "corrected flow"[1].

The total conditions and flow angle are fixed by the inlet conditions, and therefore the diffuser inlet Mach number is dependent only on the mass flow. It is therefore the corrected flow on which the matching of diffuser to impeller is completed.

In practice, it is sufficient and convenient to use the "standard day corrected flow" to match diffuser flow with impeller flow. The standard day corrected flow (SDCF) is defined as:

$$SDCF = \frac{\dot{m}\,\sqrt{\theta}}{\delta} \tag{5.12}$$

where $\theta = T_t/T_{ref}$ and $\delta = p_t/p_{ref}$. SDCF has units of kilograms per second, but is representative of the non-dimensional corrected flow (as shown in Equation 5.11) for

[1]It is also sometimes written as $\dot{m}\sqrt{RT_t}/A\, p_t\, \sqrt{\gamma}$, which changes the form of the function on the right hand side but is an equally valid non-dimensional grouping.

a device with fixed geometry and operating with a given gas (air, assumed to behave as a perfect gas). It is typically used to eliminate differences in the atmospheric conditions when experiments draw air from the local environment.

The standard day corrected flow is calculated based on the mass averaged properties of the impeller exit flow. While the mass averaged total pressure has no physical basis [13, 46], the difference between mass average and availability average total pressure at the diffuser inlet was shown to be negligible (as observed by other authors, e.g. Prasad [47], who stated that the difference was, in general, less than 0.1%).

The procedure to determine the mass flow for the isolated diffuser simulations was to adjust the mass flow either directly (near stall) using the mass flow boundary condition, or indirectly via the static pressure on the exit boundary, until the corrected flow in the vaneless space was equal to the corrected flow at the vaneless space within the single passage stage calculations.

The difference between matching based on the physical mass flow and using the SDCF (used as a proxy for corrected flow) was a reduction in the physical flow of between 1.5% and 2%. This can be explained by the minimum limits placed on radial velocity and total pressure, used to prevent backflow at diffuser inlet as discussed in the previous chapter. Once these modifications are taken into account, only a small variation (of the order 0.5%) is present; this is likely within the numerical accuracy of the averaging schemes utilized.

One further complication relates to the assumption that mixing occurs immediately, a consequence of using a mixed-out pitchwise average. The total pressure monotonically reduces downstream of the impeller blade, due to the irreversible mixing of the impeller wakes and also the growth of endwall boundary layers as shown in Figure 5-3. To allow for this, the matching of corrected flow is performed at the mixing plane radius, i.e. for the single passage stage calculation, the corrected flow is calculated on the upstream surface of the mixing plane. This captures the maximum extent of irreversible mixing and the associated loss in stagnation pressure that is present in the single passage simulations, such that the isolated diffuser simulation are as consistent as possible.

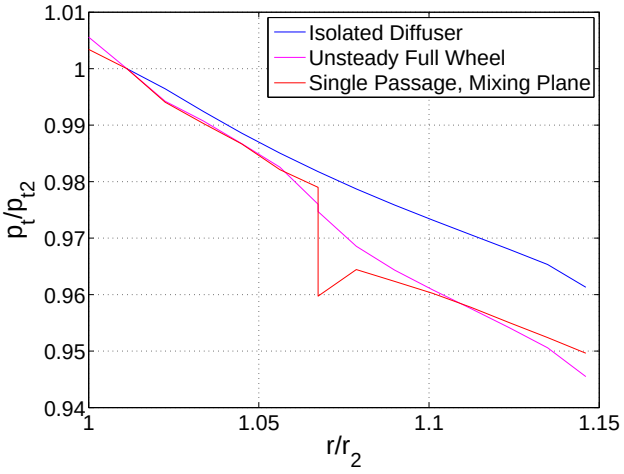

Figure 5-3: Change in mass-averaged total pressure across the vaneless space, comparing different simulations. The unsteady full wheel and the single passage simulations show greater total pressure losses due to mixing of pitchwise non-uniformity downstream of the impeller. The mixing plane simulation also shows a loss in total pressure across the mixing plane.

The matching methodology here highlights why the strict conservation of mass, momentum and energy fluxes between the impeller flow and the diffuser flow may not always be the best approach, particularly following a pitchwise averaging procedure. This highlights one of the problems encountered in formulating a mixing plane implementation in CFD codes, which require a strict conservation of fluxes for the purposes of multistage simulations. Through separating the two simulations, it is possible to make allowances for the limitations of the pitchwise averaging process.

It is noted that the matching procedure used here is a first-principles, rigorous approach, and improves considerably on the work of Hill [5]. Many of the limitations of Hill's work - specifically the use of an approximate mass-average for calculating inlet parameters, the definition of an exit boundary condition using a correlation to experimental values, and the limited operating points modeled due to the use of only a pressure exit boundary condition - have been eliminated in this work. The advances made to the isolated diffuser model allow the simulations to be consistently matched with the impeller exit flow, such that the diffuser flow more accurately represents the flow in the real diffuser (as indicated through validation, Section 5.2). This allows a more accurate assessment of the stability limit.

5.1.4 Extrapolation to Lower Corrected Flows

The steady, single passage stage simulations were run using both pressure and mass flow boundary conditions (as discussed in Chapter 4) until a limit was reached at which the simulations would not converge. There was also a region of operation where the compressor flow was significantly different from other operating points, including high incidence stall across the span. This region extended to 4% corrected flow below the last normal operating point obtained with the single passage simulations. It was considered that these points were likely anomalous; later results with the isolated diffuser confirmed this. The mixing plane is likely affecting the flow at these low flow operating points.

In performing the isolated diffuser simulations, it proved necessary to test operating points at lower corrected flows than were possible in stage calculations. This required extrapolation of the inlet conditions. Operating points were simulated at uniform increments of physical mass flow near to stall and the trend in flow angle, total pressure and total temperature variation was observed. For flow angle, the trend was a linear increase with reducing mass flow, such that the flow becomes more tangential. Radial velocity and density define the mass flow, and changes in density between operating points is small such that it can be shown that radial velocity is proportional to mass flow. The tangential velocity also changes due to the effect of backsweep, as defined by the equation $V_{\theta 2} = \sigma(\omega r_2 - V_r tan\chi_2)$. Slip, σ, is usually assumed to be a function only of rotational speed (e.g. the correlations of Wiesner or Stanitz, see [23]) which is constant in this case. This shows that the tangential velocity will vary linearly with the radial velocity, and thus flow angle will vary linearly with radial velocity. Therefore the observed linear trend of flow angle with mass flow is entirely reasonable, although the details of the distribution across the span cannot be readily calculated.

The total temperature is also observed to vary linearly with the mass flow, which is a consequence of the linear variation in tangential velocity. The Euler turbine equation can be expressed as follows, for an adiabatic machine:

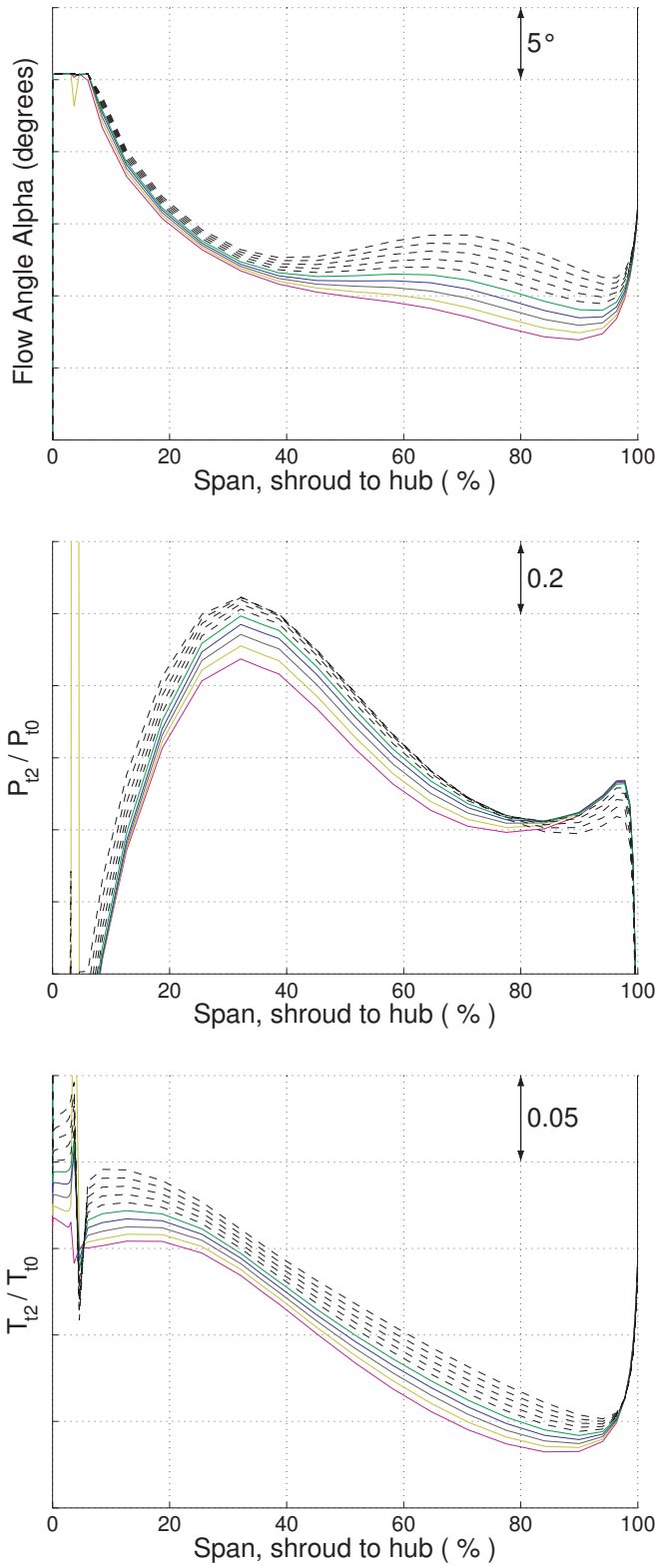

Figure 5-4: Extrapolation of flow angle alpha, total pressure and total pressure. Colored lines show inlet conditions derived from single passage stage calculations at different operating points and dotted black lines indicate extrapolation, at even intervals of mass flow.

$$\frac{T_{t2}}{T_{t1}} = \frac{\omega(r_2 V_{\theta 2} - r_1 V_{\theta 1})}{c_p T_{t1}} + 1 \tag{5.13}$$

For the centrifugal compressor, $V_{\theta 1} = 0$, and Equation 5.13 reduces to:

$$\frac{T_{t2}}{T_{t1}} = \frac{\omega r_2 V_{\theta 2}}{c_p T_{t1}} + 1 \tag{5.14}$$

Thus, for fixed inlet conditions and impeller blade speed, the total temperature at impeller exit is a linear function of the tangential velocity.

For total pressure, a more complex relationship was observed. The total pressure rise in the impeller is related to the total pressure rise via the efficiency. Using the polytropic efficiency, η_p, the relationship is:

$$\frac{p_{t2}}{p_{t1}} = \left(\frac{T_{t2}}{T_{t1}}\right)^{\frac{\eta_p \gamma}{\gamma - 1}} \tag{5.15}$$

For a lossless compressor operating with air, the exponent is 3.5. However, it was observed in the numerical experiments that a quadratic dependence of total pressure with mass flow was sufficiently accurate over the range of interest. This was implemented to extrapolate the inlet conditions to lower mass flows.

The range of validity of extrapolation is likely limited. For example, the increase in shroud side blockage due to the flow reversal is not well captured in the extrapolation process. Extrapolation of the inlet conditions extended to a mass flow 10% below the last converged and normal operating point achieved with the single passage, steady simulations.

5.2 Validation

Three full wheel unsteady simulations were performed at different operating points near stall to validate the isolated diffuser simulations, and the time-averaged results were compared with the isolated diffuser simulations. In addition, the unsteady flow features were also analyzed to examine their likely effects on the diffuser flow.

The data from experiments by Spakovszky and Roduner [7] is also available for

comparison, and this follows the discussion of the unsteady simulations.

5.2.1 Validation Against Full Stage, Full Wheel, Unsteady Simulations

Firstly, the time-averaged and pitchwise-averaged conditions at the diffuser inlet are compared between the isolated diffuser simulation (these are derived directly from the steady single passage simulations) and the unsteady full stage simulations. Figure 5-5 shows the velocity direction, total pressure and total temperature for the two cases.

The consequences of the limit on radial velocity and total pressure is clearly shown in these plots. Another difference is the higher total pressure on the hub for the time-averaged unsteady full wheel simulation; this is simply a consequence of a difference in the application of the hub boundary. In the single passage calculations the hub is modeled as stationary downstream of the impeller trailing edge (consistent with the actual compressor) and in the full stage simulations the hub surface is modeled as rotating up to the rotor/stator interface, due to a setup error. This could be readily corrected, but the unsteady full wheel simulations are computationally expensive to run, are generally only for validation, and the small difference in the hub boundary layer does not impact the remainder of the diffuser flow.

Other than these issues, the comparison shows that the impeller exit flow is well captured in the single passage, full stage simulations. The main difference lies in the flow near the shroud; this shows a larger separated flow region, lower total pressure and higher total temperature in the time-averaged unsteady simulation than in the single passage simulation. It is conjectured that this may relate to the increased viscous losses caused by impeller tip leakage in an unsteady flow which was identified by Shum et al. [22].

It is noted that an equally valid approach would be to use the unsteady full wheel simulations as a starting point for the derivation of the inlet conditions for the isolated diffuser simulations, although this would have been computationally much more expensive and thus negates one of the key advantages to performing isolated

diffuser simulations.

The time-averaged Mach number is also plotted at 10% span, 50% span and 90% span, and compared between the two simulations, as shown in Figure 5-6. The time average is computed in the stationary frame of reference, such that flow in the impeller is blended out due to the impeller rotation (the conventional approach is to time average the impeller flow in the rotor frame of reference, to show the rotor locked flow pattern). This necessitated separate post-processing, such that the colormaps of the two figures are not identical. However, it is clear to see that there is good qualitative and quantitative agreement between the time-averaged solution and the isolated diffuser solution.

One interesting point to note in the time-averaged unsteady simulation is the extent of the upstream influence of the diffuser vanes, which clearly extends into the rotor passages. This impacts not only the Mach number, but also the flow angles, as shown in Figure 5-7. It will be noted that the inlet conditions applied specify a circumferentially uniform flow angle at the impeller trailing edge in the isolated diffuser simulations. Despite this, a comparison of the vane loading between the time-average from the unsteady full wheel simulation and the isolated diffuser shows good agreement, as shown in Figure 5-8. This suggests the flow quickly redistributes with the upstream influence of the diffuser vane and capturing the mixed out average value at impeller exit is adequate. Only 50% span is shown in Figure 5-8, but similar agreement exists across the span. The variation on the suction side appears to be a consequence of the unsteady, transonic flow in the full wheel simulation. At certain time instances, the Mach number of the flow around the leading edge of the suction surface exceeds one, decelerates via a shock, experiences a small amount of further acceleration before then diffusing along the length of the diffuser channel section. While the shock is merged out through time averaging, the pressure rise through the shock is sufficiently high that its influence can still be seen in the mean loading plot. In the isolated diffuser simulation, the flow around the leading edge smoothly accelerates and decelerates in a shock free manner.

One potential improvement would therefore be to move the inlet boundary further

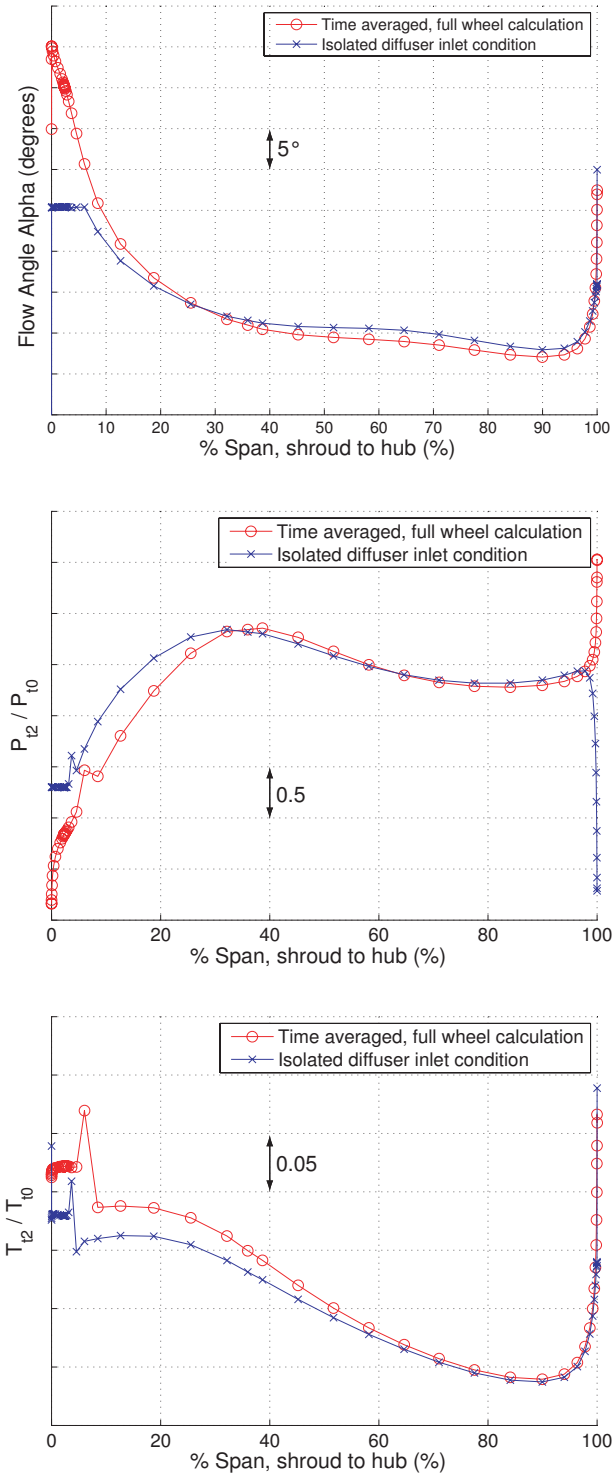

Figure 5-5: Conditions at impeller exit/diffuser inlet. Comparison between isolated diffuser inlet conditions, derived from the single passage stage calculations, and the time-averaged unsteady full wheel simulations.

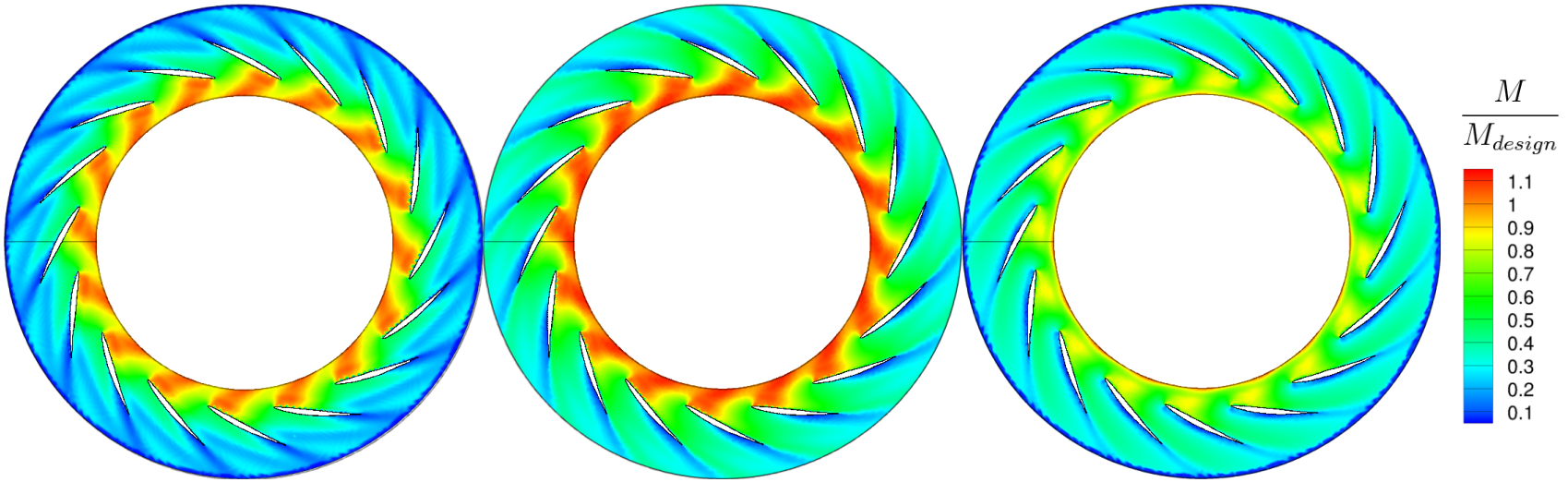

(a) time-averaged, unsteady full wheel simulations results at 10% span (near hub), 50% span and 90% span (near shroud)

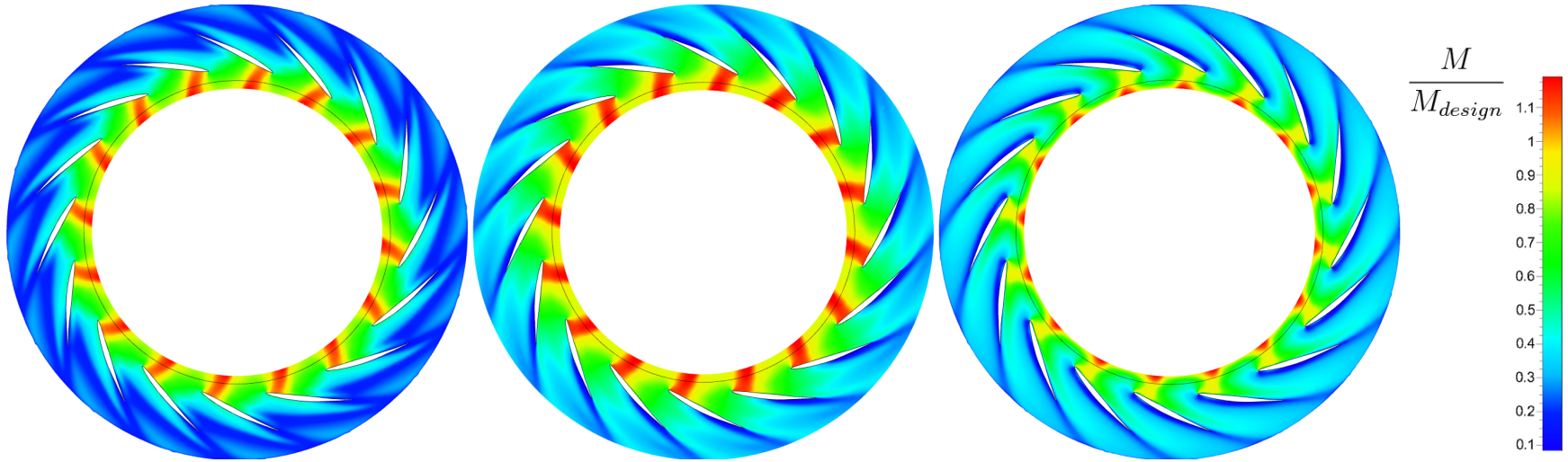

(b) Isolated diffuser results at 10% span (near hub), 50% span and 90% span (near shroud). The rotor-stator interface location is indicated by the black circle upstream of the diffuser vanes.

Figure 5-6: Mach contours at 10%, 50% and 90% span for an operating point near stall, showing good qualitative agreement between the time-averaged unsteady full wheel simulation and the isolated diffuser simulation. Note slight differences exist in the colormaps.

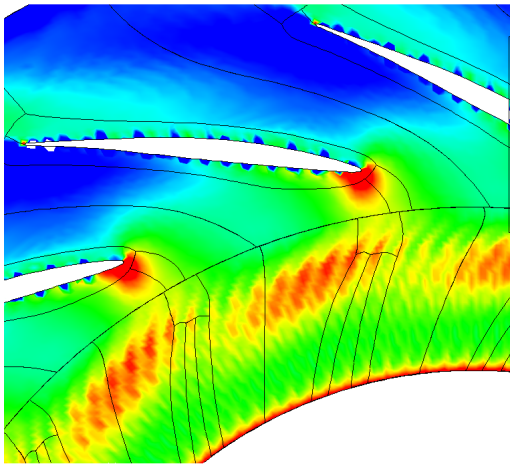

Figure 5-7: Time-averaged flow angle at inlet to the diffuser at mid-span, taken from the unsteady full wheel simulation. The upstream influence of the diffuser vanes causes pitchwise non-uniformity which extends into the impeller blade passages. Bubbles near the diffuser vane surface (caused by interpolation onto a different mesh and zero velocity inside vanes) and the striped effect at the impeller trailing edge are consequences of the time-averaging.

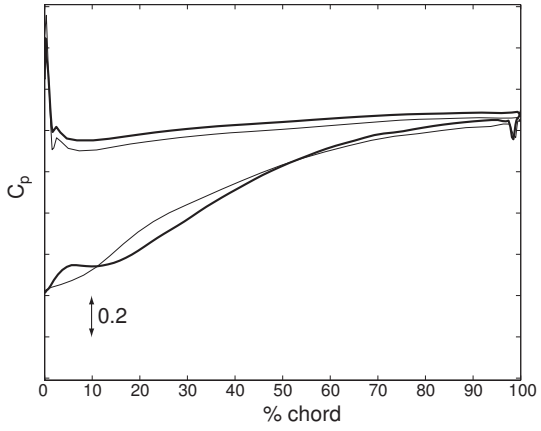

Figure 5-8: Comparison of diffuser vane loading at 50% span, between the time-averaged, unsteady full wheel simulation (bold) and the isolated diffuser simulation. Good agreement is obtained, verifying the fidelity of the isolated diffuser model.

upstream. This would require modification of the inlet conditions such that the the pitchwise averaged flow properties remain matched at the impeller exit location despite the development of the flow from the new, upstream inlet position. This was the approach taken by Shum et al. [22], whose inlet surface for isolated diffuser simulations was positioned a diffuser vane pitch upstream of the diffuser leading edge. However, this adds considerably to the complexity of the matching process, as multiple parameters would require simultaneous adjustment (both inlet and exit boundary conditions would require simultaneous adjustment).

In conclusion the correct trends are captured through the use of the single passage stage calculations to derive the inlet conditions, with excellent quantitative agreement in flow angle (which is regarded as the most important parameter defining the diffuser flow [6]) and acceptable agreement in total pressure and temperature. The contour plots of Mach number provide confidence that the flow field has the correct form in the isolated diffuser simulations, and the diffuser vane loading shows good quantitative agreement, indicating that the incidence angle on the diffuser vanes (important for stall inception) is well captured. The mixed out average flow conditions and the matching of corrected flow is shown to allow a physically consistent isolated diffuser simulation, when compared with the higher-fidelity full wheel unsteady model. Two outstanding questions remain: whether the unsteady impeller exit flow has a significant impact on the diffuser, and whether the numerical simulations are consistent with the experimental data. These are addressed in the following two sections.

5.2.1.1 Effect of Impeller Exit Flow Unsteadiness on Diffuser

Section 2.3 discussed previous research that justified the use of an isolated diffuser model which utilizes time invariant, circumferentially mixed out inlet conditions. It is not intended to revisit the analysis and conclusions of previous researchers, but it is recognized that, through performing unsteady full wheel simulations, data is available by which to review the assumption that neglecting the unsteady component

of the impeller exit flow provides an adequate model for the diffuser[2]. The analysis presented here thus adds to the evidence from Shum et al. [22], Baghdadi [27] and Cumpsty [23].

The flow features of interest are the unsteady jet-wake structure from the impeller and the impeller viscous wakes, both of which wash past the diffuser vanes at blade passing frequency. It is desired to show that these features have little effect on the aerodynamic performance of the diffuser. Figure 5-9 shows an arbitrary snapshot in time from the unsteady simulations, showing impeller wakes as regions of high entropy convecting through the diffuser. It is not evident from this, however, whether the wakes significantly affect the diffuser aerodynamics. To provide more insight, the unsteady loading on the diffuser vanes is also plotted. Figure 5-10 shows four snapshots in time for a single diffuser vane and compares this to the time-averaged loading. The operating point is close to stall. It is clear that the impeller jet-wake structure is not rapidly mixed out but can be detected throughout the diffuser, such that the flow in the diffuser is unsteady (as reported by other authors [24, 25, 26]). However, the integral value of the diffuser vane loading changes very little due to the unsteadiness, varying by less than 1% from the time-mean value. This provides an additional argument for neglecting the impeller exit flow unsteadiness in the isolated diffuser simulations.

5.2.2 Validation Against Experimental Data

Data from the experiments run by Spakovszky and Roduner on the same compressor [7] is available for comparison with the CFD simulations. The data includes quasi-steady pressure tap readings as well as fast-response pressure taps for unsteady data (which will be of more interest in Chapter 6).

The pressure taps were located such that the pressure rise across the diffuser could

[2]It has already been commented that neglecting the upstream influence of the diffuser vanes, which acts as an unsteady pressure field in the rotating frame of reference of the impeller, may cause the impeller tip leakage flow to be poorly captured in the single passage mixing plane model, which is carried forward into the isolated diffuser simulations. The specific topic addressed here is the influence of the unsteady impeller exit flow on the diffuser aerodynamics.

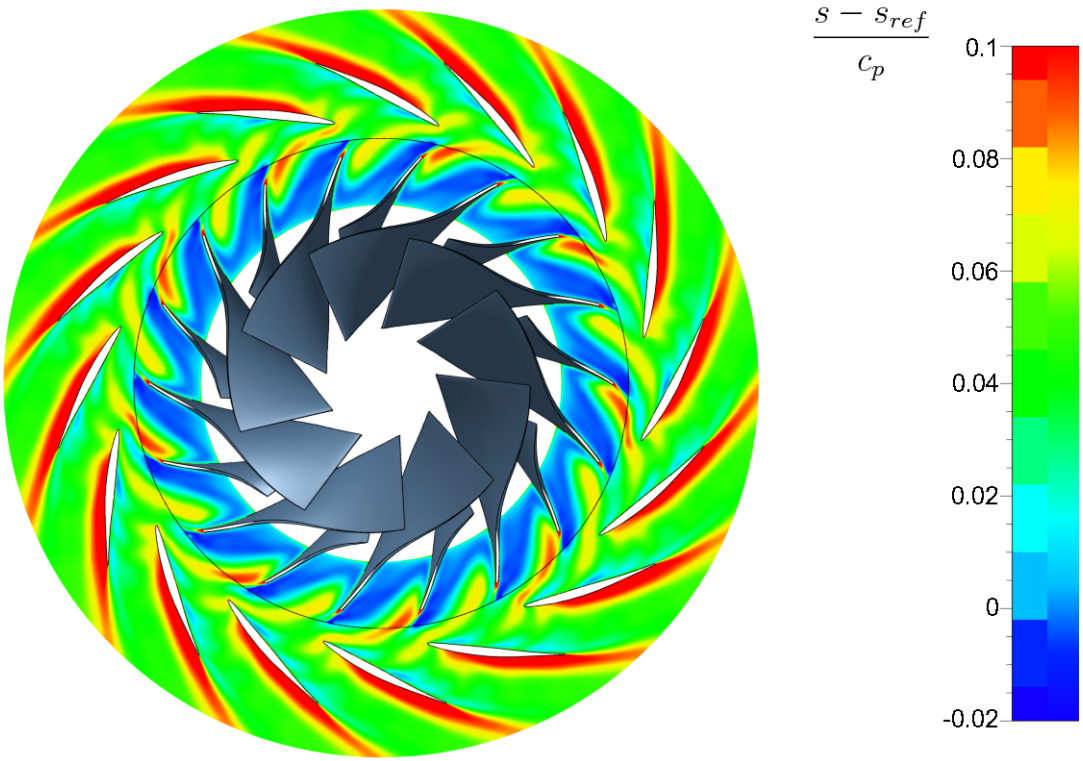

Figure 5-9: Entropy contours from an unsteady full wheel simulation, showing the convection of impeller wakes through the diffuser.

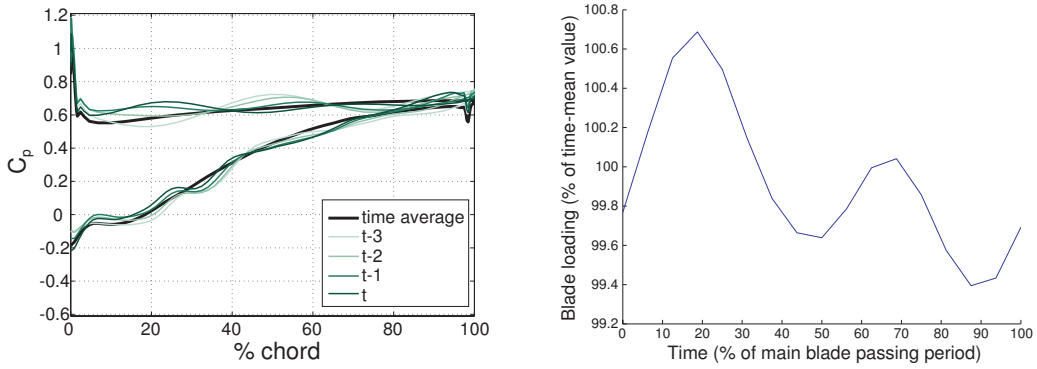

(a) Diffuser loading at 50% span for four snapshots in time.

(b) Integral value of diffuser vane loading at 50% span, showing small variation as main and splitter vane jet-wake convect through diffuser.

Figure 5-10: Diffuser loading at 50% span, showing the effect of impeller jet-wake and viscous wake on the diffuser is relatively small.

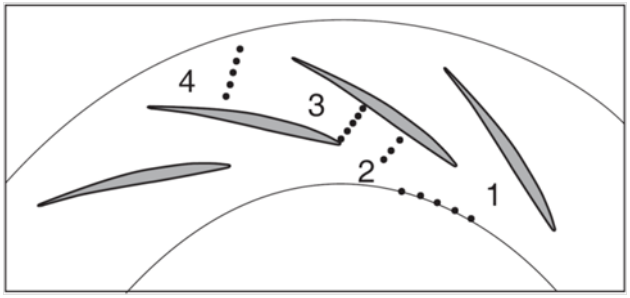

Figure 5-11: Pressure taps used in experiments, adapted from [7].

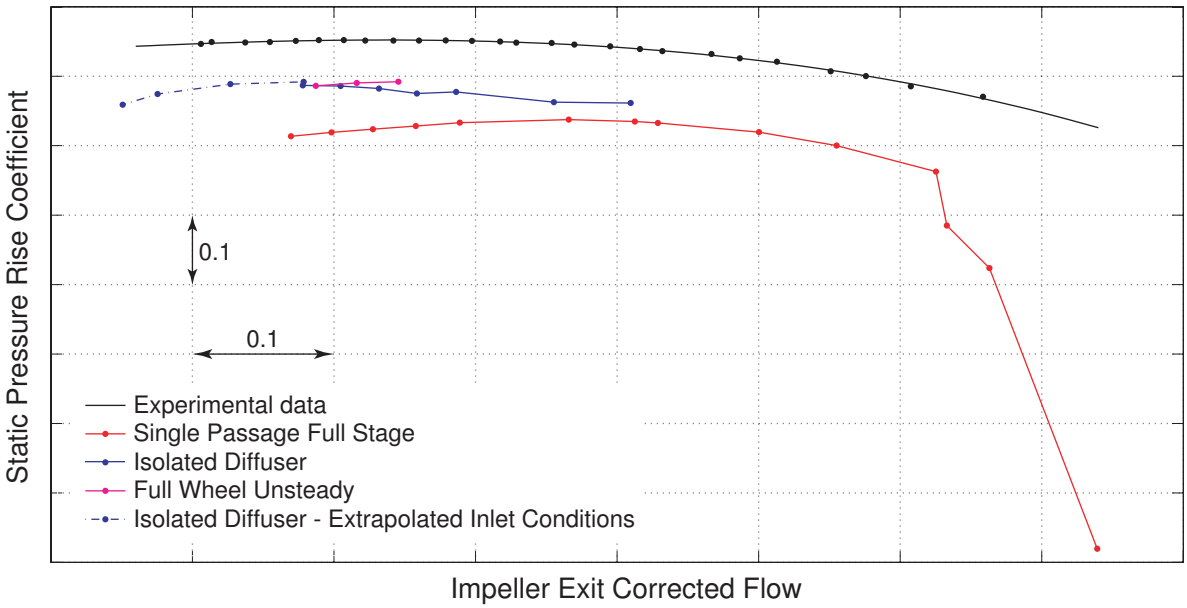

Figure 5-12: Comparison of diffuser pressure rise coefficient between different diffuser models and experimental data.

be broken down into subcomponents. With reference to Figure 5-11, the subcomponents are identified as 1 to 2: the vaneless space; 2 to 3: the semi-vaneless space; and 3 to 4: the diffuser channel. Pressures were taken as the arithmetic mean value between the pressure taps at each location. In addition, pressure taps at inlet to the diffuser (i.e. location 1) and outlet from the diffuser (outer radius in Figure 5-11) provided the overall pressure rise. The pressure rise is non-dimensionalized by the diffuser inlet dynamic head, $p_{t2} - p_2$, to provide a pressure coefficient. The pressure coefficients are shown for the design speedline in Figures 5-12 and 5-13, for a case without bleed flow which experienced spike stall inception.

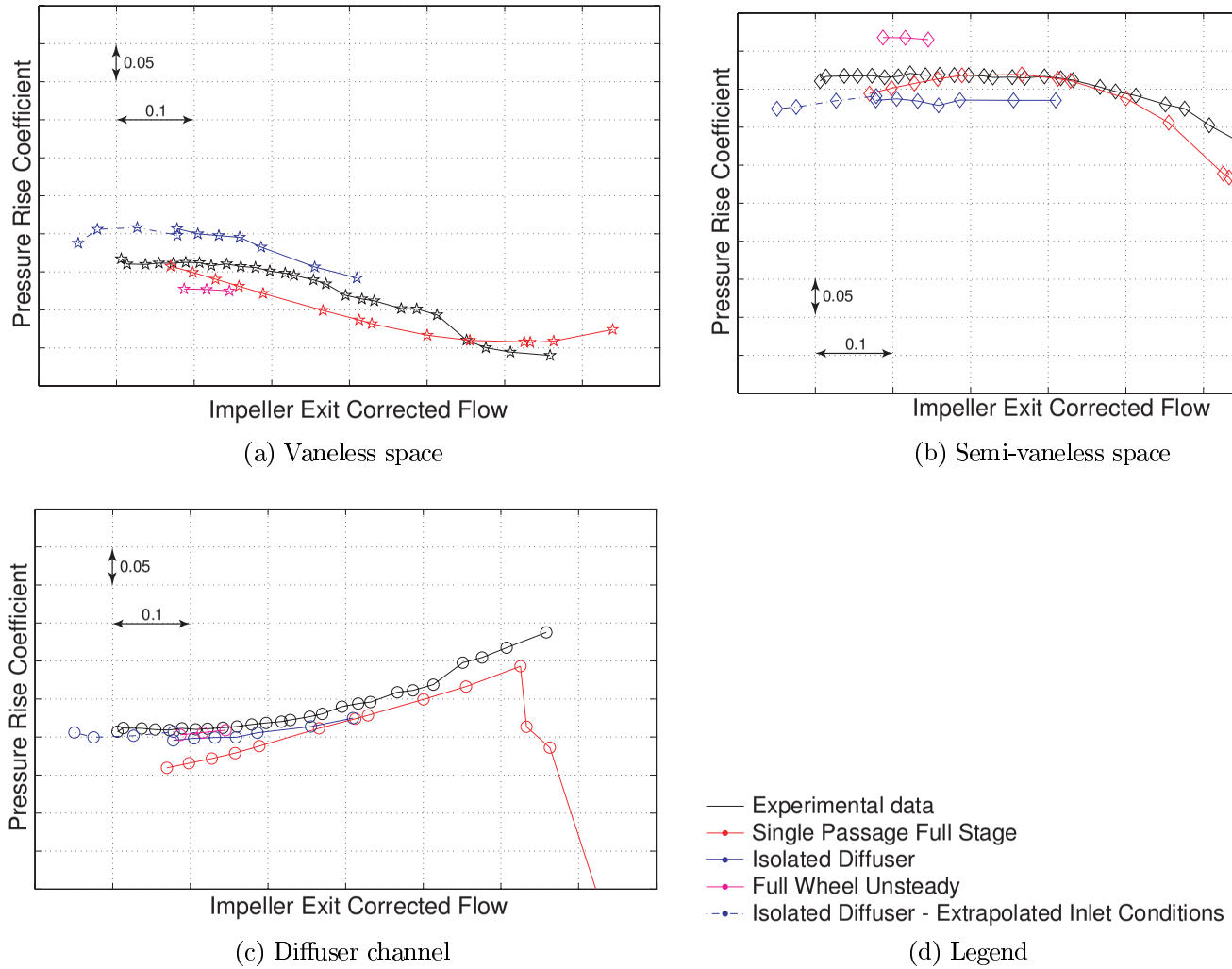

(a) Vaneless space

(b) Semi-vaneless space

(c) Diffuser channel

(d) Legend

Figure 5-13: Comparison of subcomponent pressure rise coefficients between different diffuser models and experimental data.

From the overall diffuser pressure rise characteristic curve, it is clear that all models underestimate the pressure rise achieved in the diffuser. This is consistent with other reported comparisons (e.g. [20, 21]). The pressure rise achieved in the diffuser is sensitive to the level of blockage, particularly near to stall, and the combination of unsteady effects and the limitations of turbulence modeling mean it is difficult to accurately capture the precise performance of the diffuser in the CFD modeling. Therefore, in this comparison, the factors that contribute to identifying a "good" model for analysis of the diffuser stability are as follows:

1. The trends are accurately captured. This largely relates to the slope of the pressure rise characteristic curves. Critically, the peak of the curve should be at the same corrected flow for both the experimental data and the model, as this is an important factor in the type of stall precursor encountered (see Chapter 3).

2. The critical subcomponent is identified by Spakovszky and Roduner [7] as the semi-vaneless space. The gradient of the semi-vaneless space characteristic should closely match between the experimental data and the model.

The isolated diffuser model meets both criteria. This contrasts with the single passage full stage simulations, which show poor agreement across all subcomponent pressure rise curves. The mixing plane used in this model appears not to be able to function adequately in the case of transonic impeller-diffuser interaction, where there exists strong circumferential non-uniformities due to the upstream influence of the diffuser vanes and the jet-wake structure from the impeller. The result is an anomalous diffuser flow field. This is further discussed in Section 5.3.

The most noticeable discrepancy in the isolated diffuser model is the pressure rise achieved in the vaneless space, which moves away from the experiments as the speedline moves towards stall. The removal of the reversed flow at the inlet performed in deriving the inlet conditions modifies the blockage and will improve performance in the vaneless space. Since the extent of reversed flow increases towards stall, this also explains the increasing difference between experiments and the isolated diffuser

simulation at lower flows.

The diffuser channel, which is well constrained geometrically, shows very close agreement between experiments, isolated diffuser simulations and the unsteady full wheel simulations. The full wheel simulations trade reduced pressure rise in the vaneless space with increased pressure rise in the semi-vaneless space (related to where the flow turns when entering the diffuser channel), but, for the three operating points tested, show generally good agreement in slope with the isolated diffuser simulation. It is noted that the experimental data for pressure rise in the vaneless and semi-vaneless space lies between the isolated diffuser case and the full wheel unsteady case.

5.3 Mixing Plane Limitations

It was observed in the subcomponent pressure rise curves that the single passage simulations do not accurately capture the flow field in the diffuser. In fact, when the Mach number at mid-span is compared between the single passage simulations and the isolated diffuser, significantly different flow fields are shown (compare Figures 5-14 and 5-6). The separation on the pressure side of the diffuser vane is drastically increased in the single passage simulation, and there exists a "Mach bubble", a patch of supersonic flow in the vaneless space, the form of which cannot be physically explained. Similar differences in the vaneless space were found in recent paper by Liu et al. [48], who compared unsteady full wheel simulations to steady mixing plane simulations run using the same software used here (Numeca FINE/Turbo), although the diffuser vane separation is not as severe.

The mixing plane flux variables can be rebuilt from the basic variables (e.g. mass flux from radial velocity and density) and plotted on the upstream and downstream mixing plane surfaces, which are physically concurrent, to further analyze the cause of the discrepancies. It was observed that the mixing plane does not entirely mix out the fluxes as described in Section 3.5.1. The mass flux, for example, shows significant circumferential non-uniformity on the downstream surface, showing that the mixing

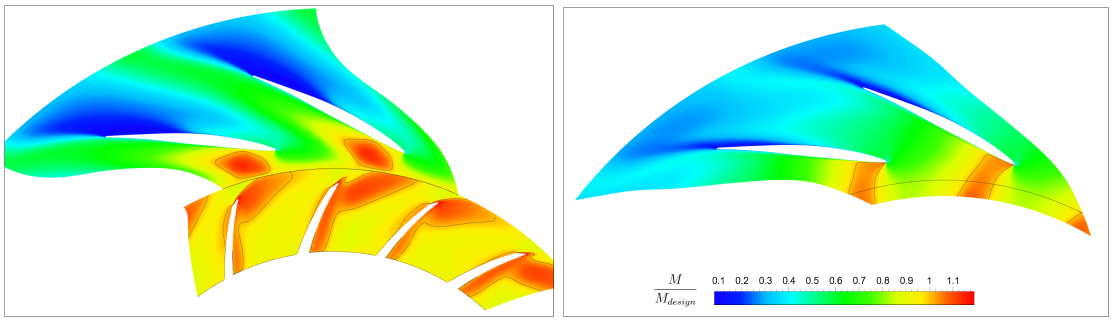

(a) Single passage simulation.

(b) Isolated diffuser simulation. For comparative purposes, location of rotor-stator interface is indicated as black line near inlet.

Figure 5-14: Significant differences between the single passage simulation with mixing plane and the isolated diffuser simulation are revealed through Mach contours at midspan for an operating point near stall. Note the supersonic "bubble" in the single passage calculation (bounded regions show extent of supersonic flow) and the severe separation from the diffuser vane pressure surface.

plane operation is not fulfilling its stated aims in these simulation of a centrifugal compressor. The same was true for the pressure on the upstream surface, as shown in Figure 5-15. This is despite the simulations converging by all typical criteria: negligible change in any particular quantity over 100 iterations, and agreement of inlet and outlet mass flow to below 0.1%.

The plots of pressure and mass flux reveal that the upstream influence of the diffuser vanes significantly affects the mixing plane. There are two significant differences between an impeller-diffuser interface in a centrifugal compressor and an axial rotor-stator interface, for which perhaps the mixing plane is better suited. Firstly, the jet-wake structure of flow exiting the impeller, caused by the Coriolis forces acting within the impeller passages, results in significantly greater circumferential non-uniformity at the exit from the impeller than would be usual in an axial case (except in severe off-design conditions, blade wakes are expected to be small in axial machines). It is suggested this strong non-uniformity is, at least in part, the cause of the circumferential pressure non-uniformity on the mixing plane upstream surface downstream of the impeller blade, given the alignment of mass flow deficit and the areas of high pressure.

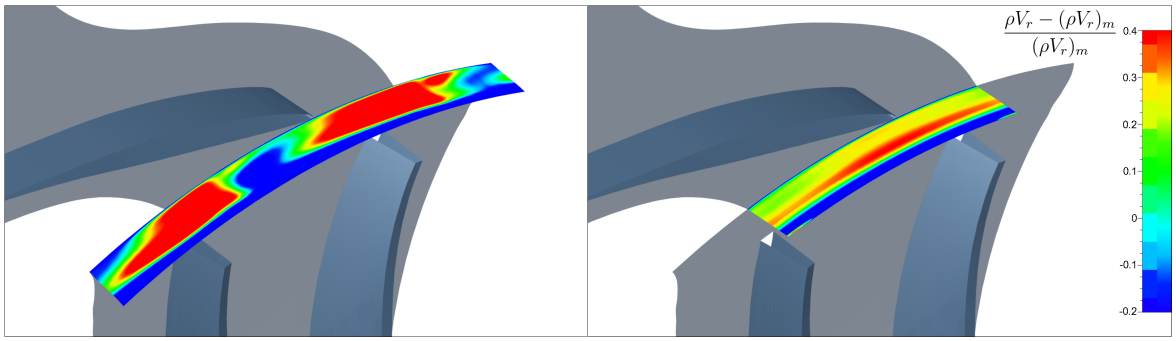

(a) Mass flux on upstream (L) and downstream (R) mixing plane surfaces

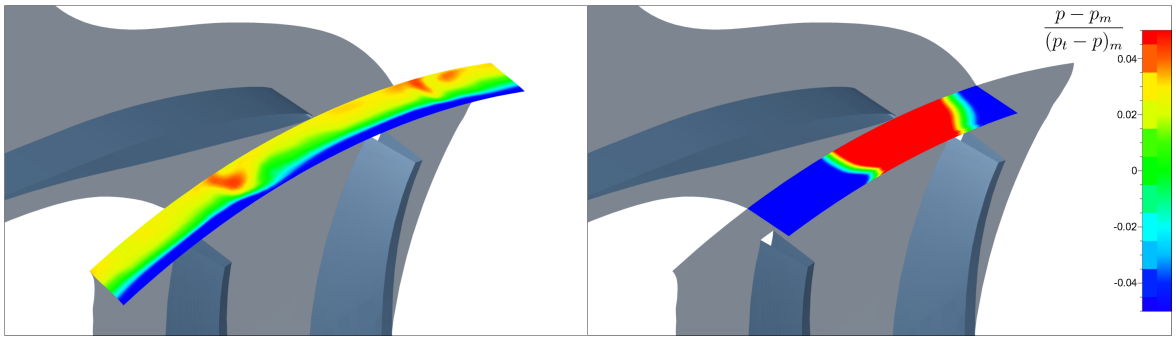

(b) Static pressure on upstream (L) and downstream (R) mixing plane surfaces

Figure 5-15: Correctly implemented and converged, the mixing plane should circumferentially "mix out" downstream mass flux and upstream pressure. The challenges presented by a transonic centrifugal compressor appears to limit its success, as shown by the circumferentially non-uniform mass flux (top right) and pressure (bottom left).

In addition, the upstream influence of the diffuser vanes in a centrifugal compressor is significantly more pronounced than for an axial machine. For a high pressure ratio compressor, the diffuser vanes are highly loaded. The influence of a blade row extends upstream to the same extent as the lengthscale which defines the non-uniformity, and the relevant dimension is the blade pitch. In the case of an axial compressor with a high hub-to-tip ratio, there are many blades, the pitch is small and therefore so too is the upstream influence of the blade row. For the diffuser of a centrifugal compressor, the number of diffuser vanes is an order of magnitude fewer, the pitch is correspondingly larger and the influence of the diffuser vane extends far further upstream than that for an axial machine. This influence is suggested to affect the mass flux as seen on the downstream side of the mixing plane.

When this is combined with the challenging flow conditions in the vaneless space of the compressor (with flow reversal near the shroud, and transonic and highly swirling bulk flow) the limitations of the mixing plane approach are exposed. The time marching scheme iterates until the mixing plane criteria are met with as small an error as possible, while meeting the overall goals of global flux conservation, but the resultant errors significant change the form of the diffuser flow.

Separating the diffuser simulation entirely from the impeller simulation allows the rotor-stator interface to be modeled differently. Firstly, it is possible to select the limits of the computational domain separately for the impeller and the diffuser, for example allowing the entire vaneless space to be modeled in the diffuser simulation. Quantities to be conserved can be carefully selected, such as conserving corrected flow across the interface rather than the physical mass flow to allow Mach number to be more closely matched. Finally, it is possible to explicitly define that variables such as the mass flux are circumferentially uniform. Combined with the selection of a suitable inlet or outlet surface (relating to the first point), this allows a more physically representative boundary condition.

In Section 5.1.4 a region of operation near to stall was identified as anomalous in the single passage stage simulations. This region extended approximately 4% below the corrected flow of the last normal operating point. The isolated diffuser simulations

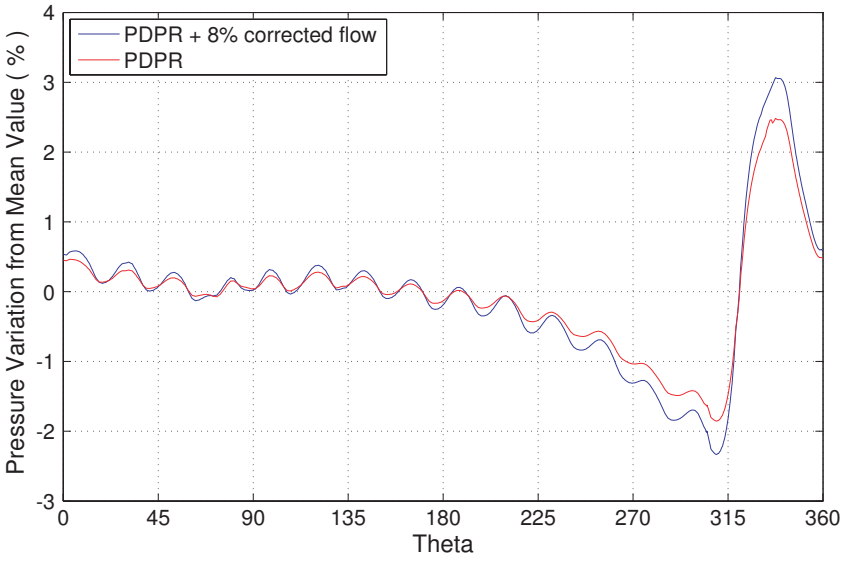

Figure 5-16: Circumferential pressure variations at diffuser exit (mid-span) for two different operating points. Theta is defined as positive clockwise from vertical (see Figure 5-17). The effect of the volute tongue, on the right hand side, dominates and pressure variations on the length scale of the diffuser are relatively small.

converge and provide smooth curves in the pressure rise characteristics of the diffuser and its subcomponents to 6% further beyond this corrected flow, without the sudden transition to stall seen in the single passage simulations. This provides evidence that the influence of the discrepancies within the mixing plane implementation are affecting these simulations, justifying the neglecting of this data.

5.4 Upstream Influence of the Volute

The presence of the downstream volute leads to a pressure non-uniformity at exit to the diffuser, as described in Section 3.4. To examine the effect of the volute in more detail, the volute was included in some of the diffuser simulations, leading to a computational domain including diffuser and volute. The simulations with diffuser and volute are particularly time consuming, as discussed in Chapter 4, and thus few simulations have been performed.

As expected, a distinct pressure non-uniformity at diffuser exit is observed, varying according to the operating point as shown in Figure 5-16. Envisaging the diffuser as

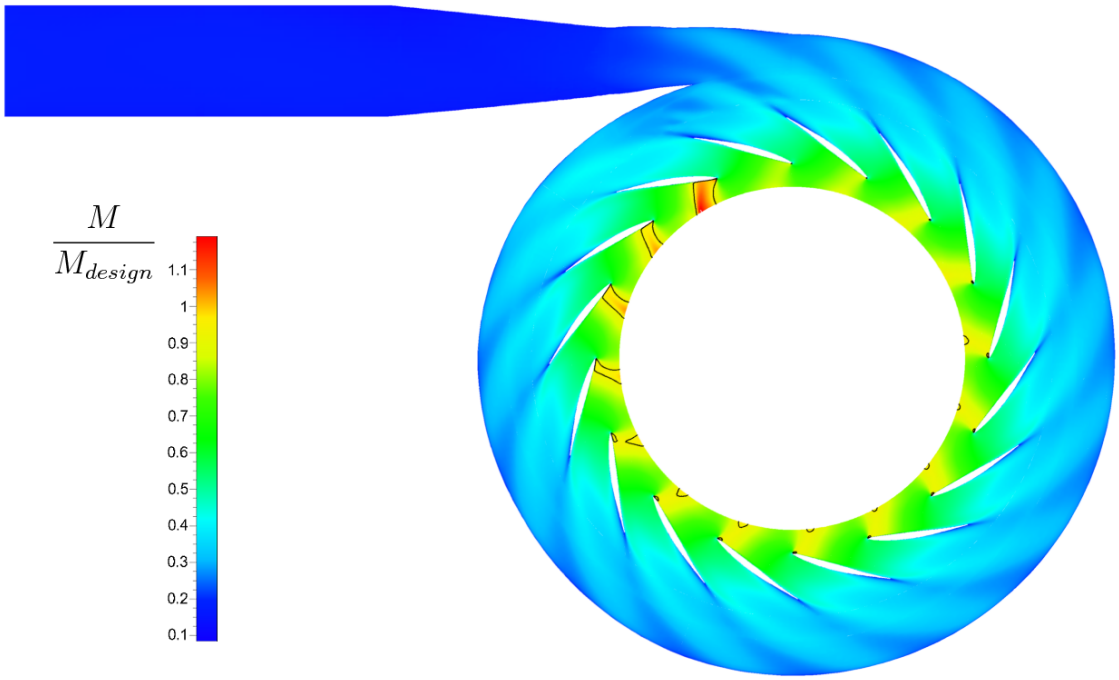

Figure 5-17: Mach contours at mid-span; M>1 is shown as bounded region.

a series of diffusing passages, it is clear that there is variation in the total-to-static pressure ratio around the circumference (noting that the inlet total pressure is fixed by the inlet conditions). The total-to-static pressure ratio controls the mass flow and the Mach numbers within the passages, and therefore there is no longer uniform mass flow distribution between the passages, as in the isolated diffuser simulations. This is the conclusion also reached in Section 3.4.

The volute is reasonably well matched with the diffuser flow in these simulations, which is evident by the fact the pressure is nearly uniform around the circumference except near to the tongue. The high pressure region seen in Figure 5-16 is directly upstream from the tongue (along a streamline). In the adjacent region, where passages experience a low back pressure, the flow into the diffuser passage chokes and flow is diverted into adjacent passages (Figure 5-17 shows supersonic flow bounded by black contour). The passages between 12 and 2 o'clock in Figure 5-17 experience higher pressure ratios and the mass flow rate through these passages is lower than average.

The diffuser and volute model suffers a shortfall in that the flow angle is not able

to respond to the upstream influence of the volute tongue, as the diffuser inlet flow angle is a defined inlet parameter. This is discussed above in context of the upstream influence of the diffuser vanes, but it is much more significant for the volute. It was suggested, in the context of the diffuser vane upstream influence, that moving the upstream domain boundary upstream could provide an improvement to the model. This is evidently not practicable for the upstream influence of the volute because the upstream influence from the volute extends through the entire impeller. In the real device, the impeller flow has opportunity to adjust to the presence of the volute at the impeller inlet, and this cannot be captured except with a full compressor (impeller, diffuser and volute) model, which is currently computationally prohibitive except for targeted calculations.

5.5 Summary

In this chapter, a methodology was outlined for deriving the inlet and outlet boundary conditions enabling a single blade-row, vaned radial diffuser simulation. The exit conditions are derived here from single passage simulations of the centrifugal compressor, although the same methodology could in principle utilize data from unsteady, sliding mesh simulations of the compressor or experiments.

A mixed out average flow state was calculated at each spanwise location to determine the pitchwise uniform total pressure, total temperature and flow velocity vector. Thus a spanwise profile was built up which supplied the inlet conditions for the isolated diffuser simulations. An adjustment was made to prevent reversed flow at inlet to the diffuser, which causes an ill-posed numerical problem.

The exit conditions, which determined the mass flow either directly or through the definition of the backpressure, were set such that the corrected flow in the vaneless space is matched with the corrected flow at the same location in the single passage, stage calculation. This completed the matching criteria.

The steady-state isolated diffuser calculations were compared to experimental data previously collected by Spakovszky and Roduner [7] for the same compressor geometry

and also to unsteady, full wheel compressor simulations run for validation purposes. The subcomponent pressure rise coefficients showed good agreement between experiments and the isolated diffuser simulations; the trends in the slopes of the curves are well captured, important for assessment of the stability of the flow, and the diffuser channel showed excellent quantitative agreement. It is suggested that the absence of pitchwise mixing and unsteady effects in the vaneless space leads to poorer agreement for that subcomponent.

Against the full wheel unsteady simulations, good quantitative and qualitative agreement was shown although the total pressure and temperature at the shroud side of the vaneless space appears to be underestimated; the total pressure, for example, is underestimated by approximately 10% of the total pressure rise though the impeller at 10% of the span from the shroud. It is hypothesized that this is caused by not capturing the unsteady pressure field felt by the impeller as a consequence of rotating through the upstream influence of the diffuser vanes (as put forth by Shum et al. [22]).

In addition, the validation of the isolated diffuser model revealed discrepancies in the results of the single passage, full stage simulations. The mixing plane utilized in this latter model, to allow the unsteady rotor-stator interface to be modeled as steady, appears unable to meet its convergence criteria for a transonic, highly loaded centrifugal compressor with vaned diffuser operating near to stall. The jet wake structure, unique to centrifugal compressors, and the diffuser vane upstream influence, which has a much greater impact in centrifugal compressors due to the larger pitch, are two causes of significant pitchwise non-uniformity which do not appear to be successfully mixed out by the mixing plane under these conditions.

Finally, the effect of the volute was analyzed through the addition of a volute to the isolated diffuser model. This presents a pitchwise non-uniform exit pressure to the diffuser, resulting in significant differences between each diffuser passage around the diffuser annulus; most significantly, the diffuser passage upstream of the diffuser tongue experiences low flow due to the high pressure caused by the stagnation point on the tongue while adjacent passages are choked due to low backpressures. Since

the upstream influence of the volute extends to the impeller inlet, it is likely that the diffuser and volute simulations are not able to accurately capture the blade-to-blade non-uniformity at the diffuser inlet, for example in total pressure or flow direction. It seems likely that, to capture this correctly, a full compressor model (with impeller, diffuser and volute) using an unsteady flow solver would be required.

Chapter 6

Diffuser Flow Stability Assessment

The assessment of stability in the diffuser flow follows a common approach for dynamic stability problems - apply a short timescale external forcing and determine how the system reacts. An analogy can be made with a mechanical system; by applying a forcing to a mass, spring and damper system, it is possible to determine whether the system adds energy to the resulting motion (i.e. negative damping) resulting in instability, or whether there exists positive damping sufficient to reduce oscillations towards a stationary equilibrium. The stability of flow within the diffuser is more complex, but the same concept applies.

This chapter describes the simulations performed using the isolated diffuser to test the stability of the diffuser flow. The structure is as follows: first the approach for assessing the stability of the diffuser flow is described, along with an introduction to the methods used to reduce the large quantity of data generated by the unsteady simulations. The methodology for applying the perturbation was described in Chapter 4.

Secondly, the results of the stability assessment are discussed, with a new development for the criteria required for spike stall precursors to form and grow in the vaned diffuser of a centrifugal compressor.

Thirdly, simulations without the buffer zone are described. These use a mass-flow exit boundary condition with velocity scaling, which is known to cause non-physical effects in unsteady simulations. However, the interaction of vorticity and pressure

waves observed in these simulations, which lead to instability, have a physical analogy with the results from Spakovszky [28] and this is explained further in Section 6.3. It is noted that these simulations were performed with a mismatched diffuser, as they occurred before the matching procedure had been finalized. For this reason, detailed results are not provided; only an overview of the observed response to the perturbation is provided.

The effects of the volute are discussed in Section 6.4. Again, these simulations were performed before the matching criteria was finalized, and the discussion is largely qualitative for this reason. The chapter is concluded with suggestions for an extended parametric study to provide verification on the proposed mechanism for stall inception, in Section 6.5.

6.1 Approach

The objective of this project is to determine why the diffuser flow becomes unstable, elucidating what features of the diffuser inlet flow play a role in the onset of instability. This can be determined through the examination of the features of the diffuser flow field as the operating point moves towards stall and eventually becomes unstable, but it can be challenging to identify the features responsible for instability. As described in the technical approach (Chapter 2), a complementary approach is to parametrically vary the inlet conditions describing the diffuser inlet flow. Using both approaches, a criterion for stall inception can be developed and Hypothesis III - that spanwise flow non-uniformity plays a role in instability - can be tested.

To determine whether the operating point is stable or unstable, two indicators are used. The use of a forced response experiment has been discussed earlier in this chapter, but the first indicator is simply the convergence of the simulation. It is common for the limit of stability to be estimated via the limit of convergence of steady simulations [36], and it is shown that this underestimates the range of stable operation. Using unsteady simulations improves the situation (as discussed below) but it is shown that unsteady simulations of the isolated diffuser can converge which

are then dynamically unstable following a perturbation.

The forced response numerical experiments utilize a total pressure forcing to perturb the flow in the diffuser. This is representative of a flow disturbance from the impeller. The stability of the diffuser flow is not expected to be particularly sensitive to the form of the perturbation, and some tests are performed to test this assumption as described in Appendix A. Future work could extend this sensitivity study.

The choices made in the definition of the perturbation are listed in Table 6.1, and the 2D definition of the perturbation is illustrated in Figure 6-1. It is desired that the perturbation is small in spatial and temporal extent, so as to excite multiple wavelengths, and this guides the choice for the period of application and the size. The location of the perturbation was chosen to be on the shroud side, as it is this side that contributes most towards the blockage at diffuser inlet (see Figure 5-2). Given the hypothesis that the spanwise variation in the flow parameters impacts the stability of the diffuser flow it seems reasonable to assume that this side will be more sensitive to the application of a perturbation. A large amplitude disturbance is chosen to improve the probability that the perturbation will trigger instability. Each of these choices could be the subject of a future sensitivity study; only changing the form from a forcing to a deficit in total pressure, and testing a shorter timescale for application were tested due to time constraints. However, neither of these changes made a significant impact on the form of the response, supporting the assumption that the response is insensitive to the precise form of the perturbation.

6.1.1 Data Reduction

Consistent with the experiments performed by Spakovszky and Roduner [7], unsteady pressure readings were taken at various points around the circumference of the diffuser. The location of the unsteady pressure taps is shown in Figure 6-2, adapted from their paper.

By plotting the pressure readings from these pressure taps offset proportionally to their circumferential position and suitably non-dimensionalized by the diffuser inlet dynamic head, it is possible to observe the formation and growth of stall precursors.

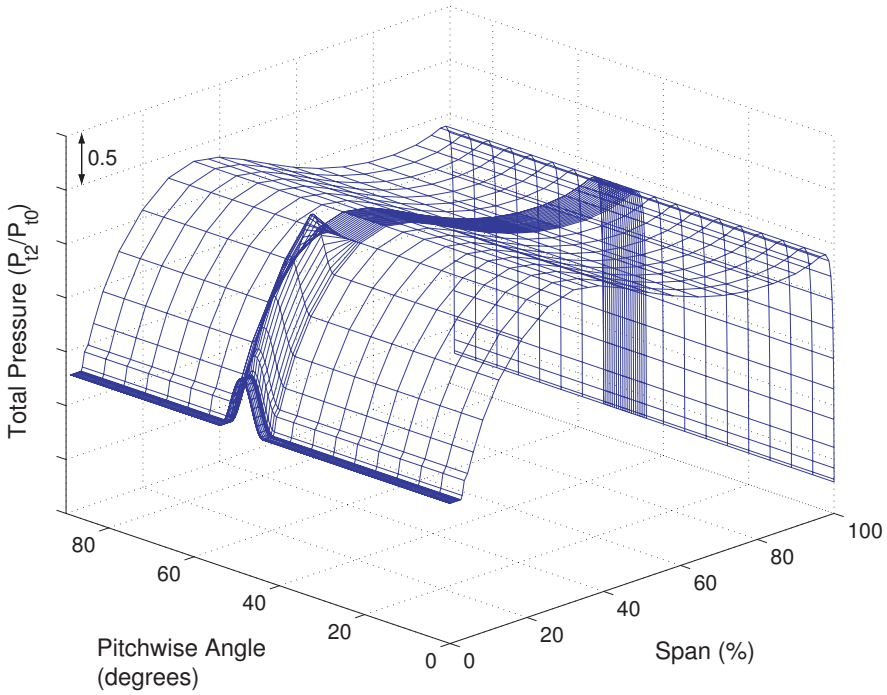

Figure 6-1: Perturbation applied in total pressure.

Property	Value
Spanwise extent	10%
Pitchwise extent	10°
Temporal extent	$\frac{1}{4}$ rotor revolution
Function	$\sin^2 x$
Amplitude	25% diffuser inlet dynamic head

Table 6.1: Summary of total pressure forcing used to perturb steady-state diffuser flow for stability assessment.

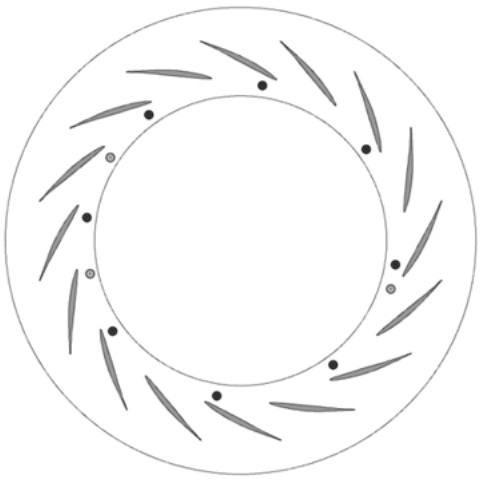

Figure 6-2: Unsteady pressure tap locations, adapted from [7]. Dark pressure taps indicate those that are evenly spaced.

This is the primary method of data reduction. Where further analysis is desired, small flow changes (perturbation quantities) can be observed by calculating the difference from the steady state flow. For example, the change in pressure over time was observed by subtracting the steady state pressure, taken from the converged, steady state solution from the initialization simulation (see Section 4.5), from the time-dependent pressure; this allows the detection of pressure waves through the diffuser. This is represented by:

$$p' = p(t) - \bar{p}$$

where p' is the perturbation in the pressure, $p(t)$ is the unsteady pressure, and $\bar{p}$ is the steady state pressure condition.

Without this step, the type of small changes evident in the simulated stall precursors cannot be detected over the large scale changes in properties across the diffuser - for example, the pressure rise through the diffuser which is of the order of the inlet dynamic pressure - masks any small changes in pressure from a rotating disturbance. Animations of vorticity waves or the perturbation in velocity at cuts at 10%, 50% and 90% span were found to be beneficial in understanding the physics of the diffuser flow. Frames from the animations are included in the discussion below.

6.2 Formation of Stall precursors in Isolated Diffuser Simulations

The isolated diffuser simulations (with the buffer zone) proved stable to the application of a perturbation throughout the range used in the steady, single passage, mixing plane solutions. This necessitated the use of extrapolation of the inlet conditions to provide inlet conditions for lower flow cases (as described in Chapter 4). The diffuser inlet corrected flow is reduced to 10% below the value at which the last converged, normal operating point is achieved in the single passage, stage simulations before becoming unstable to the application of the perturbation. Simulations at 14% lower corrected flow were attempted, but obtaining a converged steady state solution was not feasible. This suggested that the diffuser stability limit is exceeded.

For future reference the point of peak diffuser pressure rise is identified from Figure 5-12 as "PDPR". As can be seen from the figure, PDPR closely coincides with the corrected flow for the last stable operating point obtained with the single passage stage simulations.

As the diffuser inlet average corrected flow is reduced (i.e. as the speedline was followed towards stall) the response to the perturbation slowly changes. Plotted in Figure 6-3 is the response at corrected flows 4%, 8% and 10% below that of PDPR.

The perturbation is applied at time zero for a period of one quarter of a rotor revolution. For the former two operating points, the effect of the perturbation can be seen to travel around the circumference of the diffuser, as detected via the pressure taps within the vaneless space, for approximately 75% of the circumference, before they can no longer be detected.

At a corrected flow 10% lower than PDPR, the response to the perturbation becomes unstable. This operating point is identified as the lowest corrected flow (furthest to the left) for the isolated diffuser simulations in Figures 5-12 and 5-13. Following the perturbation, a disturbance travels around the circumference in a similar manner as before, but with a high frequency oscillation within the pressure traces. If the rotating disturbance (stall precursor) is broken down into the high frequency

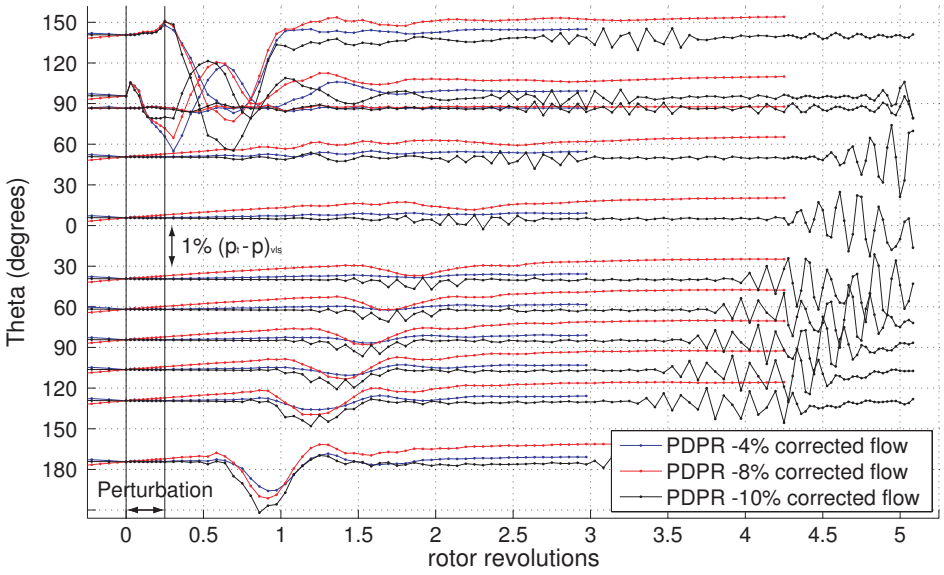

Figure 6-3: Response to perturbation for three different operating points near to stall.

component superimposed onto a first-order oscillation, it is evident that the latter is increasing in amplitude over time. This is shown more clearly in Figure 6-4. At approximately six rotor revolutions, the precursor has traveled twice around the circumference and the flow within the diffuser enters a different regime, such that an individual diffuser passage does not recover following the passing of the stall precursor, and the entire diffuser experiences unsteady flow. This is accompanied by a slight pressure drop at the position of the pressure taps, and a marginal reduction in mass flow (approximately 0.1%).

The diffuser flow field cannot be described as "stalled" but it does enter an alternative, unsteady operating regime. It is unlikely that the isolated diffuser model can accurately capture a fully developed rotating stall cell, or the embryonic stall cell envisaged by Camp and Day [4] to be the physical cause of the spike. The inlet boundary condition has pitchwise uniform flow angle and total conditions, and for a rotating stall cell, significant spanwise non-uniformity is expected. In addition, the exit boundary condition enforces a constant and uniform pressure, such that a reduction in the pressure rise across the diffuser cannot be modeled. Since the isolated diffuser model

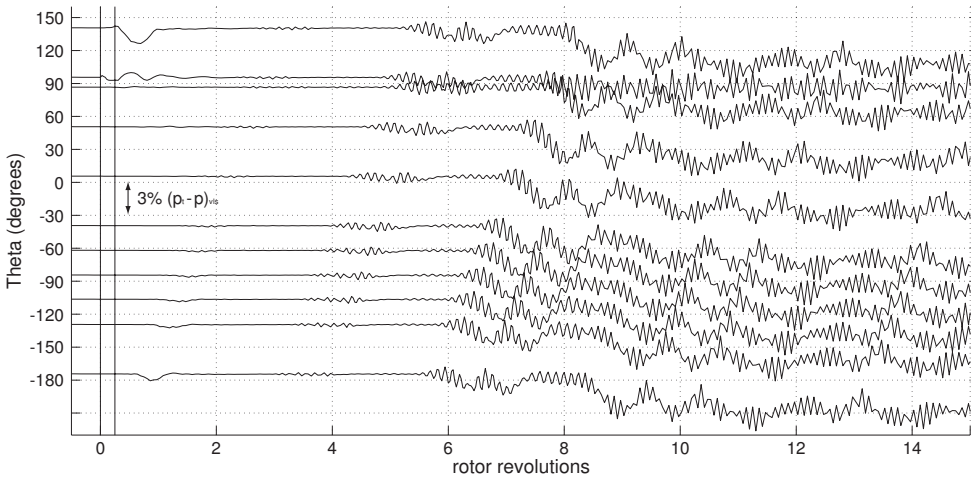

Figure 6-4: Response to perturbation at a corrected flow 10% lower than PDPR.

cannot currently capture these two features, it is likely instead that the accuracy of the solution will diminish, eventually leading to numerical divergence. As an example of this, it is noted that the global residuals from the conservation equations solved implicitly in the time-marching scheme[1] increase during the development of the stall precursor, before reaching a steady value associated with the quasi-equilibrium state seen after approximately eight rotor revolutions. The residuals increase by an order of magnitude, but the absolute value of the residuals is very small prior to the application of the perturbation such that it is considered that the development of the stall precursor is accurately modeled.

Given that the stated aim of this project is to investigate the stall precursors, it is the development of the stall precursor which is of more interest than the final developed solution, and thus the model is considered sufficient.

6.2.1 Development of a Stall Precursor

As the diffuser inlet corrected flow is reduced, the flow angle at inlet to the diffuser is increased, as shown in Figure 5-4. This has a marked effect on the shroud endwall

[1]The definition of the global residual, as defined in [38], is as follows:
Normalized residual = $RES = \sum$(fluxes / cell volume)
Global residual = $\log_{10}\left(\sqrt{\bar{RES}^2}\right)$

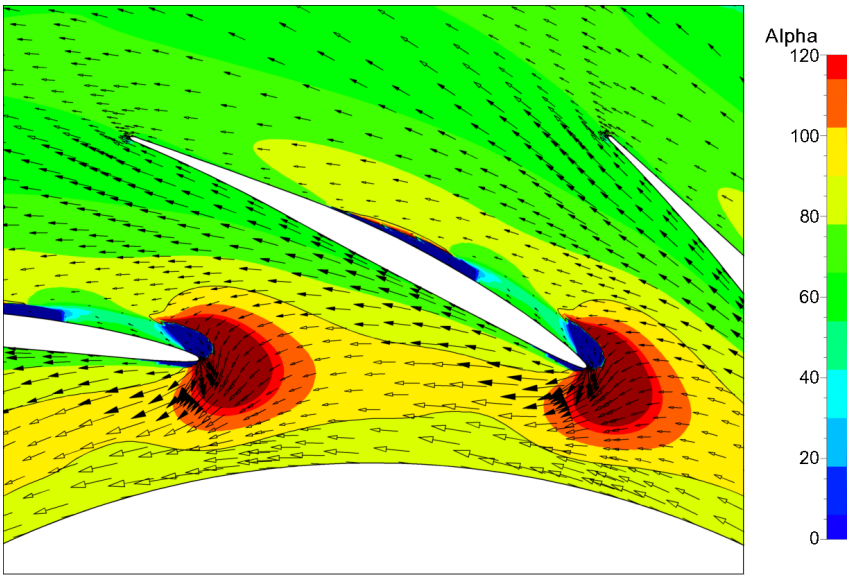

Figure 6-5: Flow angle and vectors at 94% span (near shroud) for an operating point 10% below PDPR. Radial flow reversal is indicated by regions with flow angle greater than 90° (bounded by black contour). Note beyond the colormap limits, the angle is presented as the limiting color, and a wrapping effect from 180° to -180° occurs on the pressure side near the leading edge.

flow[2].

It was observed in the stage simulations that the shroud side endwall flow is reversed at inlet to the diffuser; i.e. the radial velocity component shows flow passing from the diffuser into the impeller. This was removed by limiting the minimum value of radial velocity (see Section 5.1.2). Despite this limit, the shroud endwall flow very quickly reverses at inlet to the diffuser, as shown by Figure 6-5 (marked by the yellow and red contours).

The pressure gradient in the vaneless space is largely set by the highly swirling flow from the impeller, although the upstream influence of the diffuser vanes also has an effect in turning the flow. Neglecting the latter effect, the radial pressure gradient is a function of V_θ^2/r. The pressure variation across the span can be considered small compared to variations in either of the other dimensions, since streamlines show little axial movement which would indicate axial pressure gradients. The mass

[2]The flow on the shroud is deliberately not referred to as "the shroud endwall boundary layer" since the diffuser inlet flow is much more complex than a bulk flow with boundary layers on each endwall; the flow profile varies continuously from hub to shroud as shown in Chapter 5.

flow weighted averaged value of V_θ can be taken as the appropriate value for this purpose. The fluid near the endwalls, which has less momentum, experiences the same pressure gradient as that near the center of the diffuser, and conservation of momentum requires the endwall flow to be turned to a greater extent. This causes flow reversal near the shroud such that the radial component of velocity becomes negative, or equivalently, that the flow angle exceeds 90°.

While the radial velocity component reverses, the tangential or swirl component is still large, given the flow has just exited the impeller. What then occurs is an area of partially recirculating flow, with fluid first flowing radially outward, then reversing to flow inward toward the impeller, while swirling around the diffuser (with small axial motions allowing the switch between forward and reversed flow).

The difference between the operating point which exhibited instability (PDPR -10%) and the adjacent, stable operating point (PDPR -8%) is identified through the convection of vorticity in the flow. The total pressure perturbation locally increases the flow across the small region where it applied and this causes a change in the axial component of vorticity on either side. The forcing is applied at the shroud, where the aforementioned flow recirculation occurs. Following the perturbation, the vorticity changes convect around the vaneless space, within the area of recirculating flow. The difference between the stable and unstable operating points appears to be whether the flow recirculation allows the vorticity changes to convect out of the vaneless space through the diffuser passages, or whether they continue around the circumference, and accumulate over time. Particle traces, as shown in Figure 6-6, reveal the presence of recirculating flow in the vaneless space. This is present at 90% span for all operating points illustrated, but it is only the unstable operating point which exhibits flow circulating around the entire circumference at 80% and 70% span. It is suggested that it is the extent of the recirculating flow which allows vorticity perturbations to convect around the entire circumference. However, without a mechanism by which the vorticity perturbations are amplified, fluid viscosity would damp out the disturbance, the diffuser flow would return to the initial steady state and the operating point would be deemed stable. The separation of flow at the diffuser

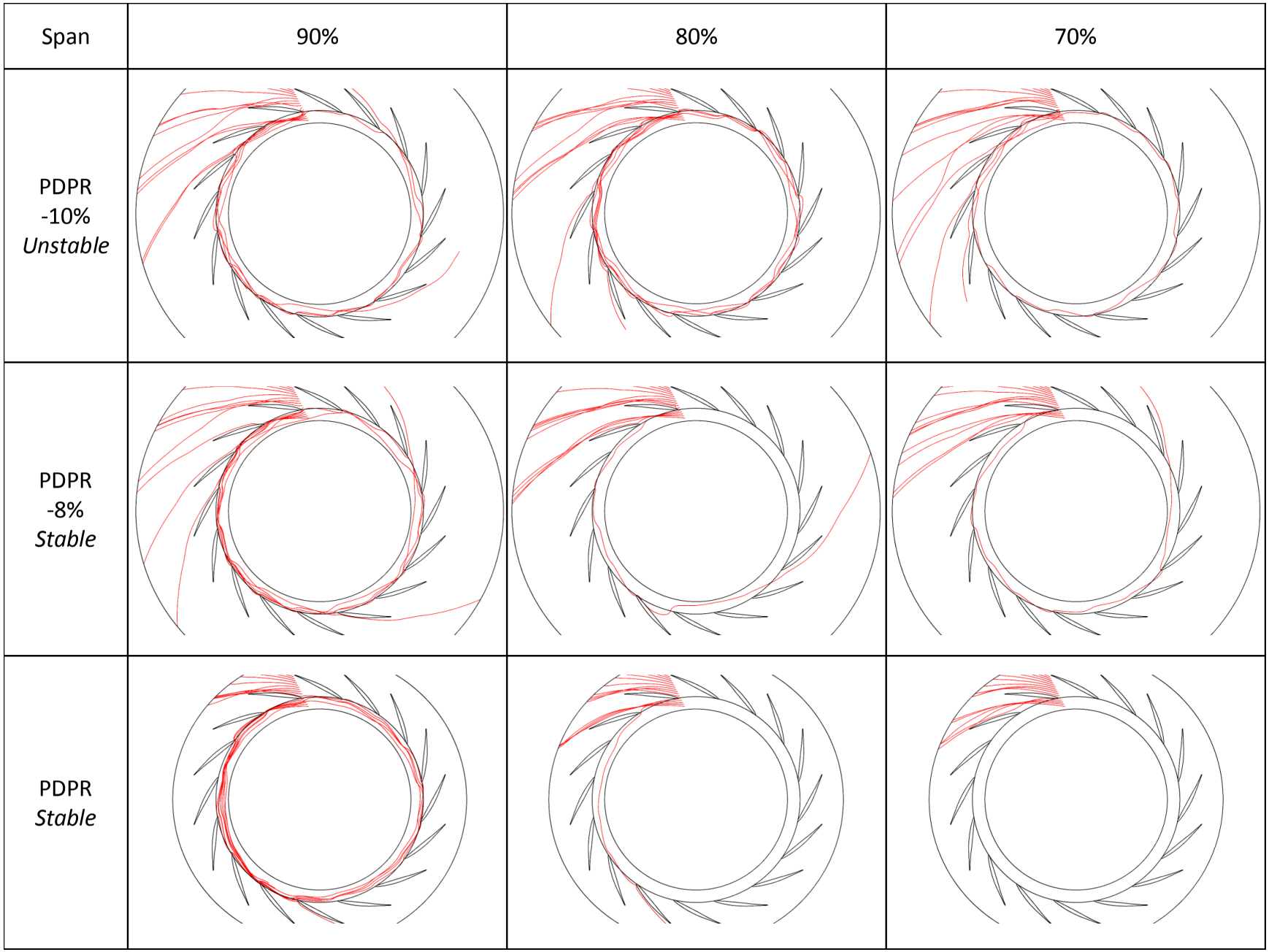

Figure 6-6: Particle traces for operating points close to stall, showing convection around circumference across 30% of the span for the unstable operating point (10% below PDPR).

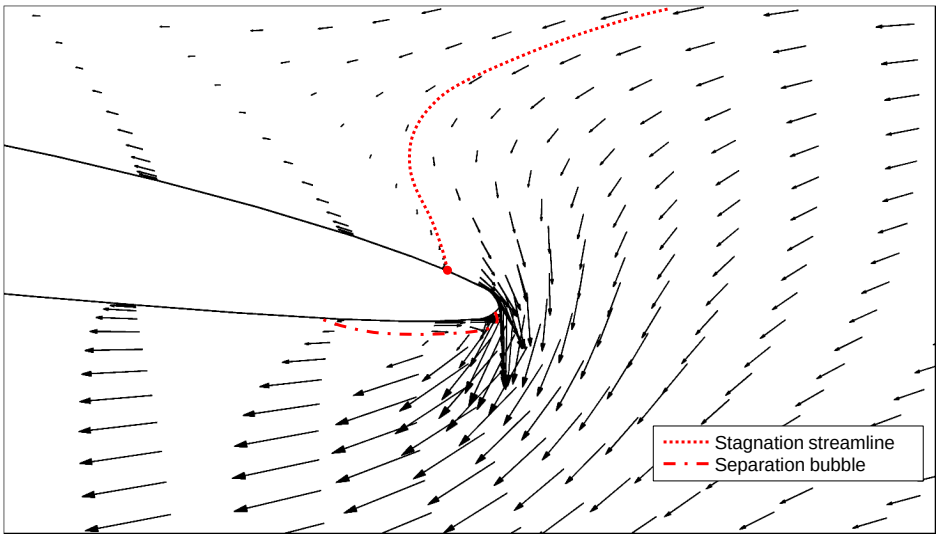

Figure 6-7: Velocity vectors at the diffuser vane leading edge 90% span indicating separation bubble at diffuser vane leading edge.

vane leading edge provides such a mechanism.

From vector plots of the velocity near the leading edge, it can be seen that the simulations predict a significant separation bubble in the corner between the leading edge of the diffuser vane (on the suction side) and the shroud endwall. This extends across approximately 18% of the span prior to application of the perturbation.

When the total pressure perturbation is applied at the inlet, as well as creating a source of axial vorticity at the diffuser inlet, it also causes a local increase in the mass flux, changing the incidence on the diffuser vane leading edge downstream of where it is applied and reducing the diffuser vane loading. The variation in incidence causes the separation bubble to change, both in terms of the point of separation and the size, and causes vorticity to be shed from the leading edge. Due to the reversed radial flow in the semi-vaneless space, this additional vorticity partly convects into the vaneless space and strengthens the vortical structures already present there. This is shown in Figure 6-8.

Some flow is spilled onto the adjacent diffuser passage as a result of the perturbation, changing the circulation on the following vane. Again, the incidence, separation location and circulation around that diffuser vane is altered, resulting in a shed vor-

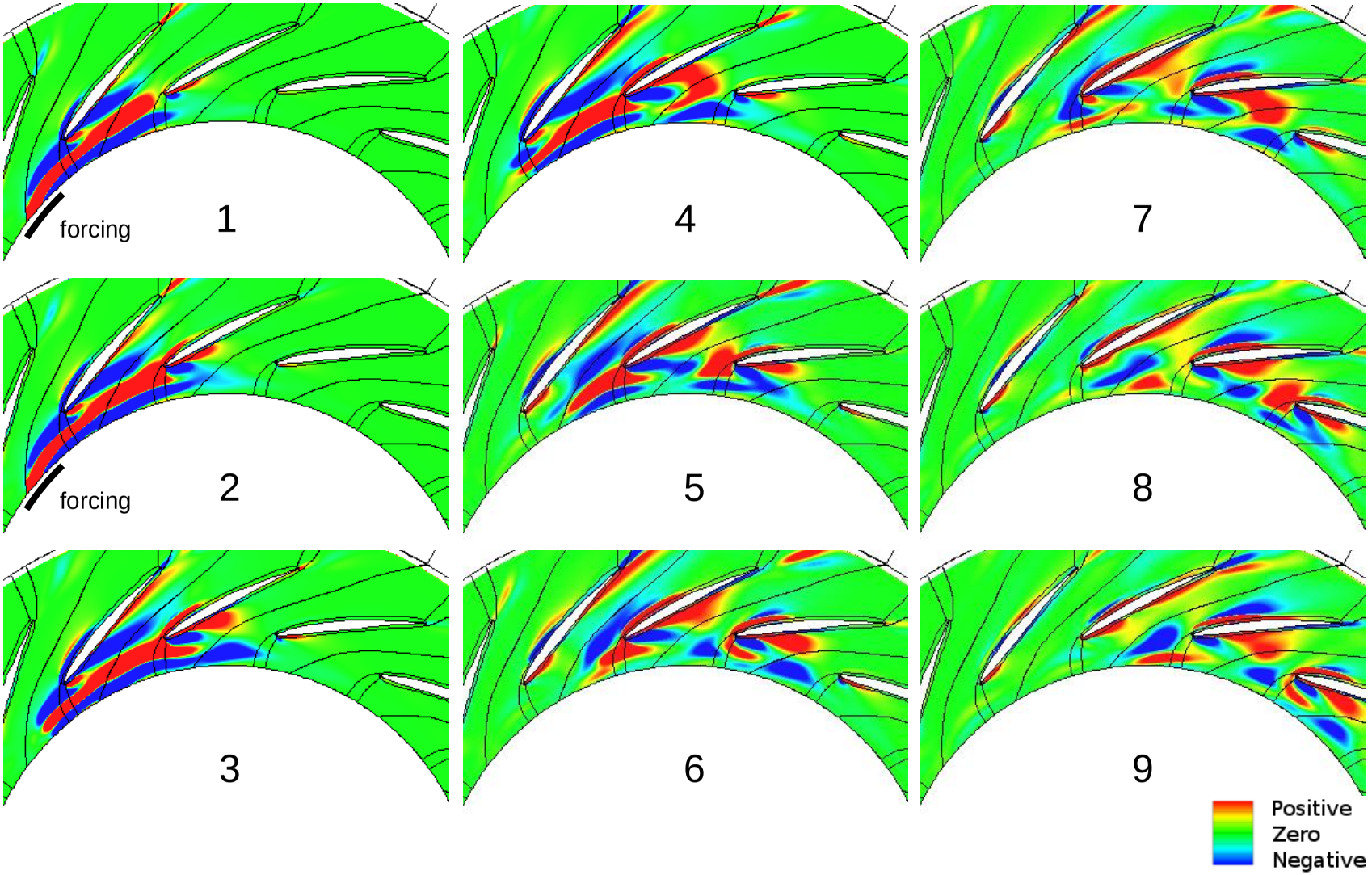

Figure 6-8: Convection of the vorticity changes ω_z' following application of the perturbation, as seen from a section at 90% span, at an operating point 10% below PDPR. Vorticity shedding from the leading edge as a consequence of the perturbation is convected into the vaneless space, as shown by region of blue convecting from the center vane. Frames are shown every 1/18th of a rotor revolution.

tex. In this manner, the effect of the perturbation moves around the diffuser (certain similarities exist with the original theorem of Emmons et al. [49] for the propagation of a rotating stall cell) and vortices in the vaneless space are strengthened.

An alternative representation of the vorticity is to plot the perturbation velocity vectors, defined by:

$$\underline{V}' = \underline{V}(t) - \bar{\underline{V}}$$

This is shown in Figure 6-9, and compared with the previous representation of ω_z'. This plot clearly represents the vortical structures which exist following a complete revolution around the diffuser.

The vortices, as represented in Figure 6-9, are present across approximately the same proportion of the span as the separation bubble, i.e. 18% span. Further across the span, the vortex lines for vorticity shed from the diffuser vane are twisted as the convection velocity becomes more radial.

The vortices convecting in the vaneless space are responsible for the high frequency oscillation in the pressure traces. Where the flow has additional rotation to that which existed prior to the perturbation, a pressure gradient is required to support that rotation, with lower pressure in the center. Thus, as the vortices convect past the pressure sensor location, the pressure falls and then rises again. This is confirmed through an analysis of the flow angles at the same radius and circumferential positions as the pressure taps (the axial position is moved to mid-span remove endwall effects); the pressure fluctuations correspond with variations in alpha in the diffuser flow, as shown in Figure 6-10. Figure 6-9 there are multiple counter-rotating vortical structures which form in the vaneless space, and this can be also seen from Figure 6-10. The number of vortical structures appears to grow over time, but their size is limited by the size of geometry of the isolated diffuser simulation and the constraint of a pitchwise uniform inlet velocity direction. This constraint is suggested to set the frequency of the oscillations in the pressure trace, which shows approximately seven oscillations at a given pressure tap per rotor revolution.

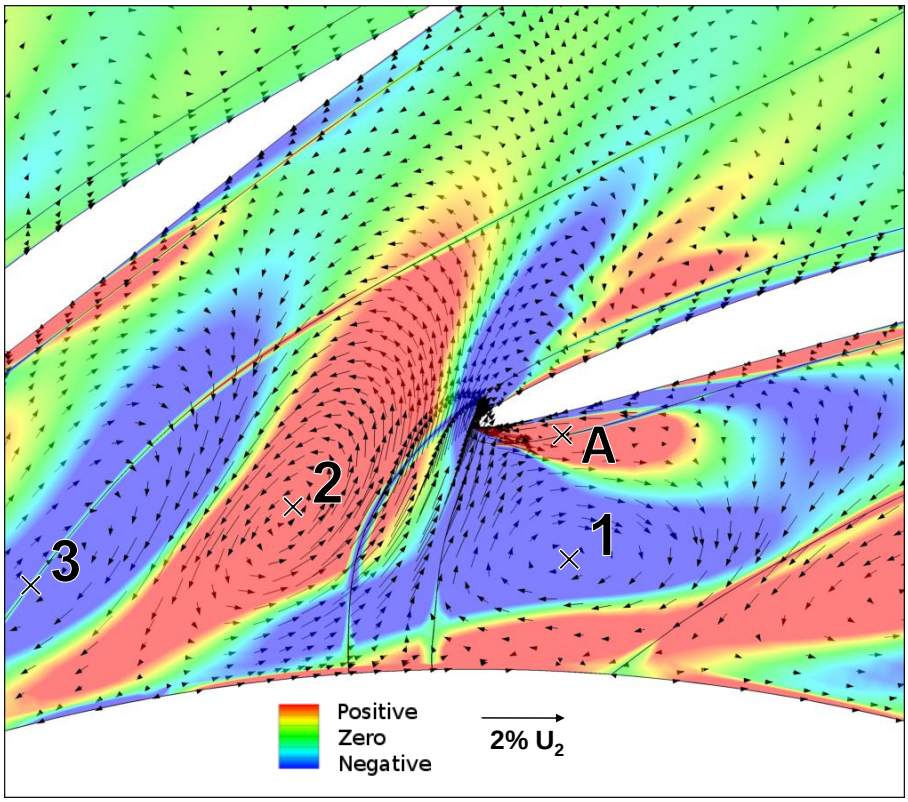

Figure 6-9: Vorticity and velocity perturbations at 3.19 rotor revolutions after application of the perturbation and at 10% span, at an operating point 10% below PDPR. The vortical structures indicated by the numbered labels convect around the vaneless space at approximately 33% rotor speed. Vorticity shed from the diffuser vane leading edge (A) convects into the vaneless space and joins vortex structure 2 as it passes by. The geometrical size of the vortices may be limited by the definition of a pitchwise uniform flow angle at the inlet boundary.

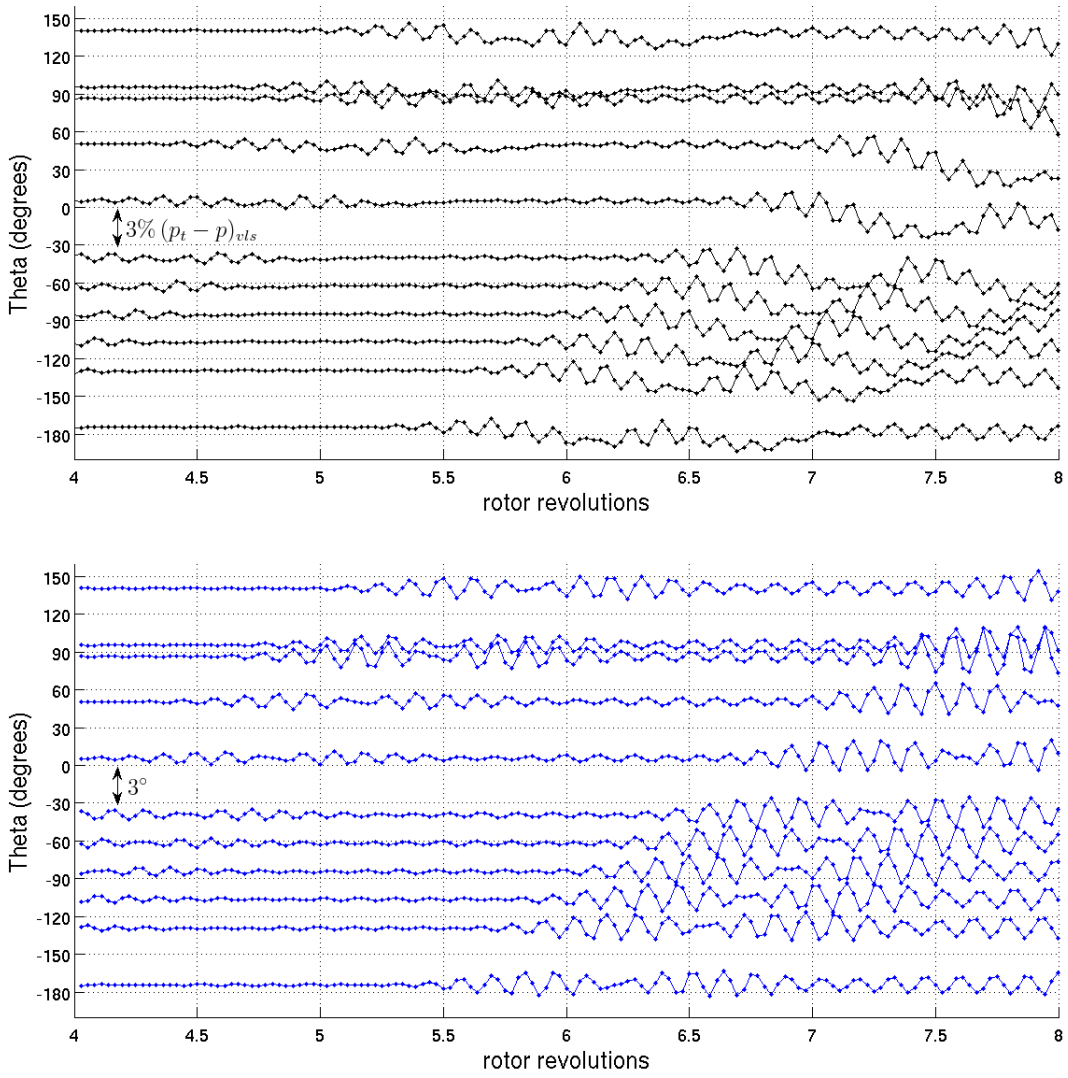

Figure 6-10: High frequency oscillations in pressure (top) correspond to changes in flow angle α (bottom) as vortex structures convect past pressure taps in vaneless space.

The occurrence of reversed flow and the convection of vorticity from the vane leading edge to the vaneless space has an analogy with one of the criteria for spike stall inception in axial machines put forth by Vo et al.[18]. The first criterion requires the tip clearance spillage flow to lie parallel to the plane of the leading edge of the blade row. The implication is that tip clearance spillage flow from one blade passage can convect to the downstream blade passage, and the significant of this occurring on the plane of the blade leading edge is that this allows the possibility of creating a loop around the entire circumference. In the diffuser flow, the tip leakage flows are replaced by the shroud endwall flow in the highly swirling diffuser inlet flow, but there remains the same criteria for the leakage from one blade tip to convect to the blade tip of a downstream blade passage (see Figure 6-6).

An early visualization of rotating stall was made by Kriebel et al. [8] in experiments between 1953 and 1958 using a radial cascade in the GTL. Kriebel [50] also developed a model for the propagation of rotating stall based on vortex dynamics, based on the observation that a stalled blade had significantly reduced circulation, requiring vorticity previously bound to the blade to be shed. While their work focused on the prediction of the propagation speed of the fully developed rotating stall cell, they presented evidence for the formation of vortices at the blade leading edge and trailing edge, as the rotating stall cell passed over the blades, through the use of interferometry and Schlieren photographs. The radial cascade geometry is similar to that of a vaned diffuser, and the similarity extends to the airfoil-profiled vanes/blades.

Figure 6-11 is reproduced from from Kriebel et al. [8]. The figure shows interferometry films with 6,000 frames per second, with time shown from right to left. The inlet Mach number is 0.47. A vortex can be seen to form at the leading edge of the blade, which increases in magnitude, convects in the pitchwise direction and partially impinges on the downstream blade. The downstream blade forms a vortex at the leading edge as the stall cell propagates.

The results of Kriebel et al. indicate that the convection of vorticity is important in rotating stall, and supports the physical mechanism proposed. However, it is not clear at this juncture how the development of the stall precursor instigates a fully

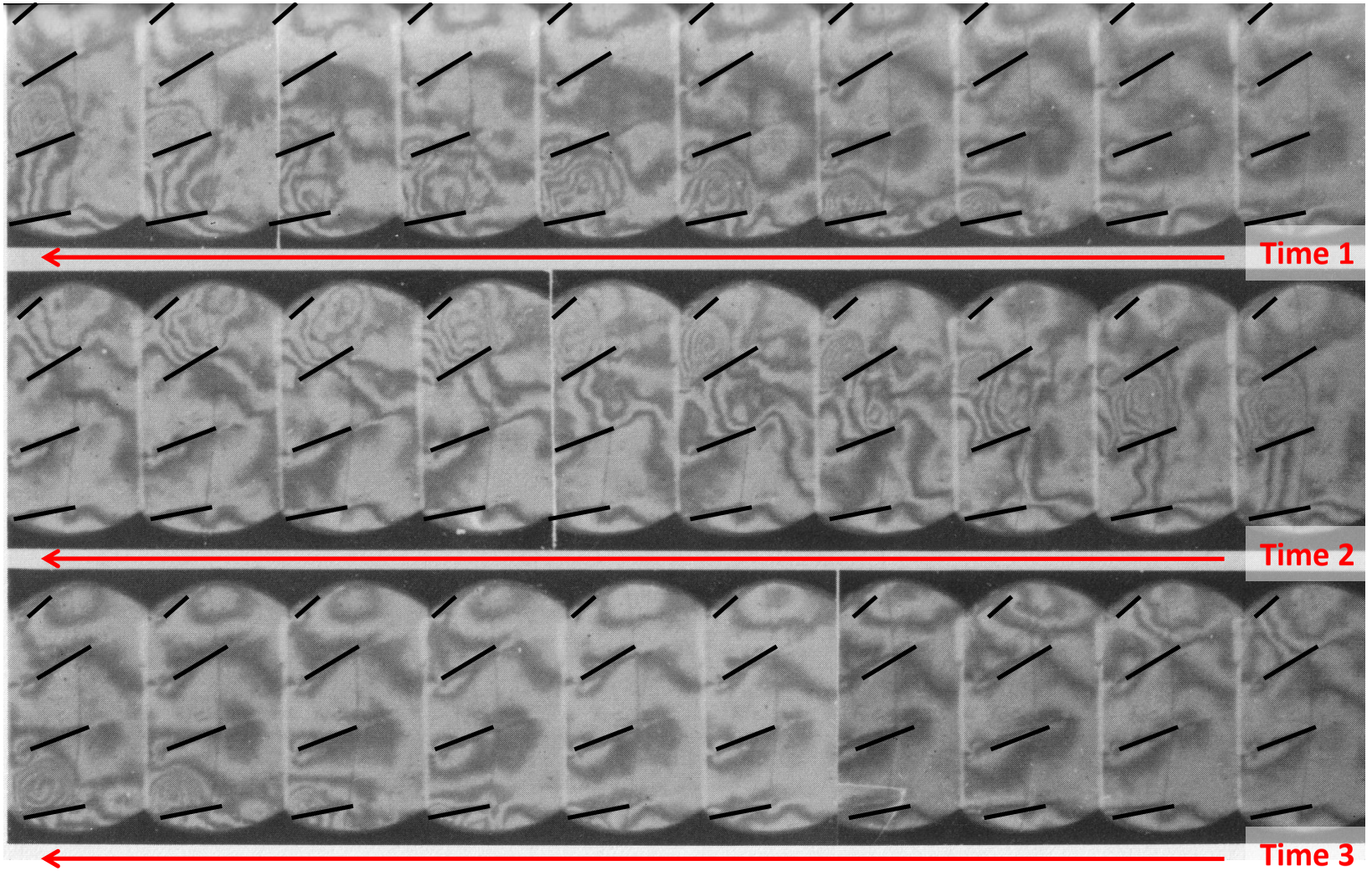

Figure 6-11: Vortices forming at the leading edge of radial cascade blades during propagation of a rotating stall cell. Interferometry photographs at 6,000 frames per second from [8]. Blades are overlaid with black line to indicate their location. Time runs sequentially from right to left and from top to bottom.

developed stall cell. It is conjectured that the vortical structures in the vaneless space of the centrifugal compressor affect a larger fraction of the diffuser span over time (vorticity can diffuse in the axial direction due to viscosity) leading to a large-scale flow breakdown on one or more diffuser passages. This process could be accelerated by the additional vorticity shed from the impeller blades, leading to the sudden flow breakdown seen in spike stall inception. However, it is noted that the phenomenon observed in the isolated diffuser simulations is caused by a reversal in the radial flow direction, and thus vorticity convecting from the impeller wakes into the diffuser is not a requirement for instability to occur.

6.2.2 Comparison with Experimental Data

The experimental data from Spakovszky and Roduner [7] is shown in Figures 6-12 and 6-13; the latter shows the experimental results with the abscissa scaled such that direct comparison can be made with the results from the isolated diffuser simulations. The most striking difference is the magnitude of the oscillation; in the experiments the spike was identified by a pressure disturbance of the order of the diffuser inlet dynamic head, whereas in the CFD results the maximum disturbance in pressure is an order of magnitude smaller. There are several possible reasons for this. Firstly, "noise" exists in the experimental results as a consequence of the limited bandwidth for the high response pressure signals, which is likely to prevent the detection of small scale, high frequency disturbances from passing vortices. Thus the initial development of the stall precursor could be lost within the noise, only revealing the spike once it has grown near to the fully developed "embryonic stall cell" described by Camp and Day [4]. The pressure rise of a significant fraction of the dynamic head is indicative of a large scale flow breakdown such as this.

Secondly, the isolated diffuser model constrains the development of the fully developed spike due to the imposition of pitchwise uniform boundary conditions at the inlet. These prevent the growth of the vortical structures to within the vaneless space (as shown in Figure 6-9), whereas in the machine it is possible that the vortical structures could extend into the impeller given the flow reversal at the shroud. This is

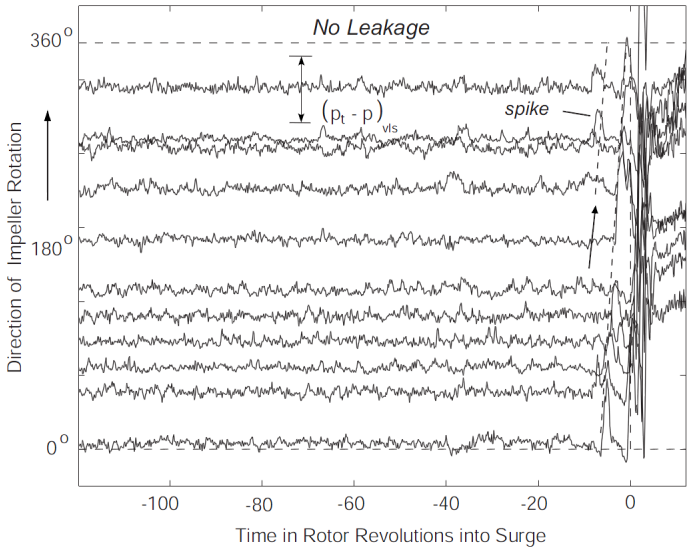

Figure 6-12: Experimental data from Spakovszky and Roduner [7]; high frequency oscillations were identified as noise.

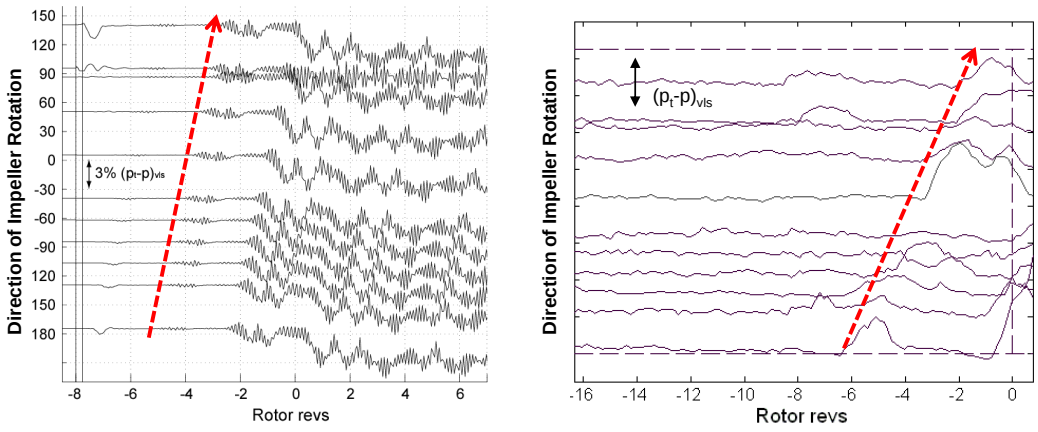

Figure 6-13: Comparison of experimental data from Spakovszky and Roduner with results from the isolated diffuser simulation, showing good agreement with rotation rate and pitchwise extent of stall precursor.

exacerbated by the removal of backflow from the isolated diffuser inlet boundary conditions, which was performed to create a numerically well-posed problem. Inclusion of the full extent of the backflow may have allowed for larger vortices.

The effect of the unsteady pressure field exerted by the rotation impeller, and the vorticity shed from the impeller blades and convected through the diffuser, is unknown. However, as the mechanism described above relates to reversed flow, the convection of vorticity from the impeller is not considered a necessary feature. Future work could examine further the unsteady simulations of impeller and diffuser, to determine the effect of unsteadiness on the flow reversal within the vaneless space. It was observed that the flow reversal in the time averaged unsteady results was present across a larger proportion of the span.

The experimental data shows good agreement in terms of a rotation rate. The rotation rate of the spike derived in experiments was approximately 20% of the rotor speed, compared to 33% in the isolated diffuser model. The similarity suggests that the mechanism for the stall precursor is accurately modeled in the isolated diffuser model. In addition, the lengthscale of the stall precursors is similar, indicated by the precursor spanning two rotor revolutions in Figure 6-13. Experiments in axial machines show spikes with very small pitchwise extent, whereas in centrifugal compressors the extent is larger; however, the solidity of a blade row in an axial machine is an order of magnitude higher than the diffuser in a centrifugal compressor, and this is likely to account for this difference.

Experiments performed by Spakovszky and Roduner suggest that the stall inception behavior changes with the extraction of bleed air from the vaneless space (see Section 3.3 and [7]). Modal wave stall inception behavior was not observed in the isolated diffuser model. Given steady inlet conditions, without the shedding of vorticity from the impeller blades, it is not expected that the isolated diffuser model can capture modal stall precursors.

The change from modal stall precursors to spike stall precursors occurred when the bleed valve, extracting flow from the vaneless space, was closed. The extraction of bleed air downstream of the impeller blade increases the loading in the vaneless

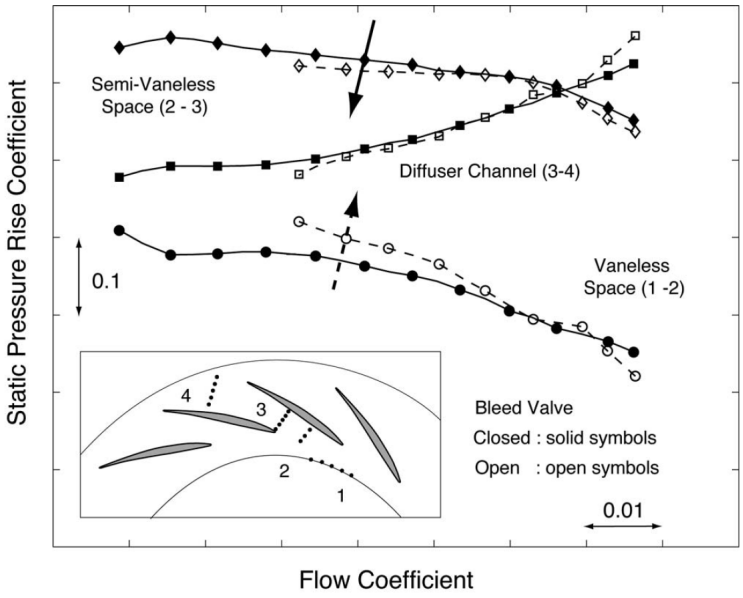

Figure 6-14: Static pressure rise characteristics of vaned diffuser subcomponents at 100% corrected speed, from Spakovszky and Roduner [7]. Loading in the vaneless space is increased due to the extraction of bleed air.

and semi-vaneless space as illustrated in Figure 6-14. The bleed cavity is on the hub surface; the extraction of bleed air is not responsible for directly removing reversed flow at the shroud. Closing the bleed valve increases the radial pressure gradient experienced in the vaneless space, which tends to increase the flow angles and worsen the flow reversal in the shroud endwall flows for a given operating point. The increase in flow angles in the vaneless and semi-vaneless space suggests that the convection of vorticity from the leading edge of a diffuser vane back into the vaneless space should occur at a higher corrected flow (or flow coefficient, as in Figure 6-14), leading to earlier onset of stall. While the latter point is observed, the stall inception mechanism also changes, and spike stall inception no longer occurs. It is hypothesized that the difference in pre-stall behavior is linked to the destabilization of the semi-vaneless space, such that the compressor is unstable to modal waves prior to the instability caused by the flow reversal in the vaneless and semi-vaneless space.

The effect of the leakage flow and the flow in the cavity would benefit further analysis. Hill [5] modeled the leakage flow in CFD but was unable to successfully replicate the change in diffuser subcomponent performance, and it was hypothesized

that the cavity may increase the vaneless space pressure rise due to a secondary effect, e.g. flow recirculation caused by the blade-to-blade variation in static pressure. This secondary effect may play a role in suppressing the shedding of vorticity at the leading edge of the diffuser vane or preventing the convection of vorticity from the leading edge to the vaneless space.

6.2.3 Proposed Spike Stall Inception Criteria

The conditions that are suggested to be necessary for spike stall inception in a centrifugal compressor are as follows:

1. Separation at the diffuser vane leading edge close to the shroud endwall, allowing vorticity to be shed from the diffuser vane leading edge with the passing of a disturbance;

2. Reversed radial flow allowing vorticity shed from the leading edge to convect back to the vaneless space; and

3. Flow in the vaneless space that recirculates around the circumference, allowing vortical structures to form and grow through the addition of vorticity shed from the diffuser vane leading edge.

The underlying cause of the effects described above is suggested to relate to the spanwise flow non-uniformity at the diffuser inlet; the radial pressure gradient set up by the highly swirling bulk flow causes flow reversal in the low total pressure, high flow angle flows near to the shroud. This in turn leads to very high incidence on the diffuser vane leading edge near the shroud.

It is recommended that further simulations are performed at different speeds and on different vaned diffuser geometries to validate these criteria.

6.3 Simulations with Vorticity Interaction at Exit Boundary

The behavior of the diffuser flow varied markedly depending on the exit boundary condition applied, as introduced in Chapter 4. In particular, applying a mass flow exit boundary condition using the Numeca "velocity scaling" option provided a significantly different result than using other options.

As the total pressure forcing is applied, the flow field changes. As discussed above, the forcing causes a jet of fluid, which can be visualized as a source of vorticity at the inlet. This convects through the domain as a vorticity wave, visualized by plotting ω_z'.

For the cases run with the velocity scaling option and without a buffer zone, the vorticity wave causes a rise in pressure as it impinges on the exit boundary. The boundary condition is applied through the scaling of the velocity vectors on the exit boundary to meet the user-defined exit mass flow criteria. At the same time, the time-marching scheme adjusts the flow to satisfy the underlying fluid mechanics expressed by the Reynold's averaged Navier Stokes equations. In the case of a total pressure forcing, which causes a local increase in flow velocities, the exit boundary condition scales the velocity vectors downwards as the perturbation impinges, causing a high pressure region. This can be clearly seen in Figure 6-15 as a region of high pressure initiated at the boundary.

Simultaneously, the pressure forcing causes flow to spill from one diffuser passage to another, as discussed above. This changes the incidence on the adjacent, downstream (in the sense of the swirl velocity) diffuser vane, changing the circulation and causing vorticity to be shed. As this shed vorticity convects to the exit boundary, another high pressure region develops, and the effect cascades around the diffuser. Of interest to note is that, at this operating point and with the different matching used in this simulation compared to the simulations discussed in Section 6.2, the vorticity is shed from the trailing edge and not the leading edge, suggesting separation at the diffuser leading edge is important for spike stall inception.

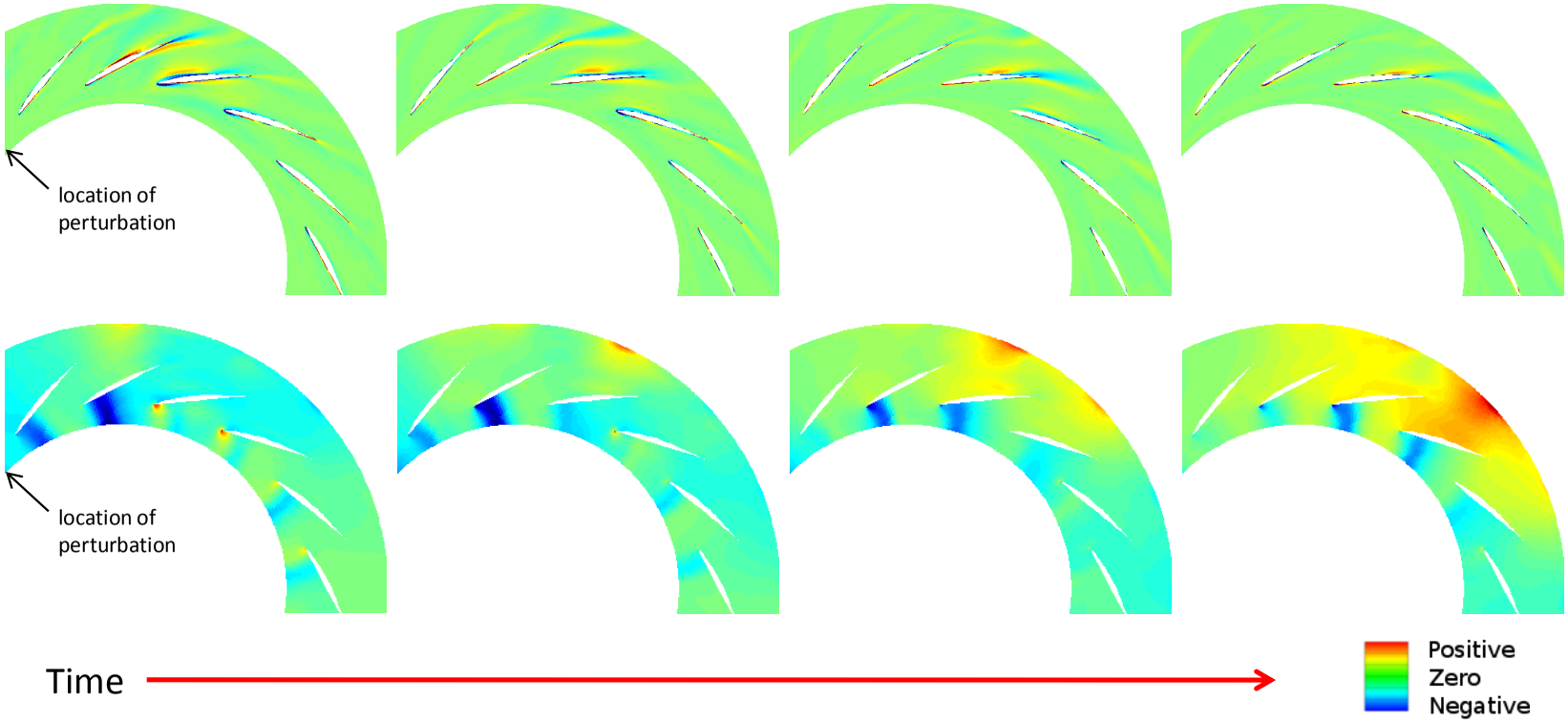

Figure 6-15: Vorticity perturbations (top) and static pressure perturbations (bottom), indicating high pressure develops where vorticity impinges on exit boundary. Frames are taken every 1/9th of rotor revolution, starting 0.64 rotor revolutions after application of the perturbation, and are taken at 90% span.

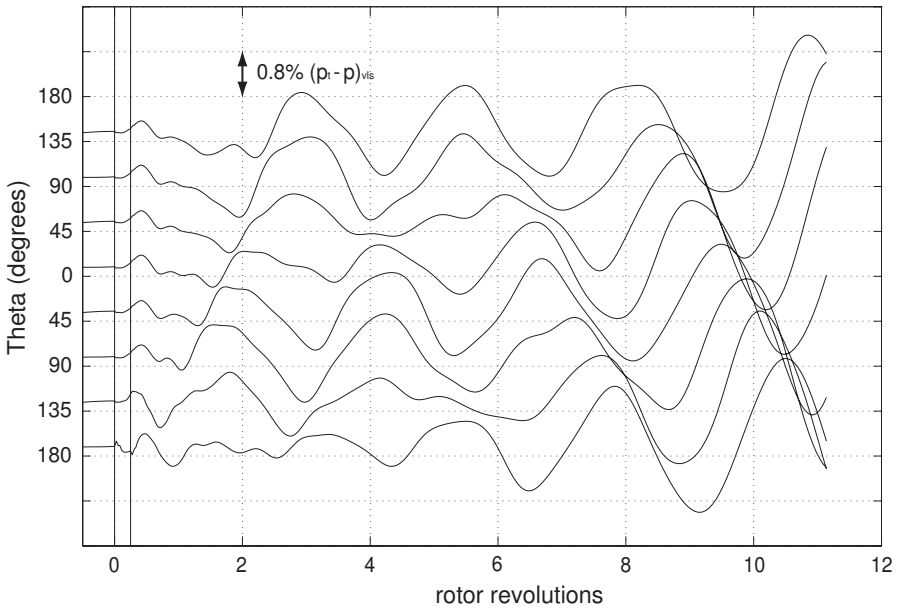

Figure 6-16: Unstable response to total pressure forcing with vorticity interaction at the exit boundary. Pressure waves initiate from the exit boundary in the direction of rotor before being replaced by a single backward traveling, exponentially growing pressure wave.

The pressure rise propagates upstream into the diffuser passages and into the vaneless space, and can be seen in the unsteady pressure traces as a forward propagating wave. The amplitude of this pressure wave is of the order of 1% of the inlet dynamic pressure. It rotates twice around the circumference of the diffuser, and in cases at higher corrected flows, is damped out. However, as lower corrected flows are reached, the disturbances grow rather than dying out (see Figure 6-16). As the disturbance grows, interaction with the diffuser vanes causes the sense of direction of rotation to change, and a backward traveling wave is formed, which grows exponentially over time.

The simulations run by Hill [5] used this type of boundary condition, and the same response was evident: a forward traveling wave replaced by a backward traveling wave, although the latter was quickly damped in Hill's simulations. The difference in amplitude between this work and Hill's could be caused to a number of factors, for example the difference in grid density, matching criteria, or location of the inlet

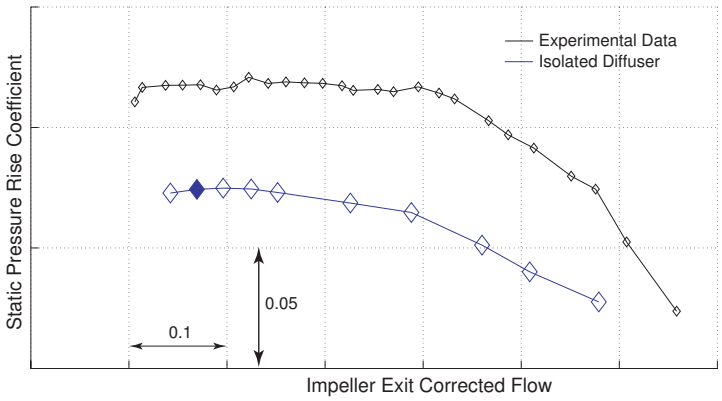

Figure 6-17: Pressure rise characteristic for the semi-vaneless space (for the mismatched diffuser). Solid marker indicates operating point illustrated in Figure 6-16.

domain.

The simulations using the velocity scaling option were run with a mismatched diffuser, in that the methodology for matching as defined in Chapter 5 was not finalized. The reason for discussion of these results (apart from explaining a numerical effect of which CFD users should be aware) is that the interaction of vorticity and pressure waves has an analogy with other findings in compressor stability analysis. Spakovszky's compressor model [28] showed that pressure waves reflected from a downstream blade row interact with vorticity waves from the upstream blade row and can cause backward traveling modal stall precursors. This appears similar to the effects seen in the numerical model here, with the non-physical interaction of vorticity waves at the exit boundary causing the same effect as reflection from a downstream blade row. In addition, the unstable behavior which resulted in the exponential growth of backward traveling waves occurs when the gradient of the semi-vaneless space changes from negative to positive (see Figure 6-17), exactly the criteria identified by Spakovszky as defining the onset of instability.

Simulations using the mass flow exit boundary condition with the pressure adaptation option were found to reflect pressure waves at the exit boundary (see Section 4.5.2) but no unstable behavior was observed with the mismatched diffuser over the operating points tested. The reflected pressure waves have significantly lower ampli-

tude than the interaction that occurs on the exit boundary using the velocity scaling option, and this could be a reason for not initiating instability. However, the iterative procedure for setting the exit pressure also leads to a pressure wave entering the domain from the exit boundary, this time in the form of a zero harmonic wave (i.e. a wave with no theta variation, uniformly traveling from the exit surface), and it is suggested that this disrupts the development of any form of rotating pressure disturbance.

In summary, it can be seen that careful implementation is required for successful modeling of the isolated diffuser, given the close coupling with upstream and downstream components and the potential for reflections and interactions at numerical boundaries. Numerical effects can, however, be explained from first principles using understanding of compression system stability.

6.4 Effects of the Volute on Diffuser Flow Stability

A perturbation analysis was performed with the diffuser and volute model, to determine the effect of the downstream volute on the stability of the diffuser flow. In addition, modeling the volute is the most representative of the possible options for the exit boundary condition for the diffuser, removing some of the numerical issues associated with other options when tested with an unsteady inlet condition. However, the inclusion of the volute also means that the diffuser inlet boundary conditions may not be adequately defined; the tongue causes an upstream influence that extends to upstream of the impeller, and as such will cause a local alteration of the flow angles and total pressure at the circumferential position corresponding to the tongue.

There also exists a caveat on the results of this section: simulations were performed prior to the finalizing the matching criteria, and as such the corrected flow at inlet to the diffuser is 2% too low.

The circumferential variations in the flow field in the diffuser and volute simulation affected the stability of the device when tested with a perturbation. The unsteady response to the perturbation is shown in Figure 6-18. From this, it can be seen

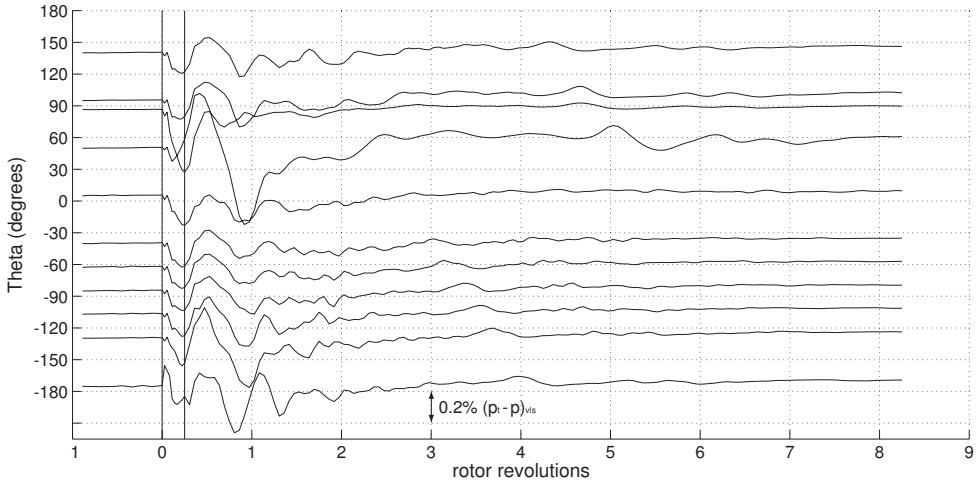

Figure 6-18: Stable response to total pressure forcing in a simulation with diffuser and volute. Backward traveling pressure wave damped near volute tongue following two revolutions around the diffuser.

that a pressure wave develops and rotates in the opposite direction to the rotor rotation for two revolutions; the rotation speed is approximately -40% of the rotor speed. The amplitude of this disturbance is very small, of the order 0.2% of the inlet dynamic pressure[3]. It is born in the unsteadiness that follows the application of the perturbation[4] and grows in magnitude prior to abruptly dying out at five rotor revolutions, in the diffuser passage upstream of the volute tongue.

The propagation of the backward traveling pressure wave is prevented by the region of supersonic flow in the passage upstream from the volute tongue, as shown in Figure 5-17. Apart from the endwall flows, the supersonic region extends across the passage, and the pressure wave (traveling at the speed of sound relative to the flow) is unable to propagate upstream. No backward traveling waves were observed in simulations with a uniform exit boundary condition, and all passages were transonic.

[3]A CFD calculation is typically considered "well converged" if the inlet and outlet mass flow agree within 0.5%. It is recognized that a pressure wave with magnitude of only 0.2% of the inlet dynamic head could simply be a consequence of the numerical accuracy of the code. The initialization simulation was allowed significant time to settle to a steady state solution with variation of less than 0.01% in any quantity over 100 iterations, which provides some confidence that this effect can be related to the flow physics. The time involved in reaching this level of convergence for the diffuser and volute simulations prevented the extension of this study.

[4]This simulation was performed with the definition of the inlet total pressure switched from 1D to 2D and back to 1D as the perturbation was applied. Refer to Chapter 4.

The physical cause of the backward traveling wave is not known at this time; given the small amplitude, the origins are difficult to determine.

While this is only a preliminary look at the effect of volutes on the development of stall precursors in centrifugal compressors with vaned diffusers, it suggests that the volute may play a significant role in the formation and subsequent growth or decay of stall precursors. The observation of the previous chapter - namely that the diffuser and volute model is limited because the diffuser inlet boundary conditions cannot allow for the circumferential non-uniformity required due to the strong upstream influence of the volute - is also relevant here: the presence of a single supersonic passage may not be representative of a diffuser downstream of a volute, if flow angles and total conditions are allowed pitchwise variation.

6.5 Uniform Diffuser Inlet Conditions

To test the hypothesis that the spanwise non-uniformity in the diffuser inlet flow has a critical role in the onset of instability, the first step of the parametric study is to perform a simulation with spanwise uniform inlet conditions. This simulation proved problematic due to Mach number effects which were not encountered when performing simulations with a non-uniform inlet condition, which benefits from being a compound compressible flow. This is further discussed below, along with suggestions for an alternative matching criterion which could potentially resolve this issue.

To derive spanwise uniform inlet conditions, the same control volume analysis is performed as described in Chapter 5 but with the entire span treated at once, such that mixing is performed in both the spanwise and pitchwise directions. This provided a single value for the inlet velocity direction, total pressure and total temperature which could be applied across the entire inlet surface.

A simulation was attempted at 8% below PDPR with the same matching criteria as developed in Chapter 5, but no convergent solution could be achieved. Analysis of the part-solved flow field during the calculation revealed that the diffuser was unable to pass the same mass flux as the case with inlet conditions defined by a spanwise

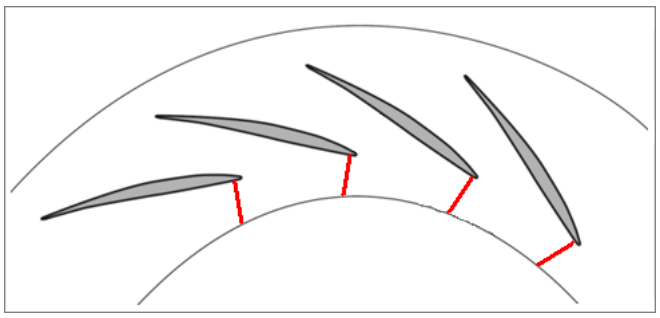

Figure 6-19: Sketch of minimum flow area encountered in isolated diffuser simulation where choking occurs; the inlet surface constrains the velocity direction and therefore acts similarly to a solid surface.

profile; the flow choked at a location defined by the minimum area perpendicular to the flow, between the diffuser vane and the inlet surface (see sketch in Figure 6-19). To achieve a convergent solution, lower mass flows were attempted, but this has the effect of reducing the diffuser inlet corrected flow and no convergent solution was possible.

The reason for choking when using a uniform inlet condition relates to the concept of a compound compressible flow (described by Greitzer et al. [13]). A uniform flow will choke at the minimum area when the Mach number reaches unity, but a non-uniform flow, for example two adjacent streams with different total conditions, chokes with part of the flow subsonic and part supersonic, and at a location offset from the minimum area. This is clearly illustrated through consideration of the ratio of total to static pressures at any given location in the diffuser. The spanwise static pressure gradient is small compared to the meridional pressure gradient; outside of corner stall regions the streamlines are largely parallel to the endwalls. However, the inlet condition is defined with a non-uniform total pressure across the span. The Mach number, as a function of the spanwise total pressure profile, can be found from:

$$M(z) = \left(\frac{2}{\gamma - 1}\right)\left[\left(\frac{p_t(z)}{p}\right)^{\frac{\gamma-1}{\gamma}} - 1\right]$$

which shows that the Mach number varies across the span. Indeed, this result explains the presence of Mach numbers greater than unity in the diffuser flow field shown in

Figure 5-6, which is not choked. The analysis can be extended to consider the criteria for choking; the reader is referred to [13] for details, but the relevant parameter for defining the point of choking for a compound compressible flow is the compound compressible flow indicator, β:

$$\beta = \iint \frac{1}{\gamma}\left(\frac{1}{M^2} - 1\right) dA$$

This presents an alternative criterion for matching the isolated diffuser simulation to the impeller exit flow, such that the compound compressible flow indicator is matched at the diffuser inlet. This is not investigated further as part of this project.

6.6 Summary

In this chapter numerical experiments are described whereby the time-invariant flow field in a single blade-row vaned radial diffuser simulation is perturbed via a short wavelength total pressure forcing applied across a small proportion of the span and pitch at the impeller trailing edge, to determine the unsteady response and investigate the stability of the diffuser flow. At a corrected flow 10% below that at which the peak diffuser static pressure rise was obtained, the response to the forcing is unstable: a disturbance rotates around the circumference which can be detected via static pressure taps in the vaneless space. The cause of the pressure disturbance is a disturbance to the vorticity in the vaneless space; examination of the perturbation in axial vorticity reveals vortices convecting around, growing in amplitude through the addition of vorticity shed from the diffuser vane leading edge. It is hypothesized that this is the cause of instability which is detected via a "spike" in plots of static pressure.

This suggests two necessary conditions for the onset of spike stall inception: (a) leading edge separation on the shroud side of the diffuser vane, allowing vorticity to be shed from the diffuser leading edge; and (b) reversed radial flow allowing vorticity shed from the diffuser vane leading edge to convect around the circumference in the

vaneless space. The suggested cause for both effects relates to the spanwise non-uniformity in flow direction and total pressure at the diffuser inlet. The fluid near the shroud has low momentum due to the low total pressure and high flow angle near the shroud at exit from the impeller. Flow across the remainder of the span has lower flow angles, but remains highly swirling, with a transonic Mach number. This highly swirling bulk flow sets a significant radial pressure gradient in the vaneless and semi-vaneless space. The low momentum fluid near the shroud is turned more by this pressure gradient than is the bulk flow, leading to flow angles in excess of 90° at the diffuser vane leading edge.

Simulations with numerical issues at the exit boundary, on which the interaction of vorticity perturbations caused artificial pressure waves to propagate back into the diffuser, were nonetheless illustrative of the mechanism by which backward traveling modal pre-stall waves are formed, and unstable operation was found (under these conditions) when the slope of the semi-vaneless space becomes positive.

Finally, performing the forced response experiments with the presence of the volute allowed the formation of a very small amplitude backward traveling pressure wave. While the exact cause of this wave has not been determined, it was observed that the propagation of the wave was disrupted by the supersonic flow which occurs in diffuser passages slightly upstream from the volute tongue, caused by the low static pressure at the diffuser exit at this location. This suggests that the volute could play a role in disrupting the development of stall precursors and potentially has the ability to delay the onset of stall.

Chapter 7

Conclusions

This thesis describes three-dimensional RANS simulations of a vaned radial diffuser, performed to gain further understanding of the mechanisms by which the diffuser flow becomes unstable at low corrected flows. The choice of an isolated diffuser simulation was made to reduce the complexity of the flow at the diffuser inlet location, removing the unsteady impeller exit flow which is not considered to have a significant impact on the diffuser performance or the stability limit. In addition, the reduced computational domain reduces the computational resources required to perform the simulations, allowing sensitivity studies to be performed on key assumptions and parametric variation of key parameters to determine their importance to stability.

The key to enabling the isolated diffuser simulations is the correct matching of the diffuser flow to the impeller outlet flow obtained from previous single passage stage simulations. A control volume approach is taken at each spanwise location to fully mix out pitchwise non-uniformities in the flow, to develop a pitchwise "mixed out" averaged flow state. This was then built up across the span to provide a spanwise distribution of total pressure, total temperature and flow direction, which provides the required level of fidelity as inlet conditions for the isolated diffuser simulations.

The matching process is completed by specifying that the corrected flow in the vaneless space is matched between the single passage stage calculations and the isolated diffuser simulations. Thus matched, the isolated diffuser simulations are shown to accurately model the steady-state diffuser flow, evidenced by close agreement with

experimental data and the results of unsteady full wheel simulations. On its own, this methodology has the potential to be a useful tool for diffuser design. Although full annulus isolated diffuser simulations were performed here, single diffuser passage simulations would also be adequate for this purpose.

It is also shown that the mixing plane implementation utilized by Numeca and representative of the standard approach for RANS CFD can cause unrealistic diffuser flows when the flow in the vaneless space is transonic and the compressor is highly loaded. Two factors are suggested to impact the failure of the mixing plane for transonic impeller exit flows, the strong upstream influence of the diffuser vanes and the jet-wake structure at outlet from the impeller. It is suggested that the mixing plane is less appropriate for centrifugal machines, as upstream influence is typically less significant in axial machines, which have many more blades and thus reduced pitch and reduced upstream influence, and the jet-wake is unique to centrifugal compressors.

Once it was shown that the isolated diffuser model well captured the performance of the diffuser, it was possible to perform the next stage of the project, testing the stability of the diffuser flow. This was performed through perturbing the diffuser inlet flow, via a forcing in the total pressure applied via the inlet conditions. For operating points at which data existed from the single passage simulations, the diffuser flow was stable to the perturbation, indicating that the single passage, steady simulations of the compressor provide a conservative assessment of the stability of the machine.

In order to achieve lower corrected flow at inlet to the diffuser, moving closer to the surge line, it was necessary to implement an extrapolation scheme for the inlet conditions. A linear trend with mass flow was determined for the flow angle and total temperature, but a quadratic dependence was used in total pressure.

This extrapolation allowed testing to the point of instability, which occurred at 10% below the corrected flow at which peak diffuser pressure rise was obtained. This was also 10% below the corrected flow at which the single passage, steady simulations began to provide anomalous results or diverged.

It is noted that modal stall waves cannot be modeled in the isolated diffuser simulation as currently implemented. It is suggested that vorticity waves shed from the

impeller are necessary to capture modal stall precursors, and these are not captured in the steady inlet conditions applied in the isolated diffuser model.

The cause of the instability was shown for the first time to be related to the convection of vorticity perturbations around the diffuser, with the stall precursor convecting in the endwall flow near the shroud at a rate of approximately 33% of the rotor speed. The unstable nature of the precursor relates to the addition of vorticity shed from the diffuser vane leading edge, where there exists a separation bubble. As the disturbance travels around, the incidence on the diffuser vanes is changed and the vane sheds vorticity. At higher flows, either no separation occurs at the diffuser leading edge, in which case vorticity is shed only from the trailing edge, or, if vorticity is shed from the leading edge, it is instead convected out of the diffuser, rather than convecting around in the vaneless space.

The corrected flow at which the diffuser becomes unstable, and the rotation rate of the stall precursor, show remarkable agreement with the experimental results, given that the proposed mechanism relates to the separation of flow from the diffuser vane, and this is governed by the wall function and turbulence model used in the RANS code (the one-equation Spalart-Allmaras model is used here). The greatest discrepancy when compared to the experimental data occurs in the magnitude of the disturbance, but it is suggested that the isolated diffuser model is unlikely to be able to capture the fully developed stall precursor, due to the constraints of the pitchwise uniform boundary conditions applied at the diffuser leading edge. At the same time, the limits of bandwidth in the experimental data is unlikely to be able to capture the small, high frequency oscillations found to occur in these simulations.

The radial pressure gradient in the vaneless space is defined by the highly swirling bulk flow, and this causes low momentum fluid in the shroud endwall flow to turn more, resulting in flow which reverses in the radial direction while maintaining high swirl. This causes a stagnation point high on the pressure side of the diffuser vane and separation at the leading edge. Thus preliminary criteria for the onset of instability can be defined: (a) leading edge separation from the diffuser vane at the shroud side; and (b) reversed radial flow such that vorticity shed from the diffuser vane leading

edge convects back into the vaneless space; and (c) flow in the vaneless space that recirculates around the circumference (also an effect of the reversed radial flows) allowing vorticity to accumulate. The root cause of the flow reversal is suggested to be the spanwise flow non-uniformity and the highly swirling flow at the diffuser inlet.

An analogy can be made with the first criteria put forth by Vo et al. [18], who observed in axial machines that tip clearance spillage flow travels from leading edge to leading edge in axial machines immediately prior to spike stall inception. However, in the case of centrifugal compressors, the cause of this flow from blade to blade (or vane to vane) is the spanwise flow non-uniformity at diffuser inlet and the high swirl, rather than the tip clearance spillage flow.

Simulations with the diffuser and the volute highlight the pitchwise non-uniformity that the downstream component causes through the diffuser. A backward traveling pressure wave was triggered in a mismatched simulation of the diffuser and volute, the cause of which is not understood at this time, but this was damped out by a supersonic passage located close to the volute tongue, where the diffuser exit pressure is lowered. This suggests that the volute has the potential to impact the onset of instability, potentially delaying its occurrence.

7.1 Recommendations for Future Work

The mechanism for instability and the criteria put forth above are based on the results of simulations of a single geometry at a single corrected speed. It is thus firstly recommended that further simulations are performed at different speeds and with other compressor geometries, to determine their generality. In particular, simulations at lower corrected speeds are recommended, as preliminary investigations at lower speeds with the same geometry suggest that this alleviates not only the problem of transonic flow in the vaneless space, which helps with the matching of isolated diffuser simulations to the impeller exit flow, but also prevents flow reversal occurring at the impeller trailing edge radius, which removes the need for alteration of the inlet conditions.

It is also recommended that simulations are performed using the unsteady full wheel model, to validate the findings from the unsteady stability assessment performed with the isolated diffuser simulation. By using a time dependent exit boundary condition with a slowly reducing mass flow, it should be possible to replicate the experimental procedure of slowly throttling the compressor into stall. It will then be possible to determine the mechanism by which the machine stalls. This is likely to take considerable computational resource; the insight found in the isolated diffuser simulation can guide the choice of corrected flow and the examination of the unsteady data.

It was not possible within the available timeframe to perform a full set of sensitivity studies or perform the proposed parametric study. It is therefore recommended that this is a future course of work; briefly, the significant studies to undertake are as follows:

1. To validate the proposed mechanism for stall inception, uniform inlet conditions should be applied to the isolated diffuser model. Should the spanwise non-uniformity play a significant role, as suggested, uniform inlet conditions should be stable to a perturbation at an operating point which is unstable using a spanwise non-uniform inlet profile. For the high speed case, this may require matching via the compound compressible flow indicator rather than the corrected flow; this needs further investigation.

2. To determine whether it is the momentum deficiency in the endwall flows that leads to the development of an unstable stall precursor, it is suggested that block profiles are applied in total pressure and/or the flow angle at diffuser inlet - i.e. a uniform profile but with a localized reduction at hub or shroud.

3. A full assessment of the sensitivity of the response to the form of perturbation may include variations in the magnitude and spanwise and pitchwise location of the total pressure forcing, as well as potentially a perturbation in flow angle. As a first step, testing a total pressure perturbation on the hub surface would be illuminating, to determine whether this is still capable of triggering instability.

4. Further optimization of the buffer layer downstream of the diffuser would be beneficial, to prevent wave reflections. Once an optimized buffer zone is implemented, it can be definitively proven whether reflections from the exit surface have any impact on the development of stall precursors in the diffuser.

5. A sensitivity study on the impact of the turbulence model used would be illuminating; here we have used the one-equation Spalart-Allmaras model in line with industry guidelines, but it is well known that turbulence models can struggle with accurately predicting transition to turbulence and separation, with the latter phenomenon important in the stall inception mechanism proposed here.

6. A sensitivity study on the grid resolution would also be beneficial. Particular areas for focus would be the vaneless space and the spanwise grid resolution, as these have the potential to impact simulations near to the stability limit given the preliminary criteria put forth in this thesis.

Finally, one potential improvement to the isolated diffuser model that is suggested is moving the inlet surface upstream to a position where the upstream influence of the diffuser vanes is negligible; it is suggested a pitch upstream would be sufficient. This may not be possible for the high speed case as the highly swirling flow is likely to choke at lower radii (see Greitzer et al. [13]), preventing the passing of sufficient mass flow to match the diffuser with the impeller exit flow. Beside this issue, there remains challenges to implementing this proposal, as it is required to control the flow profile at diffuser inlet, but boundary conditions are applied further upstream.

Appendix A

Sensitivity to Form of Perturbation

It was desired to perturb the flow on the shroud side and with sufficient magnitude to instigate instability, but the precise form, location and magnitude of perturbation selected is fairly arbitrary. Future work could perform a thorough investigation into the consequence of these choices; here we describe a preliminary investigation into two parameters thought to potentially have an effect.

A.1 Total pressure deficit

Rather than increasing the total pressure locally through applying a forcing, the effect of reducing the total pressure through a local deficit was tested. The reasoning behind this experiment was to observe whether a total pressure deficit, which fractionally reduces the mass flow and thus shifts the operating point towards the surge line, would instigate instability more effectively than a total pressure forcing.

Figure A-1 shows that applying a total pressure deficit has little impact on the form of the solution, except for inverting the response; rather than a small pressure rise traveling around the circumference as a consequence of the total pressure forcing, a small pressure deficit is seen. Both tests are performed at an operating point with corrected flow 8% lower than PDPR and both simulations indicate unstable behavior with a rotating stall precursor, including a high frequency oscillation in pressure. The simulation at 8% corrected flow below PDPR discussed in Section 6.2 is stable;

the difference is because the simulation shown in Figure A-1 was performed without extrapolating the total pressure and total temperature at inlet to the diffuser (Section 5.1.4 discusses the extrapolation process).

The result suggests that the form of the perturbation is small enough in terms of its overall effect on the full annulus diffuser flow that the response is almost linear.

A.2 Timescale for perturbation

The timescale for the perturbation was also altered, for the unstable case discussed in Section 6.2, to determine whether the form of the unsteadiness observed was related to the period of application of the perturbation. A timescale of one ninth of a rotor revolution was selected, as this represents the blade passing frequency, and this is 56% less than the original timespan chosen. As shown in Figure A-2, the effect of altering the perturbation time is small, and the unstable behavior triggered by the perturbation remains of the same; form i.e. within the limits tested, the response is insensitive to the length of application of the total pressure forcing.

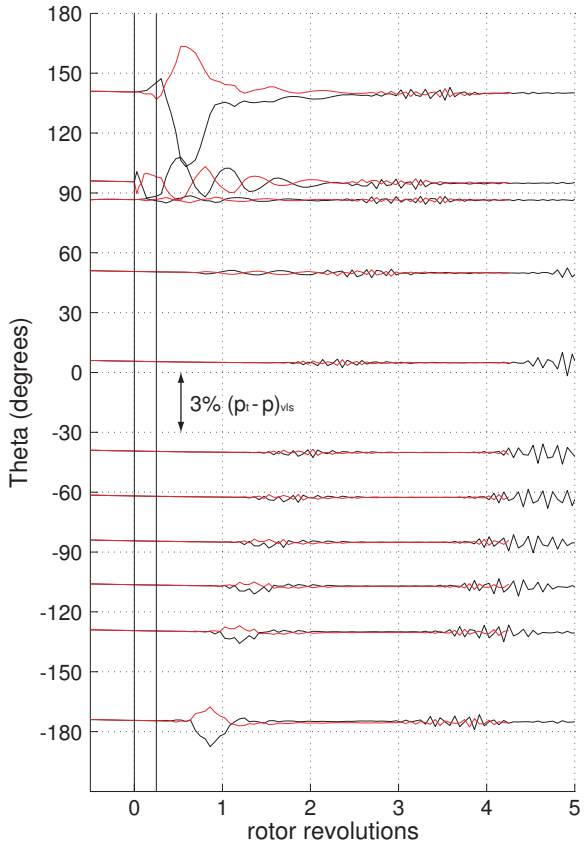

Figure A-1: Response to a total pressure forcing (black) and a total pressure deficit (red).

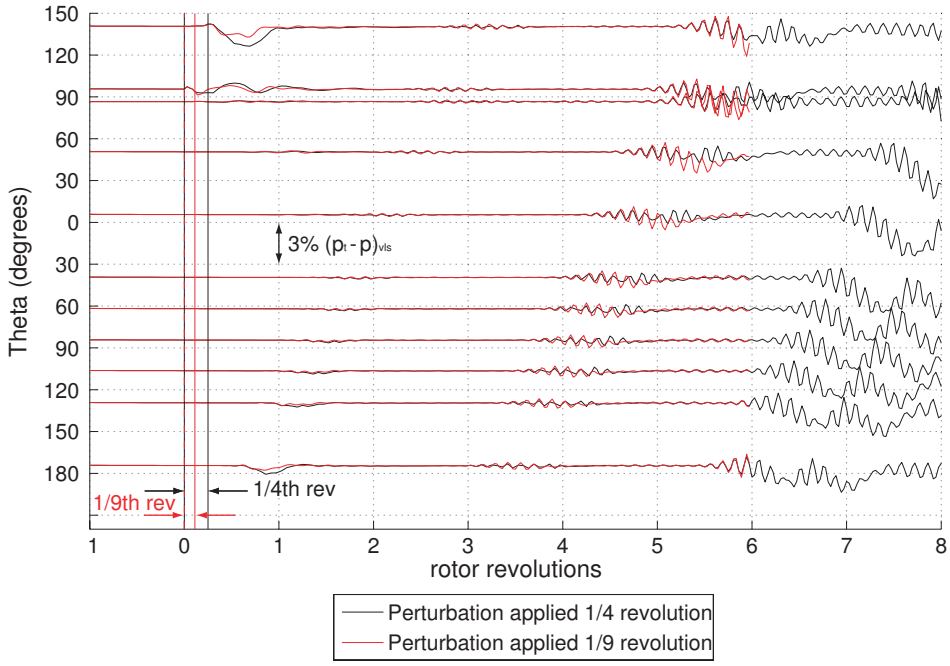

Figure A-2: Effect of altering the period of application of the total pressure perturbation.

Bibliography

[1] ABB Turbo Systems Ltd., "Product Information: ABB Turbocharging TPS..-D/E." Available online at http://www05.abb.com, downloaded 10 July 2010, July 2010.

[2] K. Toyama, P. Runstadler, Jr., and R. Dean, Jr., "An experimental study of surge in centrifugal compressors," *Journal of Fluids Engineering*, vol. 99, pp. 115–131, 1977.

[3] E. Greitzer, "The stability of pumping systems—the 1980 Freeman Scholar lecture," *Journal of Fluids Engineering*, vol. 103, no. 2, pp. 193–242, 1981.

[4] T. Camp and I. Day, "A study of spike and modal stall phenomena in a low-speed axial compressor," *Journal of Turbomachinery*, vol. 120, no. 3, pp. 393 – 401, 1998.

[5] R. Hill, "Simulation of spike stall inception in a radial vaned diffuser," master's project, Massachusetts Institute of Technology, Department of Aeronautics and Astronautics, September 2005.

[6] V. Filipenco, S. Deniz, J. Johnston, E. Greitzer, and N. Cumpsty, "Effects of inlet flow field conditions on the performance of centrifugal compressor diffusers: Part 1—discrete-passage diffuser," *Journal of Turbomachinery*, vol. 122, no. 1, pp. 1–10, 2000.

[7] Z. Spakovszky and C. Roduner, "Spike and modal stall inception in an advanced turbocharger centrifugal compressor," *Journal of Turbomachinery*, vol. 131, no. 3, p. 031012, 2009.

[8] A. Kriebel, B. Seidel, and R. Schwind, "Stall propagation in a cascade of airfoils," GTL Report 36, Gas Turbine Laboratory, Massachusetts Institute of Technology, Cambridge, MA, Aug. 1956.

[9] E. Codan and C. Mathey, "Emissions - a new challenge for turbocharging," in *CIMAC Congress*, no. 245, (Vienna), 2007.

[10] K. Heim, "Existing and future demands on the turbocharging of modern large two-stroke diesel engines," in *8th Supercharging Conference*, (Dresden), October 2002.

[11] J. Kerrebrock, *Aircraft Engines and Gas Turbines*. Cambridge, MA: MIT Press, second ed., 1992.

[12] P. Hill and R. Peterson, *Mechanics and Thermodynamics of Propulsion*. Reading, MA: Addison-Wesley Publishing Co., second ed., 1994.

[13] E. Greitzer, C. Tan, and M. Graf, *Internal Flow: Concepts and Applications*. Cambridge, England: Cambridge University Press, 2004.

[14] R. Dean, "The fluid dynamic design of advanced centrifugal compressors, Creare TN-185." Presented as lectures at von Karman Institute, Brussels, 1974.

[15] R. Hunziker and G. Gyarmathy, "The operational stability of a centrifugal compressor and its dependence on the characteristics of the subcomponents," *Journal of Turbomachinery*, vol. 116, no. 2, pp. 250–259, 1994.

[16] F. Moore and E. Greitzer, "A theory of post-stall transients in axial compression systems: Part i—development of equations," *Journal of Engineering for Gas Turbines and Power*, vol. 108, no. 1, pp. 68–76, 1986.

[17] C. Tan, I. Day, S. Morris, and A. Wadia, "Spike-type compressor stall inception, detection, and control," *Annual Review of Fluid Mechanics*, vol. 42, pp. 275–300, 2010.

[18] H. Vo, C. Tan, and E. Greitzer, "Criteria for spike initiated rotating stall," *Journal of Turbomachinery*, vol. 130, no. 1, p. 011023, 2008.

[19] B. Benneke, "A methodology for centrifugal compressor stability prediction," master's project, Massachusetts Institute of Technology, Department of Aeronautics and Astronautics, September 2009.

[20] W. Dawes, "A simulation of the unsteady interaction of a centrifugal impeller with its vaned diffuser: Flow analysis," *Journal of Turbomachinery*, vol. 117, no. 2, pp. 213–222, 1995.

[21] M. Peeters and M. Sleiman, "A numerical investigation of the unsteady flow in centrifugal compressors," in *ASME TURBOEXPO 2000*, (Munich), May 2000.

[22] Y. Shum, C. Tan, and N. Cumpsty, "Impeller–diffuser interaction in a centrifugal compressor," *Journal of Turbomachinery*, vol. 122, no. 4, pp. 777–786, 2000.

[23] N. Cumpsty, *Compressor Aerodynamics*. Singapore: Longman, 1989.

[24] C. Roduner, P. Kupferschmied, P. Köppel, and G. Gyarmathy, "On the development and application of the fast-response aerodynamic probe system in turbomachines—part 2: Flow, surge, and stall in a centrifugal compressor," *Journal of Turbomachinery*, vol. 122, no. 3, pp. 517–526, 2000.

[25] K. Ziegler, H. Gallus, and R. Niehuis, "A study on impeller-diffuser interaction—part ii: Detailed flow analysis," *Journal of Turbomachinery*, vol. 125, no. 1, pp. 183–192, 2003.

[26] B. Cukurel, P. Lawless, and S. Fleeter, "Particle image velocity investigation of a high speed centrifugal compressor diffuser: Spanwise and loading variations," *Journal of Turbomachinery*, vol. 132, no. 2, p. 021010, 2010.

[27] S. Baghdadi, "The effect of rotor blade wakes on centrifugal compressor diffuser performance - a comparative experiment," *Journal of Fluids Engineering*, vol. 99, pp. 45–52, 1977.

[28] Z. Spakovszky, *Applications of Axial and Radial Compressor Dynamic System Modeling*. PhD dissertation, Massachusetts Institute of Technology, Department of Aeronautics and Astronautics, February 2001.

[29] J. Longley, "A review of nonsteady flow models for compressor stability," *Journal of Turbomachinery*, vol. 116, no. 2, pp. 202–215, 1994.

[30] Z. Spakovszky, "Backward traveling rotating stall waves in centrifugal compressors," *Journal of Turbomachinery*, vol. 126, no. 1, pp. 1–12, 2004.

[31] Y. Gong, C. Tan, K. Gordon, and E. Greitzer, "A computational model for short-wavelength stall inception and development in multistage compressors," *Journal of Turbomachinery*, vol. 121, no. 4, pp. 726–734, 1999.

[32] A. Deppe, H. Saathoff, and U. Stark, "Discussion: "Criteria for Spike Initiated Rotating Stall" (Vo, H.D., Tan, C.S., Greitzer, E.M., 2008, ASME J. Turbomach., p. 011023)," *Journal of Turbomachinery*, vol. 130, no. 1, p. 015501, 2008.

[33] S. Deniz, E. Greitzer, and N. Cumpsty, "Effects of inlet flow field conditions on the performance of centrifugal compressor diffusers: Part 2—straight-channel diffuser," *Journal of Turbomachinery*, vol. 122, no. 1, pp. 11–21, 2000.

[34] M. Phillips, "Role of flow alignment and inlet blockage on vaned diffuser performance," GTL Report 229, Gas Turbine Laboratory, Massachusetts Institute of Technology, Cambridge, MA, Sept. 1997.

[35] Q. Guo, H. Chen, X. Zhu, Z. Du, and Y. Zhao, "Numerical simulations of stall inside a centrifugal compressor," *Journal of Power and Energy*, vol. 221, no. 5, pp. 683–693, 2007.

[36] J. Denton, "Some limitations of turbomachinery cfd," in *ASME Turbo Expo 2010: Power for Land, Sea and Air*, (Glasgow), June 2010.

[37] H.-P. Dickmann, T. Wimmel, J. Szwedowicz, D. Filsinger, and C. Roduner, "Unsteady flow in a turbocharger centrifugal compressor: Three-dimensional computational fluid dynamics simulation and numerical and experimental analysis of impeller blade vibration," *Journal of Turbomachinery*, vol. 128, no. 3, pp. 455–465, 2006.

[38] N. International, *Fine Turbo v8.7 User Manual*. Numeca International, Brussels, Belgium, v8a ed., September 2009.

[39] M. Cui, "Comparative study of unsteady flows in a transonic centrifugal compressor with vaneless and vaned diffusers," *International Journal of Rotating Machinery*, vol. 2005, no. 1, pp. 90–103, 2005.

[40] E. Casartelli, A. Saxer, and G. Gyarmathy, "Numerical flow analysis in a subsonic vaned radial diffuser with leading edge redesign," *Journal of Turbomachinery*, vol. 121, no. 1, pp. 119–126, 1999.

[41] N. International, *Fine Turbo v8.7 Theoretical Manual*. Numeca International, Brussels, Belgium, v8.7 ed., May 2010.

[42] P. Bradshaw, "Turbulence modeling with application to turbomachinery," *Progress in Aerospace Science*, vol. 32, no. 6, pp. 575–624, 1989.

[43] M. Giles, "Nonreflecting boundary conditions for euler equation calculations," *AIAA Journal*, vol. 28, no. 12, pp. 2050–2058, 1989.

[44] G. Efraimsson and C. Biela, "Analysis of aeroacousic wave propogation simulations using a higher order accurate method," in *12th AIAA/CEAS Aeroacoustic Conference*, (Cambridge, MA, USA), May 2006.

[45] M. Pianko and F. Wazelt, "Propulsion and energetics panel working group 14 on suitable averaging techniques in non-uniform internal flows," AGARD Advisory Report 182, Advisory Group for Aerospace Research and Development, Neuilly Sur Seine, France, 1982.

[46] N. Cumpsty and J. Horlock, "Averaging nonuniform flow for a purpose," *Journal of Turbomachinery*, vol. 128, no. 1, pp. 120–129, 2006.

[47] A. Prasad, "Calculation of the mixed-out state in turbomachine flows," *Journal of Turbomachinery*, vol. 127, no. 3, pp. 564–572, 2005.

[48] Y. Liu, B. Liu, and L. Lu, "Investigation of unsteady impeller-diffuser interacion in a transonic centrifugal compressor stage," in *ASME Turbo Expo 2010: Power for Land, Sea and Air*, (Glasgow), June 2010.

[49] H. Emmons, C. Pearson, and H. Grant, "Compressor surge and stall propagation," *Transactions of the ASME*, vol. 77, pp. 455–469, 1955.

[50] A. Kriebel, "Stall propagation in a cascade of airfoils," GTL Report 36, Gas Turbine Laboratory, Massachusetts Institute of Technology, Cambridge, MA, Aug. 1956.